DIGITAL URBAN TERRAIN CHARACTERIZATION FOR 1D2D HYDRODYNAMIC FLOOD MODELLING IN KIGALI, RWANDA
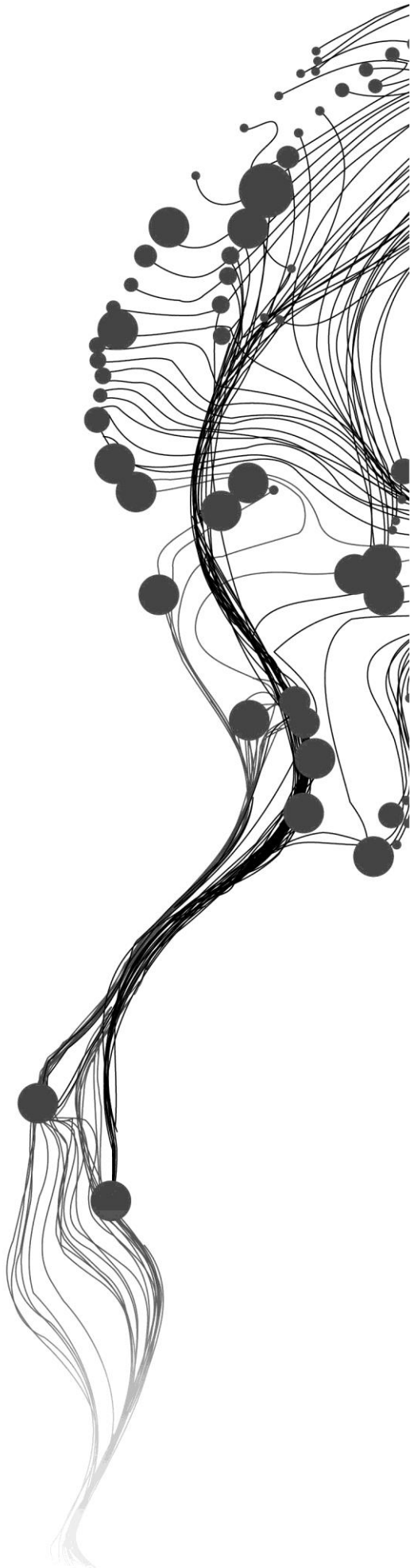
HENOCK TILAHUN ALI
FEBRUARY, 2016

SUPERVISORS:
Dr. Ing. T.H.M. Rientjes
Ir. G.N. Parodi

DIGITAL URBAN TERRAIN CHARACTERIZATION FOR 1D2D HYDRODYNAMIC FLOOD MODELLING IN KIGALI, RWANDA

HENOCK TILAHUN ALI
Enschede, The Netherlands, February, 2016

Thesis submitted to the Faculty of Geo-Information Science and Earth Observation of the University of Twente in partial fulfilment of the requirements for the degree of Master of Science in Geo-information Science and Earth Observation.
Specialization: Water Resources and Environmental Management

SUPERVISORS:
Dr. Ing. T.H.M. Rientjes
Ir. G.N. Parodi

THESIS ASSESSMENT BOARD:
Dr. M.W. Lubczynski (Chair)
Prof. P. Regianni (External Examiner, University of Siegen-Germany)

ABSTRACT

Flooding events have recently become more frequent worldwide due to factors such as the alarming rate of climate change. The effects of flooding caused by extreme weather are pronounced in urban settlements that are situated in the floodplains of rivers. Nyabugogo commercial hub in Kigali, Rwanda is a typical urban environment which has experienced frequent flooding events as it is located in the floodplain of Nyabugogo river. Terrain features such as buildings and roads govern flooding characteristics in urban environments. Hence, modelling flooding events in urban environment requires a detailed representation of the complex urban topography. In this study, a detailed digital terrain model of Nyabugogo commercial hub was developed for a 1D2D hydrodynamic modelling in SOBEK software. IDW technique was used to interpolate measured road and river point elevations and measured building height was assigned to digitized footprint of buildings. A 10m × 10m elevation grid was used to define the base DEM which was then merged with the building, river and road elevation profiles, respectively, to construct the DTM of the study area in four spatial resolutions; 5m, 10m, 15m and 20m. The effect of DEM/DTM resolution was analysed by visual inspection, error statistics and difference mapping. The topographic representation of raw satellite based DEM products (ASTER and SRTM at 30m resolution) for flood modelling was investigated by (vertical) accuracy assessment and comparison of topographic indices (i.e. slope and aspect). Vertical accuracy was assessed by using the following objective functions; root mean square error (RMSE), mean error (ME) and standard deviation (SD). It was found that ASTER DEM (RMSE=2.98, ME=0.35 and STD=1.27) has a better representation of the floodplain on the study area in comparison to SRTM (RMSE=3.07, ME=0.33 and STD=1.68). However, both unprocessed ASTER and SRTM DEMs displayed significant error as compared to reference point elevations and the base DEM (RMSE=0.72, ME=0.06 and STD=0.14). In SOBEK 1D2D modelling, the downstream boundary condition and the river bottom profile were adjusted to correct for unrealistic flooding in the model domain and the model was tested for steady flow conditions. A general increase of flood depth and inundation extent was observed while velocity slowly declined with the increase in grid size. A 1D channel representation of the road network resulted in a small reduction in flood extent while raising building height created a substantial increase in flood extent. Moreover, buildings were represented as solid, partially solid and hollow object. Maximum depth was observed when buildings were treated as solid objects while partially solid representation resulted in the largest inundation extent. The use of DTM in the flood model resulted in a substantial increase of flood depth and extents. It was also found that effect of downstream boundary condition does not propagate to the model domain. The unprocessed ASTER and SRTM DEMs failed to simulate the overland flood propagation of the Nyabugogo commercial hub.

Keywords: DTM, DEM, ASTER, SRTM, 1D2D hydrodynamic modelling, flood depth, flood extent, flood wave velocity.

ACKNOWLEDGMENT

First, I give all glory to the almighty God!!

I would like to sincerely thank my supervisor Dr. Ing. Tom Rientjes for his encouragement, guidance and critical feedback throughout the writing process of this thesis. I have learned a lot from you, Tom. I would also like to thank my second supervisor Ir. G.N. Parodi for his comments and assistance on technical matters.

I would like to extend my gratitude to the faculty and staff at the ITC, particularly WREM Department, for providing me a stimulating and facilitated study environment, and in particular for allowing me to complete my thesis with an extended timeframe due to the health condition I faced.

I would like to thank the Netherlands Ministry of Foreign Affairs for awarding me a Netherlands Fellowship Program (NFP), which covered the full costs of undertaking this MSc program at the University of Twente, ITC.

My gratitude also goes to Mr. Marc Manyifika for the provision of necessary data and his support in making my fieldwork a success.

I would like to thank my friends and colleagues at ITC for their wonderful company throughout the past eighteen months here in Enschede. Thank you very much and God bless you. Thank you Girma and Mikias for the nice friendship and the time we shared.

Special thanks to my family for their continuous support and prayer; I love you all!

Last but not least, thank you Dr. Nathanael for being right next to me in all steps of the way. I hope I made you proud!

TABLE OF CONTENTS

LIST OF FIGURES

LIST OF TABLES

LIST OF ABBREVIATIONS

1D	One dimensional
2D	Two dimensional
ASTER	Advanced Spaceborne Thermal Emission and Reflection Radiometer
CMORPH	Climate Prediction Center Morphing Technique
DEMs	Digital Elevation Models
DS	Downstream
DTM	Digital Terrain Model
GCPs	Ground Control Points
GIS	Geographical Information System
IDW	Inverse Distance Weighting
IfSAR	Interferometric Synthetic Aperture Radar
LiDAR	Light Detection and Ranging
METI	Ministry of Economy, Trade, and Industry
NASA	National Aeronautics and Space Administration
NED	National Elevation Data
NN	Nearest Neighbour
RMSE	Root Mean Square Error
RNRA	Rwanda National Resources Authority
SRTM	Shuttle Radar Topography Mission
STD	Standard Deviation
US	Upstream
WMO	World Meteorological Organization

1. INTRODUCTION

1.1. Background

Flood, an increasing and mostly catastrophic hydrologic phenomenon, is an inundation of land surface caused by an overtopping of water from its natural or manmade channels in response to excessive rainfall event(s) or snowmelt (Meesuk et al., 2014). The calamities of a flooding event extend from damage on property to claiming life. Among the several factors attributing to the increasing occurrence of floods worldwide and their associated risks, climate changes may result in extreme weather and an increasing settlement and urbanization in flood prone areas for economic reasons are the major ones (WMO, 2013). For urban settlements that are situated in the floodplains of rivers effect of flooding by extreme weather are pronounced. The high percentages of impervious areas potentially exacerbate flood impacts in urban areas (Chen et al., 2009; Tsinda and Gakuba, 2010; REMA, 2013).

The numerous steep hills and mountains have earned Rwanda the name: "Land of Thousand Hills" making several parts of the country highly susceptible to periodic flooding which occur during wet seasons. Severe rainfall resulted in major flood events in 1997, 2006, 2007, 2008 and 2009 harming people, damaging infrastructure and agricultural productivity thereby impacting economic development (Downing et al., 2009). The capital Kigali which is located on interlocking hills and valleys, is also affected by flooding in connection with on-going expansion and urbanization in the floodplains of the Nyabugogo River (Bizimana and Schilling, 2010). The Nyabugogo commercial hub is an important economic centre in Kigali where a serious flood risk upholds.

Minimizing, and if possible avoiding, the impacts of floods on urban environments such the Nyabugogo area as demands a thorough understanding of the system and an effective prediction of the probable flooding event(s). The use of computer-based flood models has since become a vital tool (Horritt et al., 2007) in simplifying the representation of reality.

Models, in particular numerical (flood inundation) models make use of several input datasets and make computations based on mathematical algorithms derived from well-established flow equations such as that of the Navier-Stoke and Saint-Venant equations. Meteorological, topographic data and data on channel layout and cross-sectional geometry constitute major inputs of models. Such data can be directly measured from the ground. Alternative to ground measurements, estimates are available from satellite and remote sensing technology. Datasets of fine spatial and temporal resolution (<10m × 10m, 1 hour) are highly desirable to accurately model flooding phenomenon. Convective rainfall systems which are common in the tropics for instance, require a short observation interval so as to capture the rain event and a relatively frequent gauge measurement makes it possible to record the rapidly changing stages of rivers during flash floods, but also riverine floods. A small spatial resolution is of high significance for topographic data where proper representation of the actual terrain is critical for accurate modelling in urban environments.

Digital Elevation Models (DEMs) are widely used for representing floodplain topography and river profile in flood modelling. Structures such as buildings and roads which are characteristic for urban areas, but also possibly other structures including dykes, drainage networks and small/local landforms, govern urban

flood propagation and hence call for the construction of a detailed Digital Terrain Model (DTM) which represents the elevation of the ground surface including the structures found on top of it (Meesuk et al., 2014). Accurate representation of topography is hence vital to minimize model uncertainties in simulating the flood properties over the complex topography of an urban neighbourhood (after Tarekegn et al., 2010).

1.2.   Problem Statement

The periodic flooding in Kigali City (Rwanda) of the Nyabugogo floodplain has endangered the lives, livelihoods and infrastructure of the rapidly increasing urban neighbourhoods of the Nyabugogo commercial hub. Due to its strategic importance, among which being a key intersection where major national roads cross (Kigali-Gatuna, Kigali-Gitarama and Kigali-Musanze); the area has embraced the continuous expansion of the city of Kigali. It had hence become an economically important town centre with a rapid increase of its dwellers and associated economic activities intensifying the danger of the frequent flood impact (Manyifika, 2015; Bizimana and Schilling, 2010; Downing et al., 2009). It is evident that more hydrologic and flood modelling studies are essential to understand the system and device appropriate mitigations.

High resolution DEM products are nowadays becoming imperative in (urban) flood modelling studies both from remote sensing sources such as LiDAR data and from sophisticated ground surveys. Both dataset are expensive to acquire and require specific technology and/or skill for collecting and pre-processing making it difficult for local authorities. The use of global elevation datasets like ASTER and SRTM hence becomes a viable alternative to supplement the acute need for DEMs in flood modelling. However, these elevation products come with several artefacts demanding adequate accuracy assessments and correction. The potential of such global DEM products for detailed urban flood modelling inn Rwanda was not addressed so far.

Hydrologic models use different input data definition formats. Raster formats often referred to as grids employ a finite difference data structure of (usually) square blocks where properties inside the block are represented by averaged single values. This approach eliminates variations within grid cells thereby possibly overruling real world sporadic behaviour and gradual changes of represented property such as elevation and it rather introduces stepped change of values. This effect is even more pronounced when a coarse scale of representation is used where the averaging of wide area is prone to miss important definitions of the real world topography that shape the behaviour of flooding in local context. Therefore, the effect of (model) resolution in representing urban topography and its consequent influence on flooding behaviour demands investigation.

The knowledge of the actual flood characteristics, such as flood depth, extent and velocity, in urban environment is critically important in determining areas of high flood risk so that authorities could plan and implement appropriate measures to avert probable flood damages. Flood propagation in urban areas is highly affected by structures such as buildings and roads in addition to the topography of the terrain surface itself. These structures alter the flood characteristics in ways that hinder, delay or initiate the overland flow. Hence, the detailed characterization of urban topography like that of the Nyabugogo commercial hub requires an appropriate representation of all major surface structures and investigation of the impact they pose on the flood behaviour.

1.3. Research Objectives and Questions

1.3.1. General Objectives

The general objective of this research is to assess the effects of DEM with incorporation of urban terrain features on flood characteristics (flood depth, extent, and velocity) when applied in a 1D2D hydrodynamic model for the Nyabugogo commercial hub in Kigali, Rwanda.

1.3.2. Specific Objectives

To achieve the general objective different DEM types were assessed. ASTER and SRTM DEM products were compared against a locally available DEM and reference elevation points to evaluate if these DEM products are suitable for simulating the urban flood of the Nyabugogo commercial hub. Furthermore the effect of urban terrain characterization on flood behaviour was investigated. In light of this, the following specific objectives were outlined:

- develop a detailed DTM of the study area,
- compare vertical accuracy of ASTER and SRTM DEM for the study area,
- assess effectiveness of use of ASTER and SRTM DEM in urban flood simulation as compared to use of a local DEM,
- study the effect of DEM and DTM resolution on urban terrain representation and flood characteristics, and
- study the effect of road and building representation on flood characteristics.

1.3.3. Research Questions

The above specific objectives were addressed by one or more of the following research questions:

- Which resolutions can represent the urban terrain features of the study are?
- How much is the mean elevation error of the ASTER and SRTM DEM as compared to the local DEM and reference elevation for the study area?
- Are there local differences between the ASTER and SRTM DEMs and how is the elevation error spatially distributed?
- How does resolution affect DEM features, such as slope, to result in a change of the flood characteristics?
- What is the effect of DTM resolution on terrain surface representation and hence on the 1D2D urban flood simulation?
- How should roads and building be represented in the flood model?
- To what extent are flood characteristics affected by introducing detailed urban terrain features into the 1D2D flood model?

1.4. Reserch Design

Three major stages of research are implemented. First, the study by Manyifika (2015) which was also conducted on the study area was reviewed. Secondly, the data collected during field work was analysed to construct a detailed DTM of the flood model domain. Finally, a 1D2D flood model was prepared based on the SOBEK software and simulations of several scenarios were conducted and analysed.

The study of Manyifika (2015) was examined and a selected boundary condition was adopted for the research. A detailed terrain mapping was carried out in the field to collect measurements of building footprint and height, roads, drainage and culvert structures. Other available GI datasets were also

collected from field offices. ASTER and SRTM global DEMs of the study area were then downloaded at 30m resolution.

A detailed analysis of the collected dataset was executed to come up with an adequate representation of the urban terrain in the required four model resolutions: 5m, 10m, 15m and 20m. Different interpolation and resampling techniques were examined and the effect of resolution was investigated. A separate raster datasets of the surface elevation, building height, river and road profiles were generated for the respective resolutions and the DTMs were generated.

SOBEK 2.12.002a version model was used to schematize the 1D channel network and coupled later with the 2D terrain model. A 1D road schematization was also tested. The effect of roads and building representation was analysed. Simulated flood characteristics such as flood depth, flood extent and flood wave velocity were finally investigated for different boundary conditions, changing grid resolutions and other system properties. Analysis of flood duration was, however, disregarded as the study area is characterized by flash floods whose effect does not last long.

1.5.   Thesis Outline

This thesis consists of six chapters. The current chapter, Chapter 1, gives some background discussion on the need for flood modelling and the objectives of the study. Chapter 2 reviews key literature concerning urban flood modelling and the use of satellite DEMs. Chapter 3 explains the study area and datasets including the fieldwork conducted. The methodology of the research is presented in Chapter 4 which describes the model structure and flow equations. Results are presented and discussed in Chapter 5. Conclusions and recommendations are presented in Chapter 6.

2. LITERATURE REVIEW

2.1. Assessment of Urban Floods

Several methodologies have been developed in the past to estimate flood impacts leading to the development of both structural and non-structural responses (Dutta et al., 2003). Integrated flood management is nowadays a preferred approaches to tackle the increasing risk of a flooding event so as to avoid human and economic losses but also to mitigate the floodplain itself sustainably (Di Baldassarre, 2012). To this effect, knowledge of the hydraulics of the river system and mechanisms by which floodplains are inundated guides decision makers towards enacting appropriate responses.

2.1.1. Hydrological Models

Models, in particular hydrological models, in this regard play a significant role in understanding the real world system behaviours and simulating catchment responses, such as floodplain inundations in urban areas (Koriche, 2012). In Rientjes (2014) a hydrologic model is defined as:

"simplified representation of a (part of a complex) hydrologic system by means of a mathematical model, model parameters, state variables, meteorological stresses and possibly boundary conditions." The physics that governs the real world physical processes is quantified by a series of equations inside the mathematical model. Figure 2.1 presents a layout of a typical mathematical model.
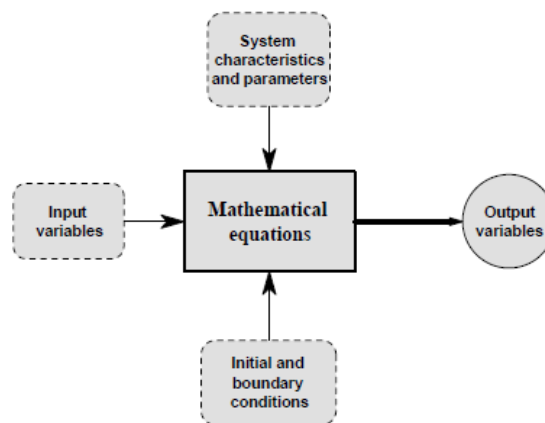
Figure 2.1: Components of a mathematical model (Rientjes, 2014).

Different types of hydrological models are increasingly being developed in an attempt to represent the catchment system as close as possible. Among the large group of available models, numerical models have become convenient tools to simulate river hydraulics and floodplain inundation as indicated by Horritt et al., (2007) and Wang et al., (2010). Numerical models make use of well-defined flow equations such as that of Saint-Venant and Navier-Stock flow equations. These numerical tools also define the representation of the model geometry (Di Baldassarre, 2012). Recent developments in computational resources have resulted in the development of sophisticated models (Bates and De Roo, 2000).

2.1.2. 1D and 2D Modelling Approaches

A variety of one dimensional (1D) and two dimensional (2D) numerical flood models are available that attempt to simulate the hydrodynamic flood behaviour as close to the real world situation as possible based on conservation of mass and momentum principles. 1D models (e.g. HEC-RAS and MIKE 11)

apply the 1D Saint-Venant flow equation with the assumption that flow velocity is perpendicular to the cross-section (i.e. flow properties vary only along the direction of flow). This modelling approach is computationally efficient but fails short of accurately representing flow over complex floodplains. 2D models (e.g. MIKE 21 and FESWMS) on the other hand overcome these constraints and offer a better description of the flood characteristics over time in terms of flood extent, depth, duration and velocity. 2D models apply the 2D (X and Y-directions) shallow water equation. However, such models are computationally expensive and suffer from increased data requirement (Horritt and Bates, 2002; Mani et al., 2014; Hunter et al., 2007; Hénonin et al., 2010; Bates and De Roo, 2000).

Channel flows that are contained within the banks are preferably simulated by 1D models. Several simulations and uncertainty analysis are hence possible in 1D models due to their high computational efficiency (Md Ali et al., 2015). Spatial discretization of a 1D model is realized by a series of cross sections defined at different locations along the channel profile. Average velocity and water depth for every cross section is calculated by the numerical solutions of the flow equations. Flood extents of a 1D model are then derived by either linear interpolation or overlay of these water depth values over a DEM (Bates and De Roo, 2000). (Hunter et al., 2007) listed some disadvantages of 1D models as follows:

- "inability to simulate lateral diffusion of flood wave,
- discretization of topography as cross sections rather than as a surface, and
- subjectivity of cross section location and orientation".

Urban environments located in floodplains are best modelled by 2D approach and consequently 2D models require continuous representation of topography (Rahman, 2006). This is achieved by means of rectangular grids (finite difference approach) or triangular mesh (finite element approach) where system characteristics inside a grid cell/mesh are represented by a single value. The use of triangular mesh has the advantage of flexibly adapting to system features however it suffers from a complex data structure and limited integration (Tennakoon, 2004). Bates and De Roo (2000) stated that water depth and depth-averaged velocity of every simulation time step can be computed at every computation node when 2D models are applied in combination with a DEM. However, 2D models are difficult to calibrate and require finer grid cells for improved topographic representation resulting in an increased computation cost making them less efficient for rapid flood assessment (Rahman, 2006; Horritt and Bates, 2002; Mani et al., 2013).

2.1.3. 1D2D Flood Modelling

For modelling flood inundation in urban environments is currently preferably simulated by integrated 1D-2D hydrodynamic modelling approaches than that of the traditional 1D simulation and the fully distributed 2D hydrodynamic modelling as it optimizes computational costs while providing a more accurate flow description (Gilles, 2010). Such approach represents the river flow by a 1D model domain while the floodplain is simulated by a 2D model domain (Bladé et al., 2012). SOBEK and MIKEFLOOD are typical examples of such flood models. Momentum conservation is ensured in coupled 1D2D modelling. However, momentum transfer among the 1D and 2D domains is ignored (Bladé et al., 2012).

According to Costabile et al. (2015), a rapid development of such models from 1D to 2D domains is attributed to the increased knowledge of the physical processes, increased accessibility of robust models and high resolution topographic information. Hénonin et al., (2013) reviewed the state-of-the-art in flood modelling approaches for urban flood simulation. In their review, Hénonin et al.(2013). asserted, in consensus to several authors including Bladé et al.(2012), Syme (2008) and Meesuk et al.(2014), that a coupled 1D2D model is preferable for urban flood simulation although it is less convenient for real-time

applications as it takes considerable amount of simulation time. Another advantage of 1D2D modelling, as indicated by Bladé et al. (2012) is the possibility to couple the 1D model with the 2D scheme in order to extend the domain when uncertainty of boundary conditions is inevitable.

2.2. Topographic Data for Flood Modelling

2.2.1. Digital Elevation Models

Among the input data required by hydrodynamic models, Tarekegn et al. (2010) suggests that digital elevation models (DEM) which provide river/channel and floodplain topographic information are the most important ones. Several authors including Mukherjee et al. (2012) and Md Ali et al.(2015) indicate the different techniques used to generate DEMs, These techniques include photogrammetric method, interferometry, airborne laser scanning, aerial stereo photograph and topographic surveys. In the absence of high quality local DEM, satellite products serve to surrogate topographic information. For hydraulic modelling DEMs from ASTER and SRTM are commonly used that are of different resolution and sources. Md Ali et al.(2015) reviewed some of these studies and also assessed the performance of different sources (topographic contour map, LiDAR, ASTER and SRTM) and resolutions of DEMs when used for flood inundation modelling. They concluded that DEM accuracy and quality are more relevant than the resolution and precision of DEM. Similarly Jarihani et al. (2015) stated that topographic accuracy, method of preparation (vegetation smoothing and hydrologic corrections) and grid size determine the extent to which DEMs of different sources can replicate landscape form so that hydrodynamic models accurately simulate real world processes.

2.2.2. Satellite Derived DEMs

So far, the use of distributed numerical models has become a popular alternative where recent advances in remote sensing technology augment limitations of observational records (Hunter et al., 2007). Significant advancement in modelling urban flood inundations has been achieved by the use of remote sensing data which provides better descriptions of the complex urban topography (Yu and Coulthard, 2015) and spatio-temporal coverage compared to observed data in the field. Remote sensing data are also used to simulate extreme rainfall events which, by means of a rainfall-runoff model, are transformed to a runoff hydrograph to be used as boundary conditions; an input in the hydrodynamic urban flood models.

Advancement in remote sensing technology has produced high resolution imageries which supplement the computational data requirements of advanced hydrodynamic urban flood models (Meesuk et al., 2014). Among these, Light Detection and Ranging (LiDAR) and Interferometric Synthetic Aperture Radar (IfSAR) data provide excellent topographic description which will significantly improve model performance in representing the flood inundation (Costabile et al., 2015). Even though a high resolution Digital Terrain Model (DTM) obtained from the sub-meter spatial resolution of these topographic datasets is desirable for urban flood modelling (Mason et al., 2014), it is not always a viable option due to their limited spatial coverage (Baugh et al., 2013) and the associated high cost of acquiring the datasets.

The alternative is, hence, to use publicly available global DEM products such as Advanced Spaceborne Thermal Emission and Reflection Radiometer (ASTER) and Shuttle Radar Topography Mission (SRTM). ASTER is an advanced multispectral imaging system onboard the Terra satellite having a Visible and Near-Infrared sensor with a stereoscopic capability to generate a near global photogrammetric DEM

available since 2009. SRMT, on the other hand, is a high-resolution near global topographic dataset acquired by an interferometric Synthetic Aperture Radar technique (IfSAR) (Colosimo et al., 2009; Frey and Paul, 2012; Thomas et al., 2014). These satellite DEM products are widely used in hydrologic modelling and have proved to be invaluable sources of topographic information for flood inundation simulation, especially over dry land river basins and remote locations (Jarihani et al., 2015) including much of Africa and other developing parts of the world where high resolution DEM is virtually unavailable. These sensors are readily accessible to any user though they suffer from artefacts due to low contrast, clouds and radar shadow resulting in erroneous topographic information as depicted by Frey and Paul (2011).

Both ASTER and SRTM DEMs come in different spatial resolution with the different versions released by the developers; The Ministry of Economy, Trade, and Industry (METI) of Japan and the United States National Aeronautics and Space Administration (NASA) for ASTER and NASA alone for SRTM. The ASTER GDEM has a spatial resolution of 1 arc-second (30m) while the SRTM DEM is available in 1 arc-second (30m) resolution for the United States (released for most of the world in 2014), 3 arc-seconds (90m) and 30 arc-seconds (1Km) for the rest of the world (Frey and Paul, 2012; Thomas et al., 2014). Several (urban) flood modelling studies (such as Haile and Rientjes, 2005; Jarihani et al., 2015; Manyifika, 2015) have indicated that a fine DEM grid is capable of representing the flow dynamics with appreciable accuracy but is computationally expensive while a coarser DEM grid would allow for efficient computation at the expense of reduced characterization of topography thereby introducing significant uncertainties in the flood simulation. The choice of DEM resolution for urban flood simulation however shall consider a sufficient representation of prominent urban terrain features that affect the flood propagation. Hence, a reasonable compromise is inevitable in defining an appropriate DEM resolution that can accurately simulate urban flood inundations.

Several authors and documentations provided along with these satellite DEM products discuss the specifications and usability of the products for hydrodynamic flood modelling. ASTER GDEM product provides better elevation definition on relatively flat and gently sloped area whereas contains artefacts and anomalies on steep surfaces, inadequately (solar) illuminated, forested and snow covered areas. The product has an absolute vertical accuracy of around 20m and 30m horizontal posting. On the other hand, SRTM product generally has a better accuracy on open areas but it suffers from voids on water bodies and on steep topography as a result of the radar energy-atmosphere-ground target interaction of the IfSAR technique. It has an absolute vertical accuracy of abound 16m and horizontal accuracy of around 20m. It is also affected by the presence of forests and urban structures such as buildings. The accuracy of these DEMs should be tested for specific study areas and necessary corrections should be made to avoid the propagation of errors on to the flood models (e.g. Patro et al., 2009; Jarihani et al., 2015; Colosimo et al., 2009; Tarekegn et al., 2010; Md Ali et al., 2015).

2.2.3.   DTM for Flood Modelling

Geometrically complex and small structures make high resolution urban flood modelling a challenging task (Schubert and Sanders, 2012). To accurately model an urban flood, the effect of terrain surface features which obstruct or alter the flow of water on the land surface should also be analysed. Buildings and roads constitute the major urban terrain features influencing flood propagation and characteristics of the flood such as depth and velocity. In addition to the bare earth surface elevation commonly referred to as Digital Elevation Model (DEM), Digital Terrain Models (DTM) contains elevations of buildings,

(often) elevated roads and high trees (Meesuk et al., 2014). Many 1D2D flood models assign high surface roughness values to account for the dissipated energy of the flood water as it is forced to change its direction and speed when encountered by these urban terrain features (Syme, 2008). Hence, an accurate DTM of the urban neighbourhood is vital for reliable simulation of an urban flood.

A. S. Chen et al., (2012) argues that the approach of using higher or lower local roughness values (Manning's 'n') when a large grid size is used fails to accurately describe local inundation processes; however, raising the ground elevations with fine grid size would be computationally expensive in addition to the demand of high resolution topographic data such as LiDAR. Rahman (2006) similarly stated that overestimation of flood behaviour (extent and depth) could occur by representing buildings as solid objects whereas underestimation of these flood behaviours might happen when bare earth elevation with associated roughness values are used. The DTM grid size is of important significance for accurate representation of urban terrain features. In this study however, high resolution topographic data was not available, hence, an attempt is made to construct a DTM from field measurements of buildings and roads. Moreover, the combined effect of raised elevation and high surface roughness values was assessed for the Nyabugogo commercial hub.

3. STUDY AREA AND DATASET

3.1. Study Area

Kigali, the capital city of Rwanda is located in the centre of the country between elevations of 1300 and 1600 meter above sea level (m.a.s.l) with the peak of Mont Kigali extending up to 1850 m.a.s.l. Hills, ridges and valleys of very high slopes dominate the city which has two rainy seasons: February to May and October to December. The city is affected by a frequent flooding attributed to its rugged topography and high seasonal rainfall. Kigali is a rapidly expanding city where an on-going urbanization is observed on the floodplains of the Nyabugogo River. The Nyabugogo commercial hub located in the north west of Kigali city is an active urban neighbourhood susceptible for the periodic flooding of the Nyabogogo River (Manyifika, 2015; Bizimana and Schilling, 2010; Tsinda and Gakuba, 2010; Research and Public Awareness Unit/MIDIMAR, 2012; REMA, 2013).

The Nyabugogo River drains a catchment with an area of 1647 sq. km. covering large parts of Kigali city. A total of sixteen sub-catchments make-up the Nyabugogo catchment with a highest annual average rainfall between 1100mm and 1600mm. Only Mpazi and Yanze sub-catchments discharge directly inside the study area thereby constituting two upstream boundaries of the model domain whereas Lake Muhazi sub-catchment collects all the upstream drains of the river and hence represents the major Nyabugogo river upstream boundary Figure 3.1 presents the Nyabugogo catchment and the study area.
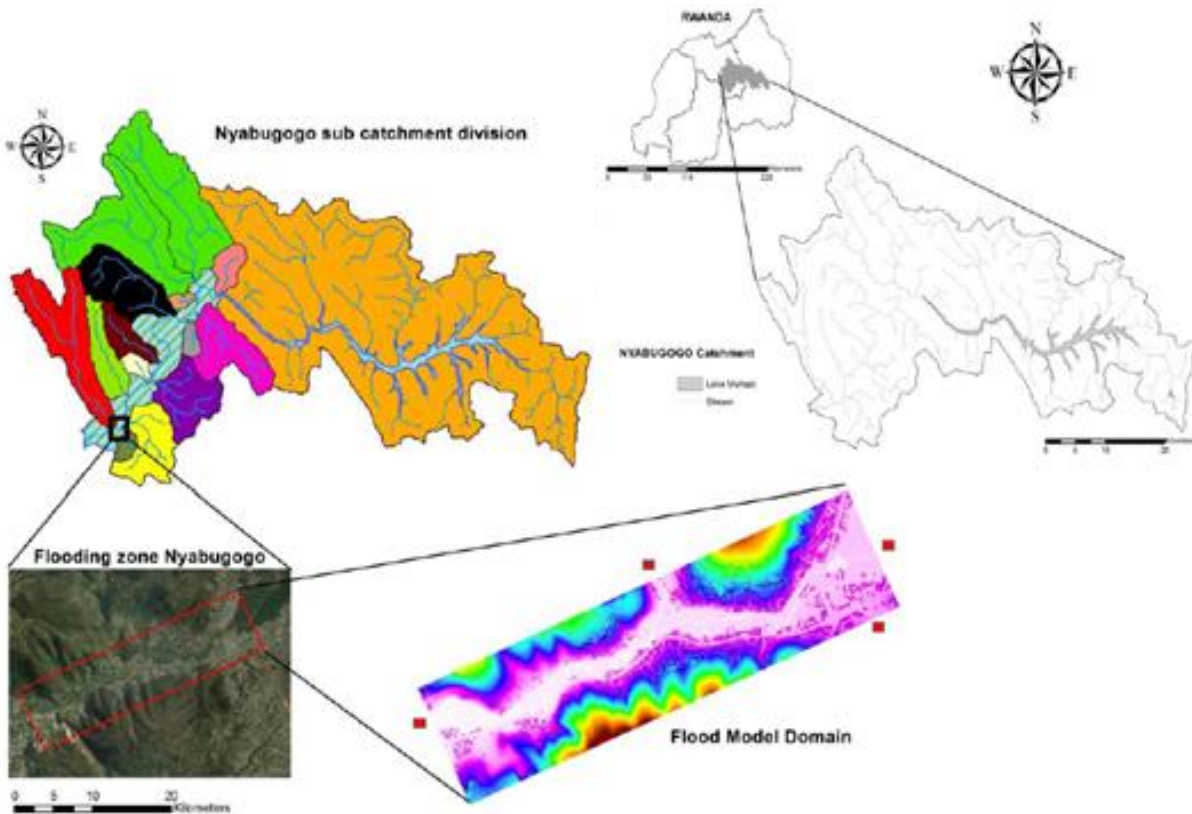
Figure 3.1: Study area: Nyabugogo commercial hub (Manyifika, 2015).

3.2. Climate

Due to the high elevation of Kigali, as is the case for Rwanda in general, temperate climate prevails though the country is located on the tropical belt. It experiences a temperature ranging between 19 and 21^0c with the highest annual average rainfall of around 1200mm with long rains occurring during the March, April and May period (Rwanda Meteorological Agency website; http://www.meteorwanda.gov.rw).

3.3. Topography

The elevation of the study area varies between 1360 and 1590 m.a.s.l. and is dominated by steep hills confining the relatively flat floodplain of the Nyabugogo River. The Nyabugogo commercial hub with elevation around 1370m is a relatively flat system that is affected by recurring floodings.

3.4. Dataset

Several primary and secondary datasets were collected during a two weeks long fieldwork at the Nyabugogo commercial hub, Kigali in September, 2015. Among the collection of topographic data, detailed data on urban terrain representation has been collected.

3.4.1. Secondary Data

Accurate topographic representation is of high interest for distributed flood models. Flood modelling studies simulate flood inundation characteristics resulting from excessive rainfall and discharges of river systems where flow on land follows the elevation profile of the surface once it overtops the river banks. Hence, adequate topographic representation can be regarded as a prerequisite for any flood modelling exercise. In line with this, the Rwanda Land Use and Development Master Plan Project has conducted an aerial photography mission and ground surveying campaigns to produce a 0.25m × 0.25m digital orthophoto and 10m × 10m elevation grid (see Figure 3.2) of the whole Rwanda in May, 2010 (SWEDESURVEY, 2010). These datasets were collected from the Rwanda National Resources Authority (RNRA) during the fieldwork. However, attempts to collect surveying benchmark data from the concerned government offices were not successful.

3.4.2. Satellite Data

Freely available global elevation datasets of ASTER (Advanced Spaceborne Thermal Emission and Reflection Radiometer) and SRTM (Shuttle Radar Topography Mission) were downloaded (respective tiles containing the study area) from the websites given Table 3.1. Figure 3.3 shows a section of the extracted DEM of ASTER and SRTM.

Table 3.1: Satellite based DEM products

DEM Product	Resolution	Version	Source
ASTER	30m	2	http://gdex.cr.usgs.gov/gdex/
SRTM	30m	3	http://earthexplorer.usgs.gov/
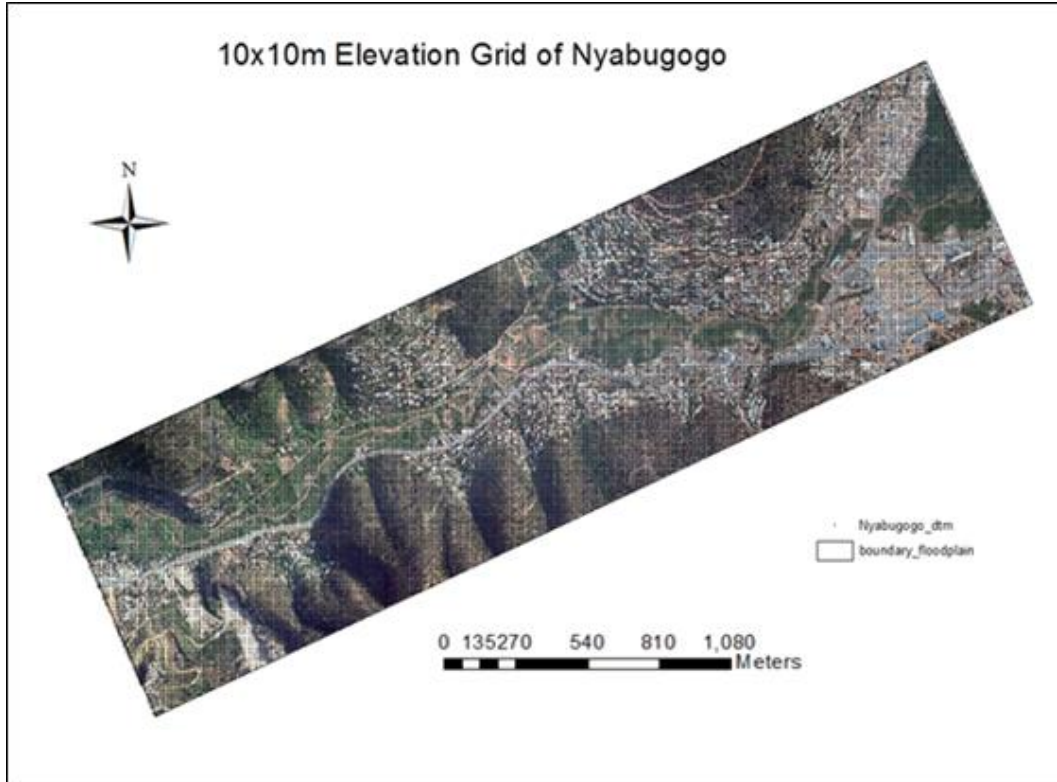
Figure 3.2: 0.25m × 0.25m orthophoto and 10m × 10m elevation grid of the study domain.
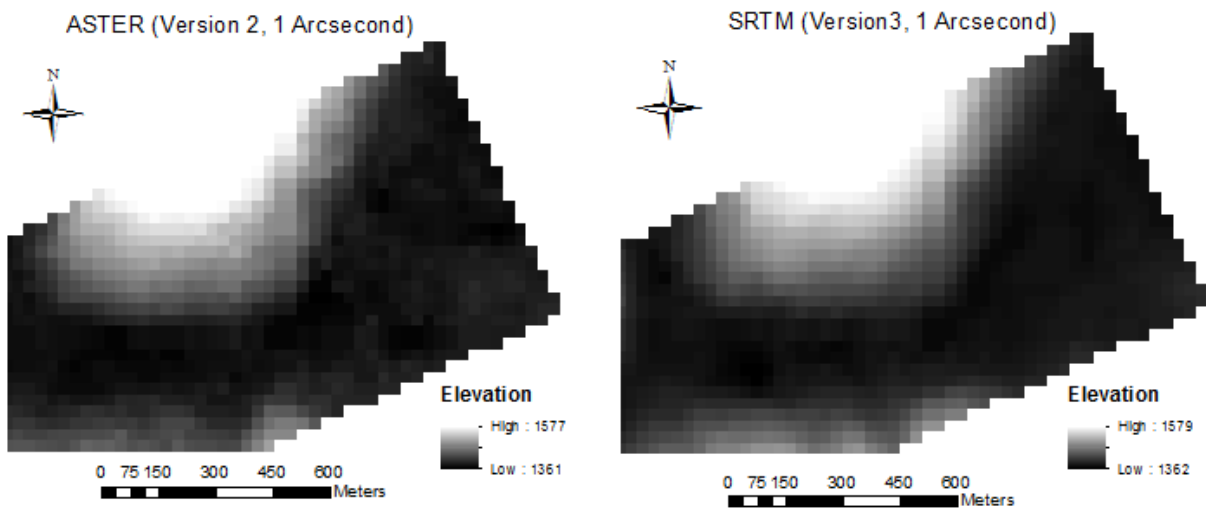
Figure 3.3: Extracted ASTER V2 (left) and SRTM V3 (right) DEM of (part of) the study domain.

3.4.3. Data from previous work

Manyifika (2015) utilized an 8km by 30min CMORPH satellite rainfall product to analyse four extreme rainfall events that took place in the Nyabugogo catchment and applied the HEC-HMS NRCS CN model to prepare runoff time series for all four events. The simulated stream flow served as inflow from upstream areas to model the Nyabugogo, Mpazi and Yanze drains. Of these four events, the second event, i.e. the rainfall which occurred on from 4th to 5th of May 2012 was selected for the current study. This event not only produces the largest discharge but also it occurs between relatively small intervals triggering overflow as a result of the filling up of the river channel by the earliest fall. Figure 3.4 shows the upstream

runoff hydrograph of this rainfall event. The upstream boundary flows of Nyabugogo river, Mpazi drainage channel and Yanze river are given in Annex 1.
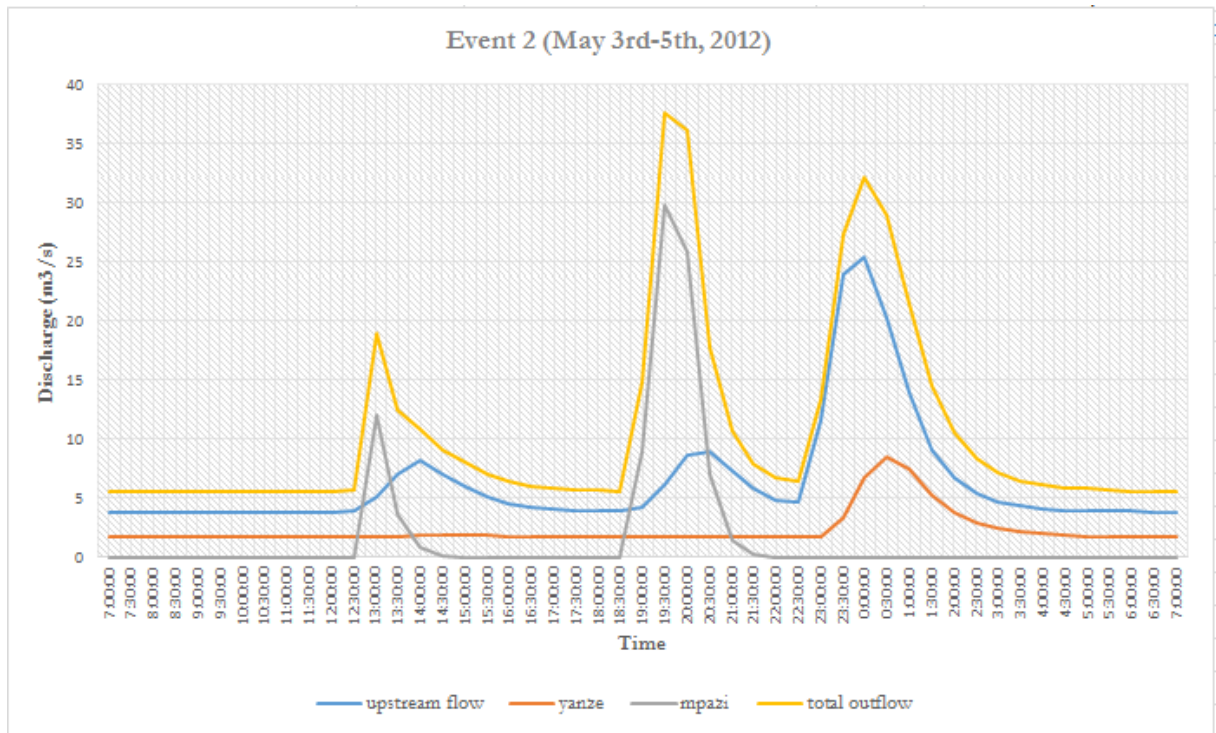
Figure 3.4: Upstream boundary inflow by Manyifika (2015)

A dataset with cross section and longitudinal profile of the river bottom and its banks was also measured by Manyifika (2015) using a total station surveying instrument. This data was adopted in the current study to enhance the dataset collected during period of fieldwork as shown in Figure 3.5. Moreover, the previous researcher also collected some flood depth measurements by identification of flood marks and interviewing local people. These observations are given in Figure 3.6. However, the direct use of such dataset must be exercised with care as both the flood marks and people's claims on flood extent were uncertain given the time frame of the selected event and the data collected. Even though the use of these flood depth records was ruled-out in the current work, a valuable insight of inundation by a typical recurring flood could be obtained.
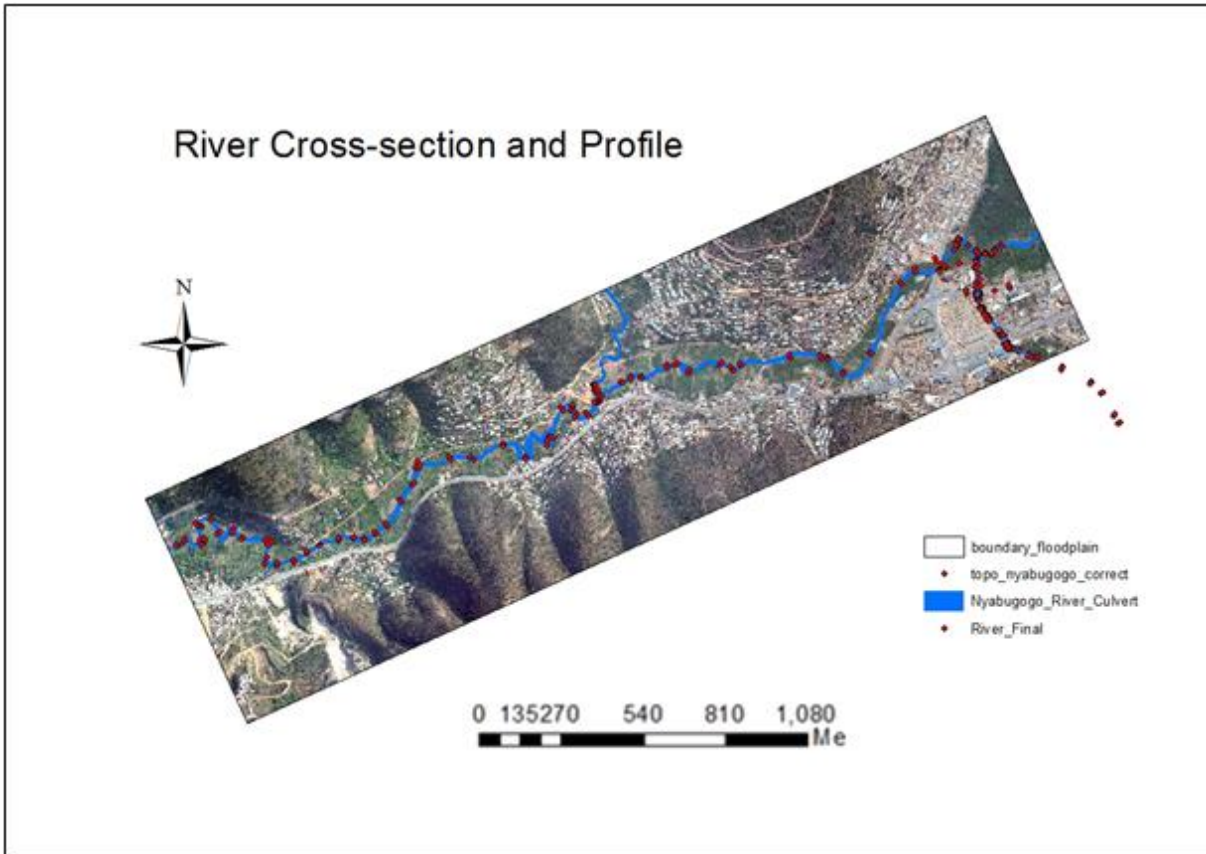
Figure 3.5: River (and bank) cross-sections and profile points, after Manyifika (2015).

#	X	Y	Depth m
1	504964.20	4785307.41	0.60
2	505107.27	4785412.58	0.20
3	504910.67	4785424.90	0.40
4	504951.89	4785510.64	0.30
5	505217.65	4785563.70	0.30
6	504872.77	4785498.80	0.50
7	504975.57	4785554.23	0.50
8	504895.04	4785663.18	0.30
9	504871.83	4785588.34	1.20
10	505005.89	4785511.12	0.50
11	504919.67	4785560.38	0.60
12	504940.52	4785640.03	0.70
13	505054.21	4785325.89	0.60
14	505105.38	4785371.37	0.50
15	505005.42	4785359.05	0.70
16	505143.75	4785515.86	0.40
17	504919.67	4785385.11	0.60
18	504984.10	4785477.00	0.50
19	504931.52	4785551.86	0.70

Figure 3.6: Collected flood depth of the Nyabugogo commercial hub by Manyifika (2015)

3.5. Fieldwork Data

3.5.1. Roads and Ditches

An attempt was made to measure the location, elevation and span of the major roads and associated roadside ditches of the study area excluding those which were located high on the hills and far from the floodplains of the Nyabugogo River. Starting from the downstream boundary of the model domain measurements were taken on both sides of the road in such a way that changing cross-sections, alignments and slopes were recorded as much as possible. As such more measurements were taken on curving sections of the road segment unlike the relatively straight road segments. A fixed measuring interval was not implemented for reasons of instrument convenience, visibility and time constraint. Location and dimensions of roadside ditches (both natural and manmade) were measured as shown in Figure 3.7 (here, for example, the ditch is found on the left of the road):
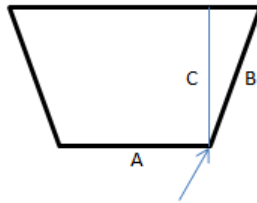
Figure 3.7: Example of a roadside ditch measurement; Where A stands for bottom width, B for side length, and C for depth and location was measured at the point indicated by the arrow (location changes with the alignment of the ditch by the two sides of the road).
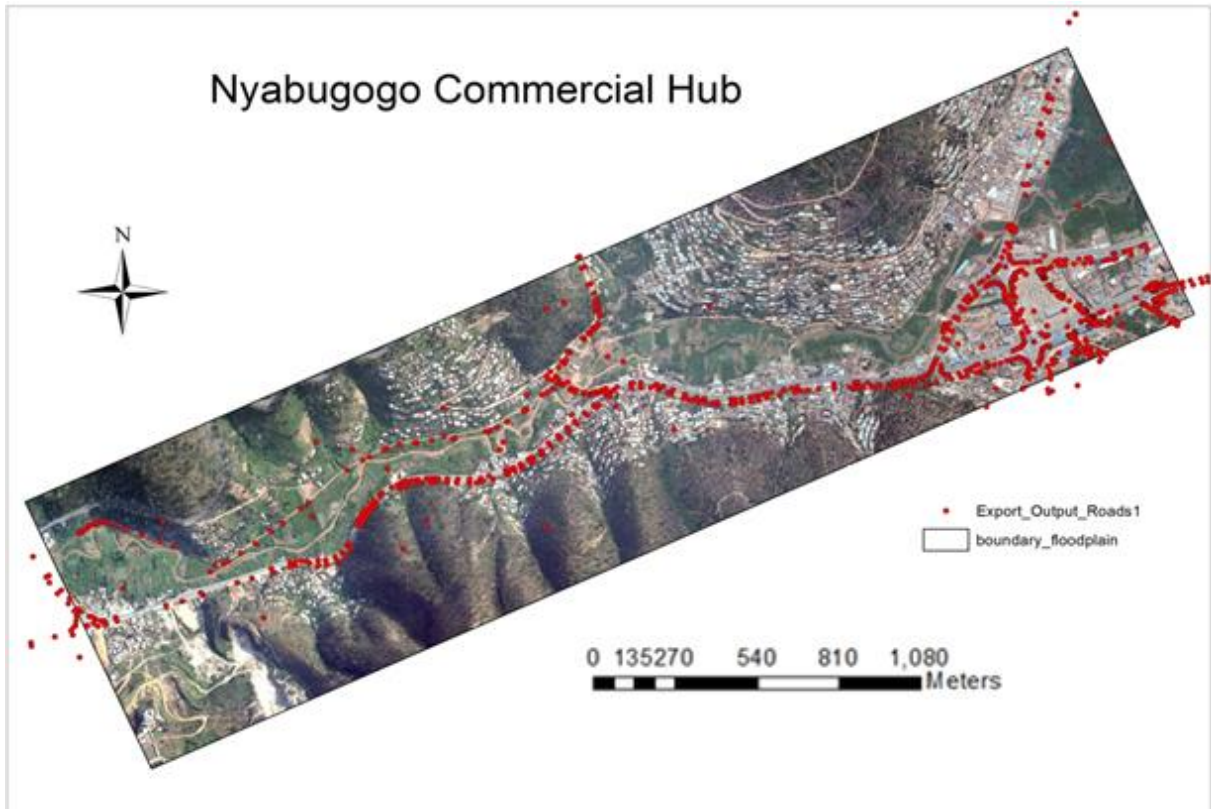
Figure 3.8: Map of the collected road points in the study domain.

For the small roads by the banks of the river, a centreline measurement was taken, noting the width of the road wherever it changes. This was because the span of these roads was between 2 and 3 meters throughout and the dense vegetation and tall trees by the sides of the road impair visibility. In total more

than 900 road and ditch points were measured as displayed over the orthophoto of the study domain in Figure 3.8.

3.5.2. Drainage, Culvert and Bridge

The Nyabugogo River cross-section was surveyed by Manyifika (2015) hence it is adapted here as it is. The detailed cross-section of the major drainage line, named Mpazi, constituting one of the model-boundary inflows was measured including its two major culverts. Moreover, small culverts on the major roads of the domain were also measured Figure 3.9 shows photos taken while culverts were measured in the field. However, only the location and elevation of the two major and two minor bridges were measured as it was impossible to get additional information (such as elevation of the bridge crest).

Figure 3.9: Sample photos taken while measuring location and cross-sections of culverts.

The measurement of these roads, ditches, drainage and culverts took the first four days of the field work.

3.5.3. Building Height

The Remote Height Measurement (RHM) function of the total station allows height measurement of any structure (including vegetation). However, the field crew was not aware of this function hence I gave a brief introduction so as to measure the footprint and height of buildings located by the roadsides as indicated in Figure 3.10.
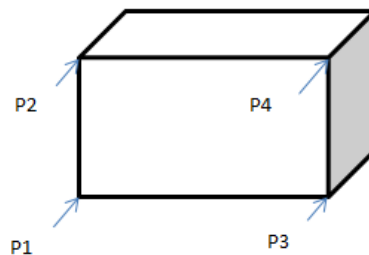
Figure 3.10: Example building footprint and height measurement

Where P2 and P4 represent the height of the building at points P1 and P3 respectively, hence having similar coordinates as that of the footprint points.

As it was impossible to obtain such two pairs of building footprint and height measurement of every building in the given time, a decision was made on the field to consider buildings of similar height from

the measurement of one and to complement the construction of building height with the footprints digitized from the orthophoto by Manyifika (2015), certainly incorporating possible changes from alternative sources such as GoogleEarth and photographs taken on the field. However, due to visibility problem few shifting of building footprints was made and for some buildings only one set of measurement was taken. Moreover, for the buildings constructed on the hillsides a height measurement of sample buildings was made with a measuring tape so as to adopt this height for all inaccessible buildings as it was observed that much of these buildings were residential buildings with similar attributes (shape and height).
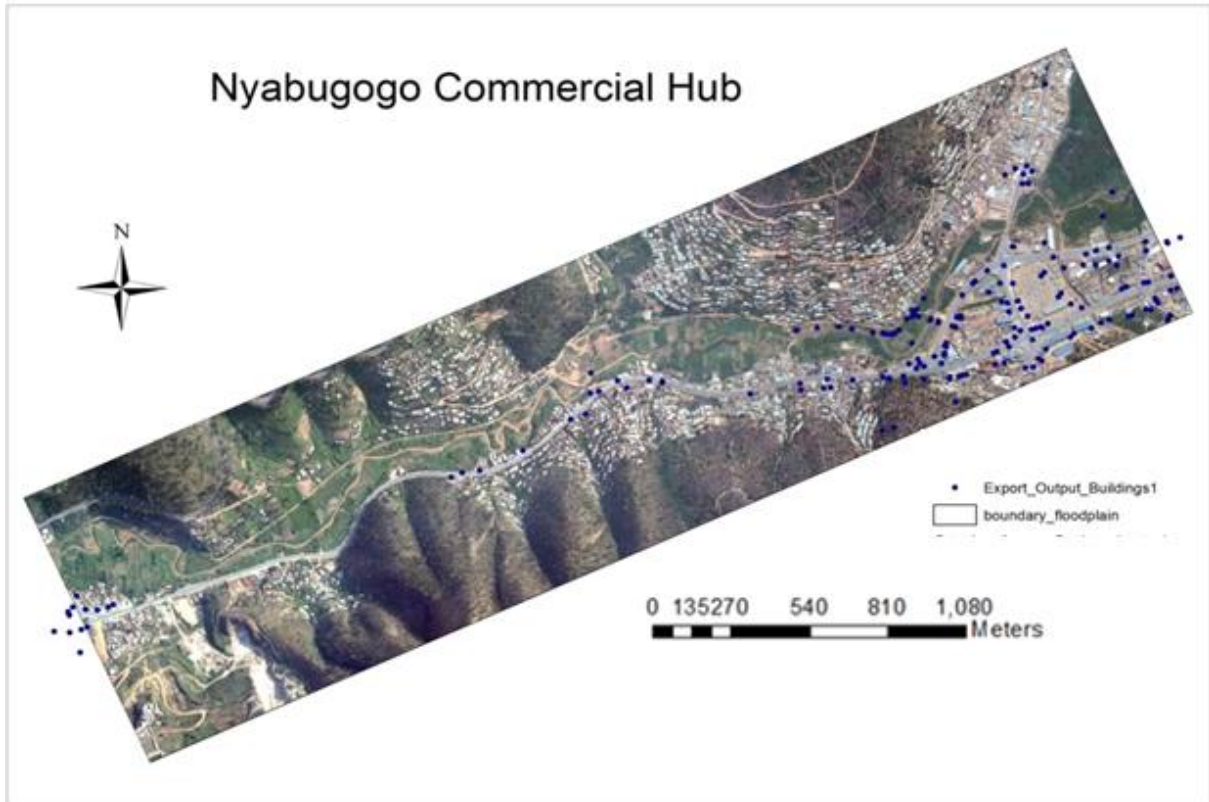
Figure 3.11: Map of the collected building footprint and height points in the study domain.

A total of more than hundred pairs of building footprint and height measurements were taken in the last two days of the fieldwork as shown in Figure 3.11, much of it being concentrated around the central bus park where the highest flood risk holds and some along the road where a large flood extent was observed from the simulation made by Manyifika (2015).

3.5.4. Ground Control Points (GCPs)

Around hundred Ground Control Points (GCPs) were collected with a hand held Garmin 52S GPS with maximum accuracy i.e. +/- 3m An attempt was made to distribute the GCPs in both flat (relatively flat) and hilly areas in the study domain as shown in Figure 3.12.. However, it was not possible to collect more points (especially on the high hills) due to inconveniency/inaccessibility and time constraint.
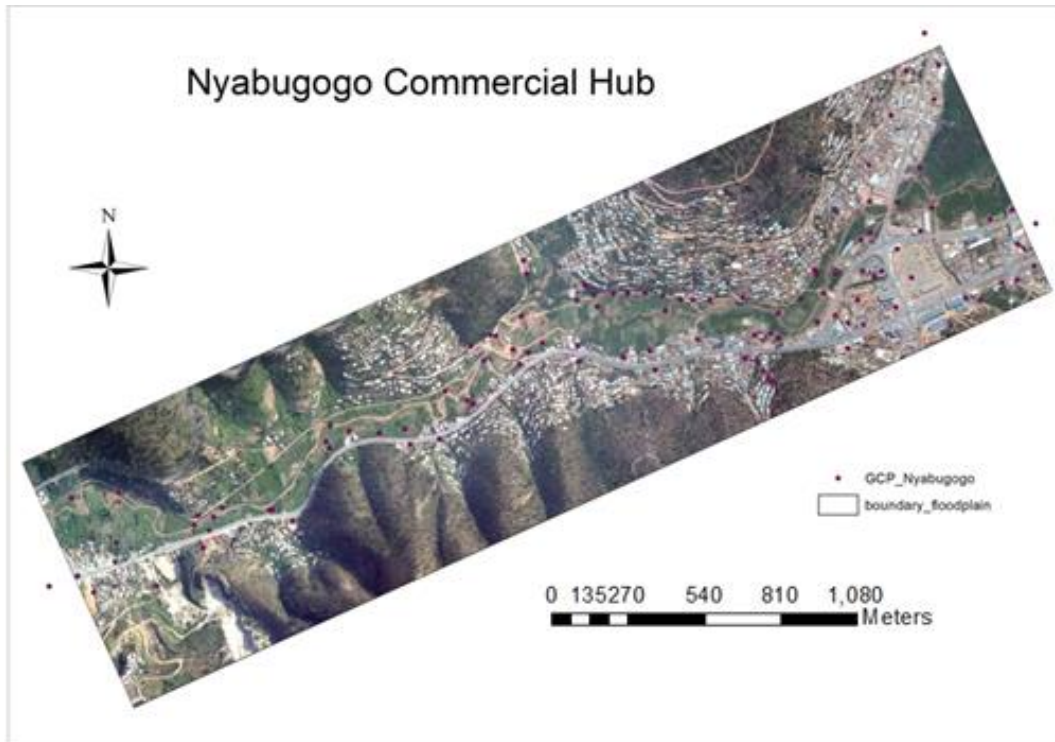
Figure 3.12: Map of the collected GCPs in the study domain.

The collection of these GCPs was made during all days of the fieldwork in parallel to other measurements. Figure 3.13 shows photos taken during the collection of GCPs in hilly and floodplain areas and building footprint and height measurements as well.

Figure 3.13: Sample photos of GCP collection and measurement of building footprints and height.

4. METHODOLOGY

4.1. General

The tasks carried out in this research are summarized in the flowchart below. The three major components are: (i) comparison of ASTER and SRTM DEM with local DEM and all the three DEMs with the ground control points (GCPs) collected from field work, (ii) generation of different resolution DTM from the local DEM and (iii) incorporation of major urban terrain features in the DEM from field survey and other data collected, i.e. buildings and major roads were added on to the DEM to generate a DTM of the study area. Finally the effect of the different DEM, resolution and urban terrain characterization were further analysed from the flood model outputs showing flood depth, extent and velocity simulated by the SOBEK 1D2D hydrodynamic model. Figure 4.1 summarizes the methodology.
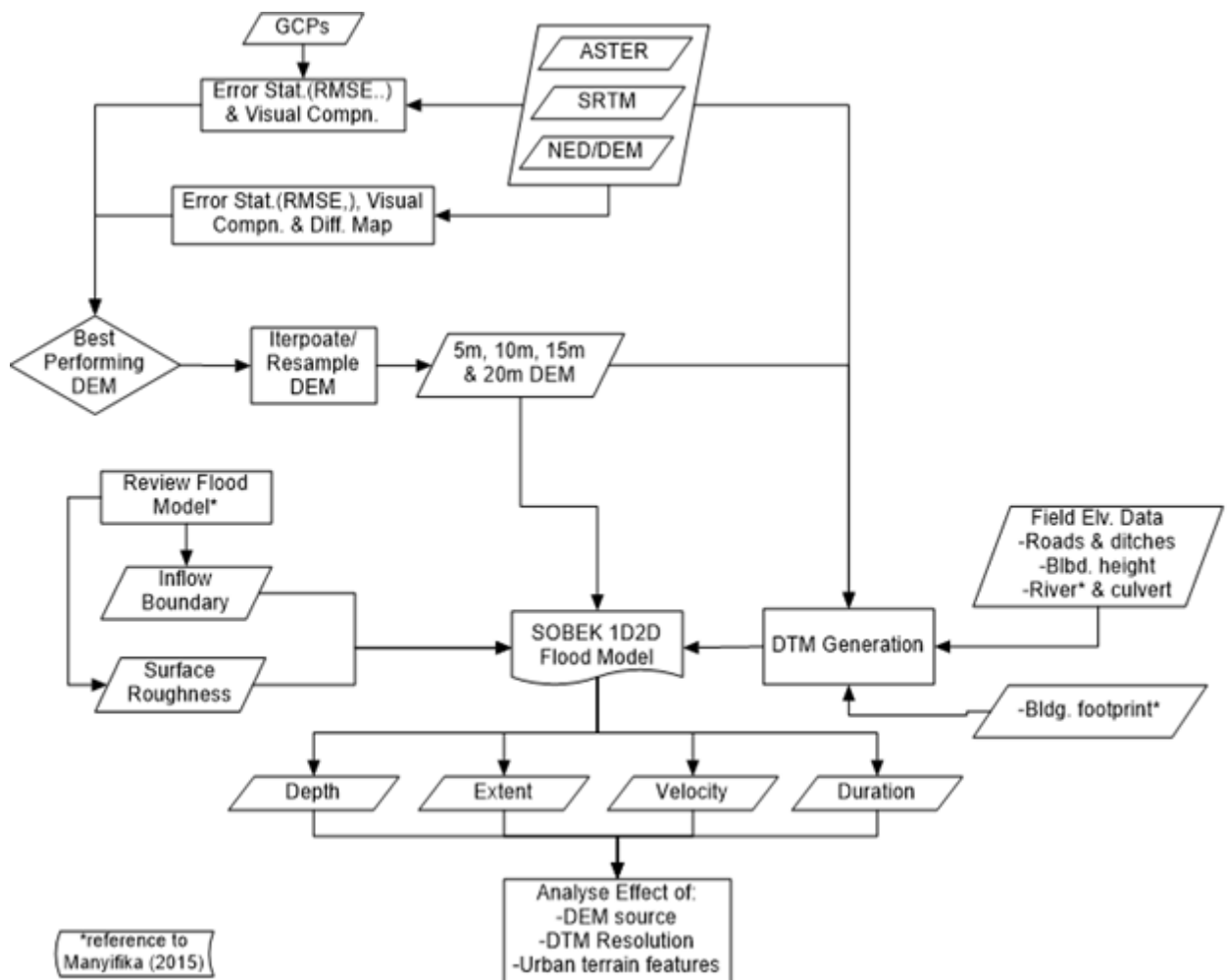
Figure 4.1: Flowchart of the methodology.

4.2. Digital Terrian Modelling

Topographic representation is one of, if not the most, fundamental inputs for hydrodynamic modelling of floods in urban environments. During events of flooding and inundation, overland flow commonly follows the natural topography with flow direction defined by the steepest descent, subject to obstacles like buildings, dykes and types of land cover with specific roughness. Elevation of terrain and surface structures that alter this flow and thereby govern the resulting inundation in urban environments are represented by a digital terrain model (DTM). Hence, an accurate DTM construction is at the core of reliable urban flood modelling. For this purpose, a detailed analysis of the available topographic dataset including the fieldwork data was carried out as summarized below.

4.2.1. Fieldwork data processing

The pre-processing of the collected road and building elevation dataset of the Nyabugogo commercial hub was performed in ArcGIS 10 environment and ILWIS 3.31 Academic version. Collected elevation point data was filtered to exclude redundant and erroneous measurements from further use. Locational (X,Y) and elevation (Z) offsets were then corrected in reference to the 2010 orthophoto (0.25m × 0.25m) and the associated 10m × 10m elevation grid dataset developed by the Rwanda National Land Use and Development Master Plan Project. The integration of surveyed ground control points, areal triangulation and bundle adjustment were used to ensure the quality of the orthophoto. Necessary corrections and quality checks were performed to ensure accuracy. The detail of the orthophoto generation is provided in (SWEDESURVEY, 2010) and associated documentation. The orthophoto and elevation grid were hence used as reference elevation dataset for pre-processing, DEM generation and accuracy assessment works and evaluation of the flood model simulations.

4.2.2. Interpolation of Point Data

Data collected from fieldwork were point elevation datasets measured at distinct locations along the road/river where significant change of system characteristics was observed. The reference elevation data was also a grid point dataset at 10m × 10m dimensions hence interpolation was required to obtain a consistent elevation representation throughout the study domain. In this study nearest neighbour (NN), inverse distance weighting (IDW), kriging and spline interpolations were tested. However, the application of interpolation techniques results in uncertainty of elevation values and hence several techniques were employed to select the appropriate method as explained below in section 4.2.3.

4.2.3. DEM Accuracy

Two approaches were followed to analyse the elevation surface representation resulting from the different interpolation techniques:

   i. The study domain is a small area containing an urban environment along with the floodplain of the Nyabugogo River and the confining hills on both sides of the river banks. An areal comparison was done via visual assessment of distinct terrain features and their representation in the DEMs by means of hill-shade views and difference mapping (Tighe and Chamberlain, 2009; Mukherjee et al., 2012; Frey and Paul, 2012).

   ii. Accuracy of the DEMs was tested by means of error statistics against the reference elevation point dataset. According to Van de Sande et al. (2012), Bourgine and Baghdadi (2005), Thomas et al. (2014) Mukherjee et al. (2012) and Guo et al. (2010), vertical accuracy of DEMs could be assessed by the following statistical measures:

a. **Root-Mean-Square-Error (RMSE)**: measures the vertical accuracy of DEMs with respect to a true/reference value. It represents the random and systematic errors arising from data generation processes such as applied interpolation and techniques by which data is inquired (for satellite based DEM) and reads:

$$RMSE = \sqrt{\frac{1}{n}\sum_{i=1}^{n}(DEM_i - REF_i)^2}$$

[4.1]

where REF stands for the reference elevations.

b. **Mean Error (ME)**: measures the spatial distribution of elevation errors of the DEMs from the reference values. A positive ME value indicates higher values in the DEMs while a negative ME value indicates lower values in the DEMs as compared to the true/reference elevations. ME reads:

$$ME = \frac{1}{n}\sum_{i=1}^{n} DEM_i - REF_i$$

[4.2]

where REF stands for the reference elevations.

c. **Standard Deviation (SD)**: measures the spread of differences indicating the variation in the magnitude of the elevation errors. It also gives insights as to how these errors are associated with height/elevation of the study area. It is given by:

$$SD = \sqrt{\frac{\sum\left((DEM_i - REF_i) - ME\right)^2}{n-1}}$$

[4.3]

where REF stands for the GCP elevations and ME stands for the mean error.

For the flood simulation DEMs with grid resolution of 5m, 10m, 15m and 20m were prepared. DEMs served for preparation of terrain models with roads, rivers and buildings added so to represent the main terrain characteristics that affect a flooding. The effect of resolution on topographic representation was analysed by the above described comparison techniques and other important topographic parameters such as slope and aspect (Grohmann, 2015; Vaze et al., 2010).

Moreover, the effect of DTM resolution was analysed in the SOBEK 1D2D hydrodynamic model for flood simulation. Analysis aimed at flood characteristics such as flood depth, flood extent and flood propagation velocity as further described in section 4.3. In addition, the different components of the model properties (such as boundary conditions and assumptions involved) were examined in an attempt to justify the changes on flood behaviour that resulted due to the changes of DTM resolution (Haile and Rientjes, 2005; Horritt and Bates, 2001; Jarihani et al., 2015).

4.2.4. Satellite Based DEM: ASTER and SRTM

ASTER and SRTM global elevation datasets of 30m resolution were compared with a 30m DEM generated by the 10m × 10m elevation grid and the accuracy of the satellite DEMs was also assessed. Similarly, the effectiveness of the freely available global satellite DEMs for urban flood modelling of the Nyabugogo commercial hub was tested by comparing the resulting flood characteristics to those generated by the local DEM.

4.2.5. Urban Terrain Model Preparation

A detailed digital terrain model of the Nyabugogo commercial hub is made up of the raster datasets of the base elevation surface-DEM, the building height, the road and the river elevation profiles. The building height values map was combined with the base DEM to raise the elevation of the pixels representing the building footprint. The road and river elevation profiles were developed and cleaned from artefacts to be merged with the building height layer, respectively, resulting in the DTM of the study domain.

The effect of urban terrain features in blocking, storing and conveying the surface flow of the flood waters was studied by applying the following techniques (Syme, 2008; Aktaruzzaman and Schmitt, 2009; Schubert and Sanders, 2012; Haile and Rientjes, 2005; Meesuk et al., 2015):

a. **Assigning surface roughness value**: surface roughness values (refer Table 4.1)were assigned to pixels representing the different urban terrain features from roughness values provided in the literature supplemented by field observation of the feature properties, and

b. **Raising elevation**: elevation values of such pixels were raised to the appropriate height of the terrain feature it represents such as buildings and roads as was measured in the field.

To account for their effect in altering the flood propagation in urban neighbourhood, these urban features (specifically buildings) were analysed as:

- Solid objects,
- Partially solid objects, and
- Hollow objects

with their corresponding roughness values after Haile and Rientjes (2005). The resulting flood characteristics of flood depth, flood extent and flood wave velocity by of SOBEK 1D2D simulations under these different scenario were further investigated to conclude on the effect of urban terrain feature characterization in flood modelling of the Nyabugogo commercial hub.

4.3. Flood Modelling

4.3.1. SOBEK 1D2D

As mentioned earlier, the WL/Delft-Hydraulics SOBEK 1D-2D is a typical distributed hydrodynamic flood model suitable to simulate an urban flood inundation making use of the full Saint-Venant (shallow water) flow equation (Haile, 2005). A 1D river network and 2D rectangular grids representing the floodplain topography comprise the spatial model domains to allow simulation of complex urban flood events including street flow, drainage flow and overland flow on paved surfaces. The 1D and 2D components are coupled for the conservation of mass and treated separately when momentum is analysed (Haile and Rientjes, 2005). DEM, model inflows and outflows (i.e. mathematical boundary conditions), surface roughness for river and floodplain, and channel cross section constitute the major inputs of SOBEK 1D2D hydrodynamic model. It can model the effect of hydraulic structures such as culverts, bridges, weirs etc. SOBEK has a user friendly environment that enables the import of GIS data and also the export of simulation results to basic GIS environments. Moreover, it provides network validation and model check wizards before running simulation that prevents system crash upon lengthy simulations (Delft/Hydraulics, 2014).

SOBEK 1D2D is an integrated raster based model. The 1D flow module simulates the channel flow whereas the floodplain topography is represented by the overland flow (2D) module. Integration of the

two modules is achieved by geometrically connecting the map coordinates of 1D channel network when overlaid and merged with the 2D floodplain representation (Haile & Rientjes, 2005). The Delft-scheme in SOBEK 1D2D models the hydrodynamic water flow by numerically solving the complete De Saint Venant flow equations. The spatial discretization follows a staggered grid where networks of reaches are connected at connection/linkage nodes and calculation points are assigned in between where the flow equations are numerically solved. Discharges and velocities are defined on reach segments while water levels and cross-sections are defined on calculation points and connection nodes as shown in Figure 4.2.
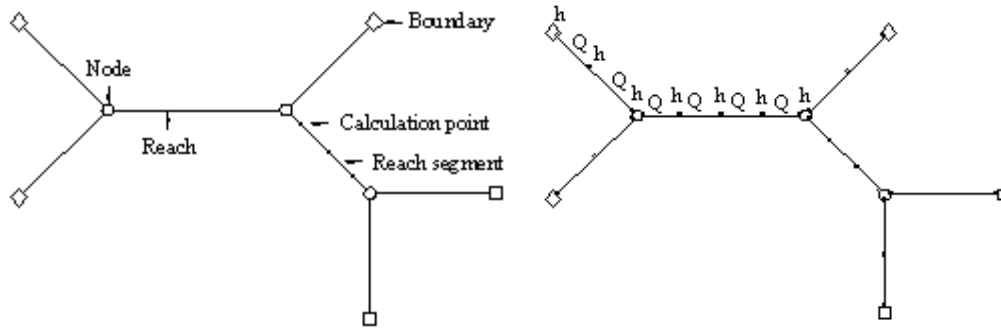
Figure 4.2: Representation of 1D Channel network (left) and Staggered grid (right)

4.3.2. Flow Equations

The flow equations of SOBEK 1D2D are described in Delft/Hydraulics (2014), the summary of which is presented below. Further descriptions on numeric aspects of the model are available at www.sobek.nl.

1D Flow equations

Channel flow is modeled by 1D Saint-Venant equation where two equations are solved:

Continuity Equation-1D

$$\frac{\partial A_f}{\partial t} + \frac{\partial Q}{\partial x} = q_{lat}$$

[4.4]

Momentum Equation-1D

$$\frac{\partial Q}{\partial t} + \frac{\partial}{\partial x}\left(\frac{Q^2}{A_f}\right) + gA_f\frac{\partial h}{\partial x} + \frac{gQ|Q|}{C^2RA_f} - w_f\frac{\tau_{wind}}{\rho_w} = 0$$

[4.5]

Where:

A_f	flow area [m²]
T	time [s]
Q	discharge [m³/s]
X	distance along the channel axis [m]
q_{lat}	lateral discharge per unit length [m²/s]
g	gravitational acceleration [m/s²]
h	water level [m]
C	Chézy's coefficient [m$^{1/2}$/s]
R	hydraulic radius [m]
w_f	water surface width [m]
τ_{wind}	wind shear stress [N/m²]
ρ_w	density of fresh water [kg/m²]

The first term in equation [4.5] above represents inertia, the second is a convection term, the third term describes water level gradient, the fourth term denotes bed friction while the influence of wind friction is given by the last term.

2D Flow Equations

Overland flow is modelled by the shallow water equation solved by three equations (non-linear):

Continuity Equation-2D:

$$\frac{\partial \zeta}{\partial t} + \frac{\partial(vh)}{\partial x} + \frac{\partial(vh)}{\partial y} = 0$$

[4.6]

Momentum Equations-2D:

In the x-direction:

$$\frac{\partial u}{\partial t} + u\frac{\partial u}{\partial x} + v\frac{\partial u}{\partial y} + g\frac{\partial \zeta}{\partial x} + g\frac{u|V|}{C^2 h} + au|u| = 0$$

[4.7]

In the y-direction:

$$\frac{\partial v}{\partial t} + u\frac{\partial v}{\partial x} + v\frac{\partial v}{\partial y} + g\frac{\partial \zeta}{\partial y} + g\frac{v|V|}{C^2 h} + av|v| = 0$$

[4.8]

Where,

ζ	Water level above the plane of reference [m]
u	velocity in the x-direction [m/s]
v	velocity in the y-direction [m/s]
V	velocity, V=SQRT(u²+v²) [m/s]
h	total water depth, ζ+d [m]
d	depth below plane of reference [m]
a	wall friction coefficient [1/m]

The terms above in equation [4.7] and [4.8] represent local acceleration, horizontal pressure gradient, convection, bottom friction and wall friction. In order to save computational cost, turbulent stress terms of sub-grid momentum transfer among grid cells are not included in the above terms pertaining to their limited importance in flood flow. On the other hand, the additional resistance created by vertical obstacles such as buildings is accounted by the wall friction term. However, this was not considered in the study as it requires an intensive data including detailed geometry of buildings and wall roughness properties.

In SOBEK 1D2D the continuity and momentum equations ensure the conservation of mass and momentum respectively. SOBEK handles large networks and/or long time series by a means of a minimum degree algorithm that runs an iterative simulation. Momentum balance is solved in SOBEK by a means of a fractional time step. Discharge and volumes of the previous time step define the estimation of time step where, for instance, a smaller time step which result in a longer simulation period is set when large discharges are withdrawn from locations of little storage. Such incidents occur when calculation points are placed at close distances. On the other hand, large distances despite misrepresentation of the natural flow process are prone to inaccuracy of simulation results. SOBEK temporarily adjusts time steps to insure numerical stability.

4.3.3.   1D2D Integration

Coupling of the 1D channel network with the 2D grid in SOBEK 1D2D is made through the connection between the calculation points and/or connection nodes with the corresponding 2D grid cell, where only one connection is allowed. The 1D2D connections are determined by the computational code based on the map coordinates of the calculation/connection nodes and the cell centres of the underlying 2D grid, expressed mathematically as follows:

$$if\,(|X1 - X2| \leq DX/2)\ and\ (|Y1 - Y2| \leq DY/2)$$

[4.9]

Where,

X1, Y1	x and y map coordinates of 1D point respectively
X2, Y2	x and y map coordinates of 2D grid cell centre respectively
DX	width of grid cell in x-direction
DY	width of grid cell in y-direction (NB: DX=DY for a square grid)

Then it is assumed that the 1D point (calculation point/connection node) is completely inside the 2D grid cell.
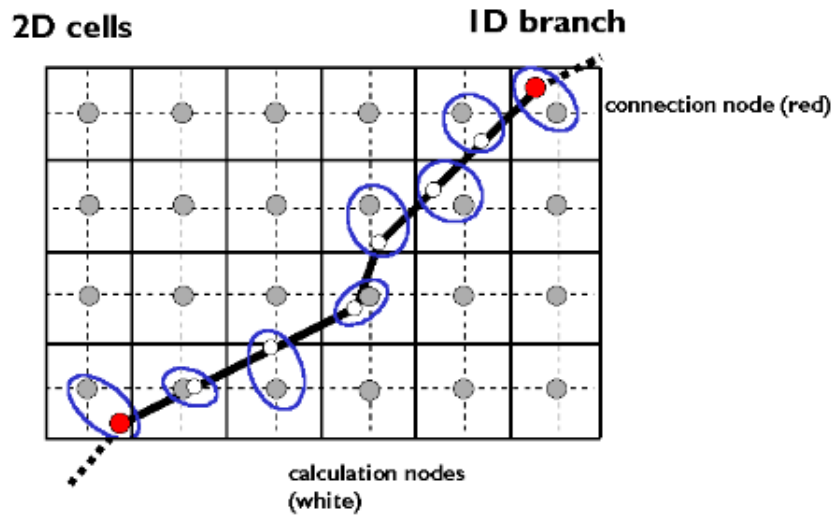
Figure 4.3: Connection between 1D network and 2D grid

Once the above criteria is met, the 1D2D coupling is established by internally moving the center of the 1D node towards the center of the 2D grid cell without altering the reach characteristics as shown in Figure 4.3. SOBEK then considers the 2D grid cell as part of the 1D calculation node/connection point thereby any flow above the 2D grid level is treated as 2D flow covering the area of the grid cell, if not flow will remain as 1D flow.

4.4.   Model Schematization

A GIS-based network and grid are used to represent the system to be modelled in SOBEK's interactive graphical platform called NETTER. It is a network editor that allows the setup of 1D channel network over a background GIS map and the import and manoeuvre of the overlaying 2D grid. It also contains advanced analysis tools to view the model simulation results. SOBEK-Rural 1D Flow module was used to model the river flow and later coupled with SOBEK Overland Flow (2D) module. Several functionalities of NETTER were used to schematize the 1D channel network of the study domain which comprises of a series of reaches connected to each other by connection and linkage nodes with a number of calculation

points placed in between. The three upstream boundary conditions and the downstream flow were defined by means of 1 and 2D boundary nodes while culvert and bridge nodes were used to define the hydraulic structures existing in the domain. Figure 4.4 shows a 1D2D schematization of the study area,
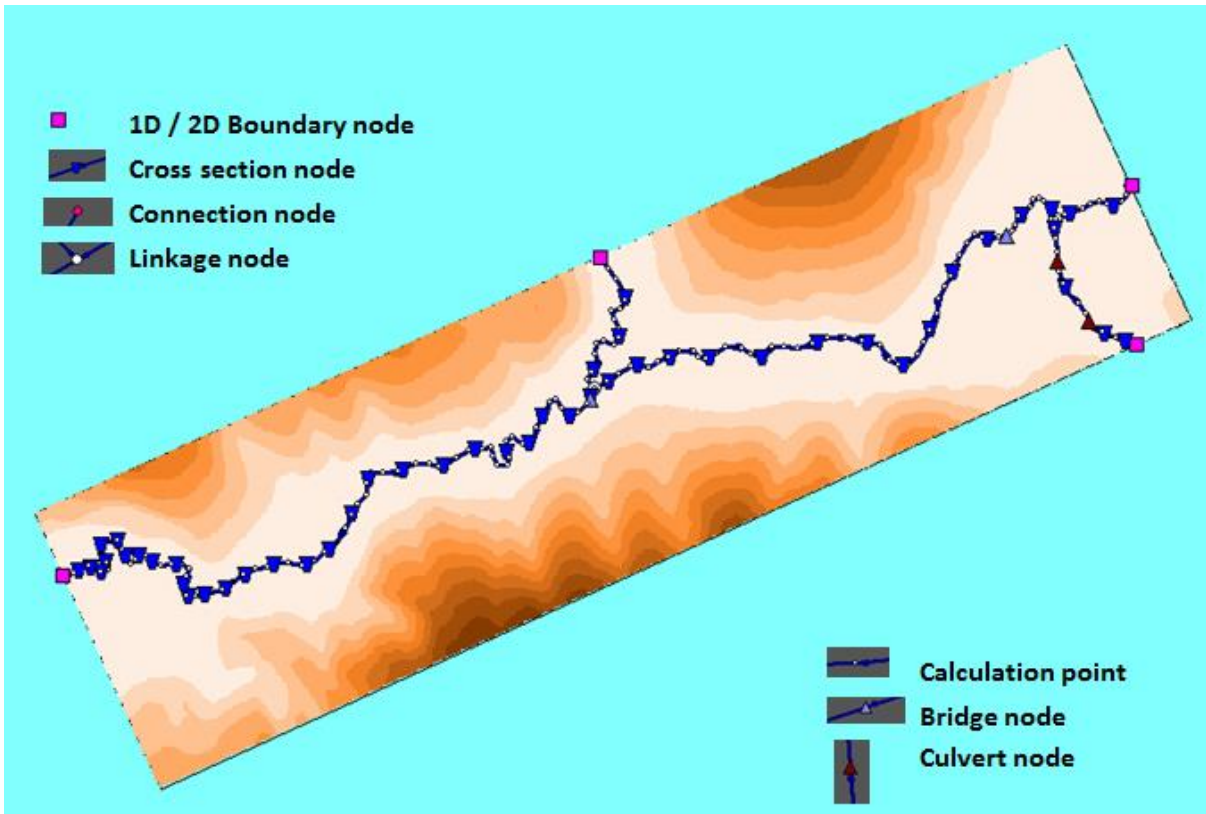
Figure 4.4: SOBEK 1D2D schematization of Nyabugogo commercial hub flood model.

The background GIS map was imported as an ArcInfo shapefile from ArcMap, also the 2D elevation grid and distributed roughness values were imported in ASCII file format. Moreover, a trapezoidal river channel profile was defined at several key locations including the channel bottom and top width, side slope, bed friction, bottom and surface levels. History stations were also set to record the simulation results of every time step at important locations such as the Nyabugogo central bus/taxi area. (NB: River channel data was collected by Manyifica (2015)).

A 1D schematization was first completed and simulation was tested before the 2D mode was activated. The model simulation results in an inundation of a 2D grid cell whenever the calculated water level at each calculation point and/or connection/linkage node is above the embankment level of the cross section (i.e. surface level). The resulting storage on the 2D grid empties back to the node/reach when the level drops. The results of the simulation are presented in *maps* with animated flow of every time step, *charts* reporting flow properties at all nodes, reaches and structures for every time step and *tables* that summarize the simulation history. A side view functionality of NETTER allows for a longitudinal animation of the flow in the channel. Results were exported as ASCII files for further analysis in a GIS environment. Figure 4.5 shows the NETTER interface.
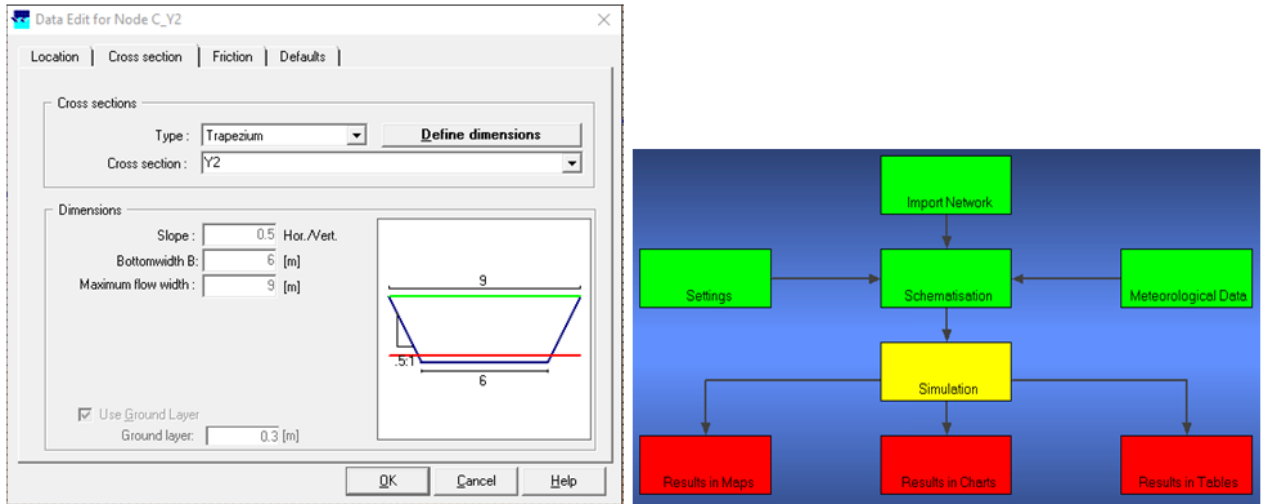
Figure 4.5: Channel cross section definition wizard in NETTER (left), SOBEK user interface (right).

4.5.   Model Calibration and Sensitivity

Model calibration, often termed as 'model fine-tuning', is the process of optimizing model parameters with the objective to match observed measurements of the real world process being modelled. Parameter values, model structure and boundary conditions amount for the major sources of uncertainty of model (Rientjes, 2014). In this study surface roughness was the only possible model parameter to be optimized as the other model inputs such as cross section, slope and profile were defined after field measurement. However, there were no actual flood measurements of whatsoever collected during the inundation of the peak rainfall under analysis. Although Manyifika (2015) has collected few flood depth measurements by interviewing locals and measuring available flood marks, they were not considered as true values since they were results of mere speculation of local people and does not relate to the event under consideration. Only to obtain some insight of the flooding in the Nyabugogo commercial hub, an attempt was made to calibrate the model with these flood depth value.

Surface roughness given by the Manning's coefficient (n_m) was applied in this study. SOBEK computes the actual Chézy's coefficient from the Manning coefficient by:

$$C = \frac{R^{\frac{1}{n}}}{n_m}$$

[4.10]

Where,

C	Chézy's coefficient [$m^{1/2}/s$]
R	Hydraulic radius [m]
n_m	Manning's roughness coefficient [$s/m^{1/3}$]

The six land cover classes used in (Manyifika, 2015) were adopted (shown in Table 4.1) as the major focus of this study is the highly urbanized Nyabugogo central bus/taxi park area where the land surface is mostly lined thereby requiring insignificant need for a detailed land cover classification. Shapefiles with the corresponding roughness values assigned were made for classifications with the three building treatment types after spatial analysis operations in ArcMap. These shapefiles (given in Figure 4.6) were then converted to raster of different resolution as required by the model and exported as ASCII files to SOBEK

Table 4.1: Manning's roughness coefficient after Tennakoon (2004).

Class	Land cover		Manning's Roughness Coefficient, n [s/m^{-3}]
1	River		0.03
2	Roads		0.025
3	Residential area		0.035
4	Commercial area		0.032
5	Green area		0.04
6	Buildings	Solid	1
		Partially solid	0.7
		Hollow	0.033
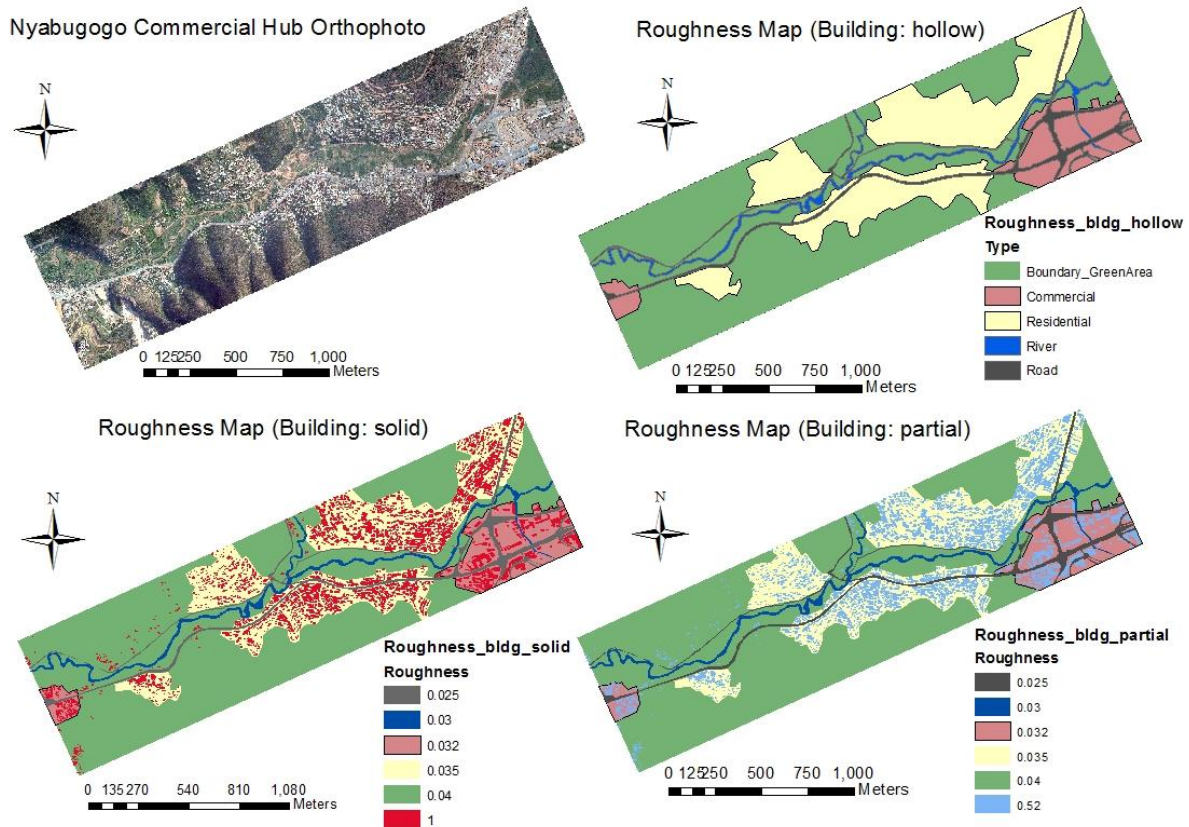
Figure 4.6: Manning's roughness coefficient maps for the different building treatments

Quantification of the uncertainty of a calibrated model is achieved by a sensitivity analysis where the model is parameterized and stressed differently (Rientjes, 2014). As such sensitivity of the model for both the upstream and downstream boundary conditions was tested. Moreover, the different resolutions applied were evaluated to determine the effect of model resolution on the resulting flood characteristics.

Finally, to draw conclusions, the SOBEK 1D2D flood model outputs for the different simulations were visually and statistically analysed both in the SOBEK and ArcGIS environment upon exporting as ASCII file format. However, validation of the simulation results was not possible as there was no measured or satellite observed flood data of the study domain.

5.   RESULT AND DISCUSSION

5.1.   DTM Processing

5.1.1.   Fieldwork Data Analysis

After a general pre-processing of the elevation shapefiles in ArcGIS (transformation, projection etc.), analysis started with a general overview and assessment of the collected point elevation measurements. This was done with respect to the 2010 Orthophoto and its associated 10m × 10m elevation grid. It was observed that much of the collected points were closely aligned to the locations of the terrain features they represent, i.e. roads, ditches and buildings. The observed systematic shifts (either in the horizontal or the vertical) of small extent were not identical throughout the study area pertaining to the human induced errors of measurement which mostly occurred during the shift of total station points for reasons of visibility. Erroneous and redundant data were left out resulting in 769 road, ditch and culvert point elevations and 110 pairs of building footprint and height points.

These (X, Y, Z) measurements were then compared to their location on the orthophoto and the corresponding elevation grid for the application of appropriate correction. The elevation measurements were kept intact given the vertical accuracy (in millimetres) of the total station used. However, a comparison of these elevation measurements with the elevation grid of the orthophoto revealed a systematic difference pertaining to the ellipsoidal height measurement collected by the total station. Hence to convert the ellipsoidal height to orthometric height a geoid correction was required to all point measurements so as to maintain a similar reference system to that of the elevation grid. To obtain an optimum geoid correction a detailed investigation of the correspondence between the two elevation datasets was carried out resulting in:

- Only a single pair of points was found to fall within the same 0.25m × 0.25m pixel (original resolution of orthophoto) having a difference of 27.8m,
- Twenty two pairs of points fall within 1m distance from each other resulting in a mean difference of 27.81m,
- Nearly all (739 pts.) road points fall within 10m distance from the elevation grid resulting in an average of 26.66m difference. Though the figure was indicative of a rough estimate of the elevation difference, it was not used for the final selection of the required correction for the reason that the 10m buffer, actually the resolution of the 10m × 10m elevation grid, potentially includes many points regardless of a possibly large elevation variation, which was the case on the hillsides of the study domain,
- Twenty two pairs of points carefully selected at or near known total station point (serving as conventional benchmarks) resulted a mean difference of 28.29m, and
- A random selection of a group of points at the different locations of the domain (81 pair points) along the road resulted in a mean difference of 27.6m where nearly 57% of the difference being above the mean.

From the above results a **28m** geoid correction was selected attributing to the fact that the mean of pair of points within 1m distance from each other and the total station points would give a rather realistic estimate of the elevation difference. Also there is a limited elevation variation within 1m buffer and the known total station points were stationed at convenient and relatively flat surfaces, respectively, making it

convenient for correlation with the elevation grid. Then this correction was applied on all road points, however the building points were left out since only the height difference between the footprint and building height measurement was needed for the DTM construction.

The minor locational shifts on the road and their associated roadside ditch measurements collected in and around the floodplain of the Nyabugogo river were then compared with the 10m × 10m elevation grid points using known matching locations. These were then corrected by applying the resulting offsets to all remaining measurements in the different zones of the study domain, where the observed offsets vary. A 2.8m wide buffer was setup for the small riverside roads following the field inspection of road width. The SOBEK modelling environment dictates the use of raster cells (the minimum pixel size being 5m × 5m in the case of this study) which undermines the significance of incorporating the exact cross-sections (mostly trapezoid as observed in the field) of the roadside ditches. Hence, to account for the effect of roadside ditches in conveying discharge of flood waters, it was made certain that all these ditch points along with their corresponding bottom width were included in the digitizing of the roads polygon shapefile.

In the case of the Mpazi drainage canal and its two major culverts, hereafter referred to as culvert measurement, however, a strange deviation of the collected points was observed. It tends to increase on the points further away from the onset of the total station points fixed at the beginning of culvert (in the domain) using the Garmin 52S GPS. The accuracy of the handheld GPS used (± 3m) and inevitable human and instrument error in the setting and initial measurement of the total station locations could have possibly amounted to such observed difference as compared to orthophoto. Location corrections applied based on deviations of the five total station points within the culvert from the 10m × 10m elevation grid have failed to generate the proper orientation of the culvert further indicating an instrument error at the beginning of the culvert measurement. However, a manual rotation and a slight shift supported by field knowledge of the researcher proved to produce a favourable result as the five total station points, and accordingly all the remaining points, were properly positioned in alignment with the reference, the orthophoto. These points together with the river bottom measurements collected by Manyifika (2015) were then similarly digitized to generate the river polygon shapefile.

Finally, the building footprints digitized from the orthophoto by Manyifika (2015) were corrected according to field observation to incorporate the changes which took place during the period of five years since the production of the orthophoto and measured building heights were manually assigned in the attribute table after a similar location correction was applied. Field knowledge, captured photographs and small movie shoots were coupled with the orthophoto and GoogleEarth to identify and confirm the measured building height. A minimum building height of 3.2m was assigned for the domain after the sample one story building heights measured in the field representing conventional residential and small business buildings. Moreover, a local adoption of building height values was applied to buildings inaccessible for height measurement during the field campaign. Figure 5.1 gives the final road and river points and building shapefiles prepared.
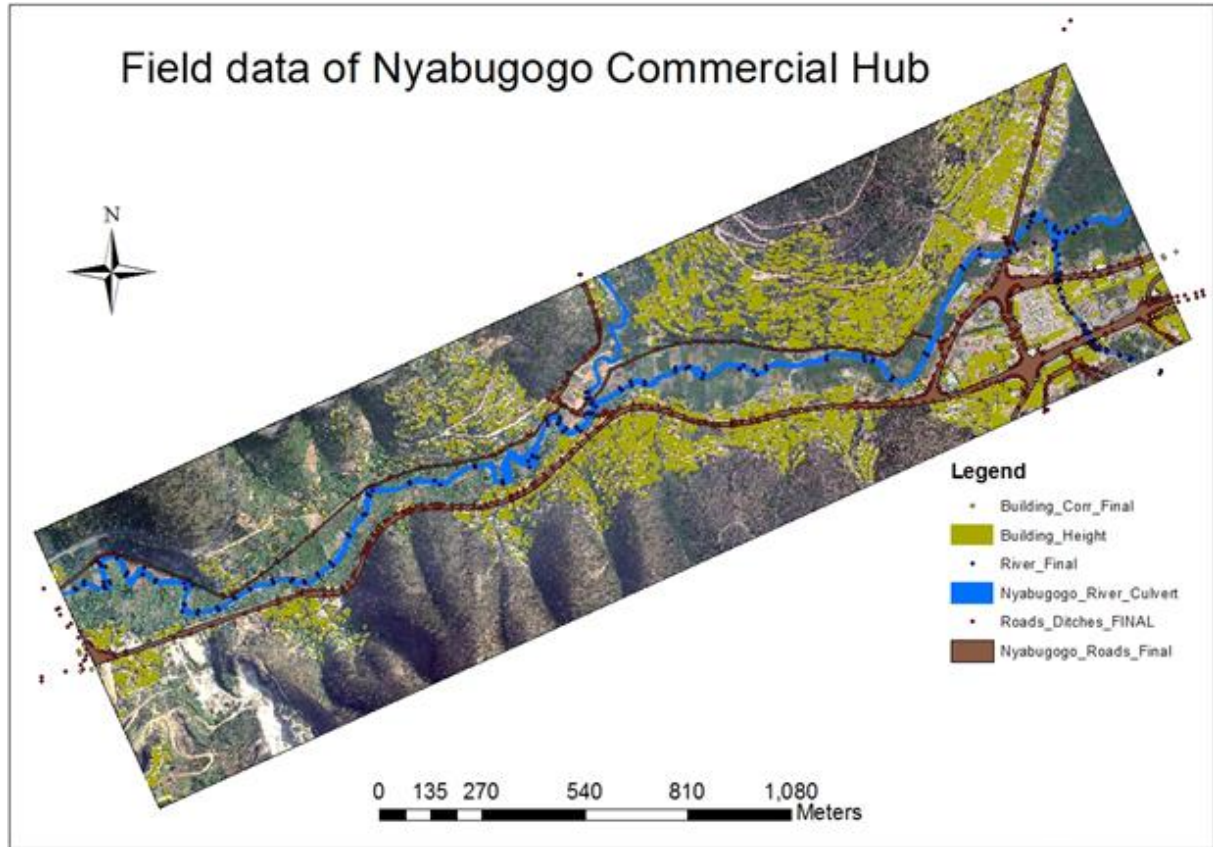
Figure 5.1: Corrected roads and ditches, river and building height data of the study domain.

5.1.2.   Selection of Interpolation

The effect of the different interpolation techniques (inverse distance weighting-IDW, Kriging, Spline and nearest neighbor-NN) was investigated using the 10m × 10m elevation grid points at 5m resolution as this resolution would, presumably, better capture topographic variability of the study domain in comparison to the other coarse resolutions applied in the study (large pixel sizes, here 10m, 15m and 20m resp.). Three techniques were applied for the analysis, namely visual inspection using hillshade maps, difference mapping of the interpolated elevation surface and statistical comparison using separate control points. Apart from minor differences such as smoothing effects on steep hillsides, the four hillshade maps Figure 5.2 shown below depict no significant elevation variation especially in the floodplain area and the relatively flat central taxi station area where frequent flooding occurs.
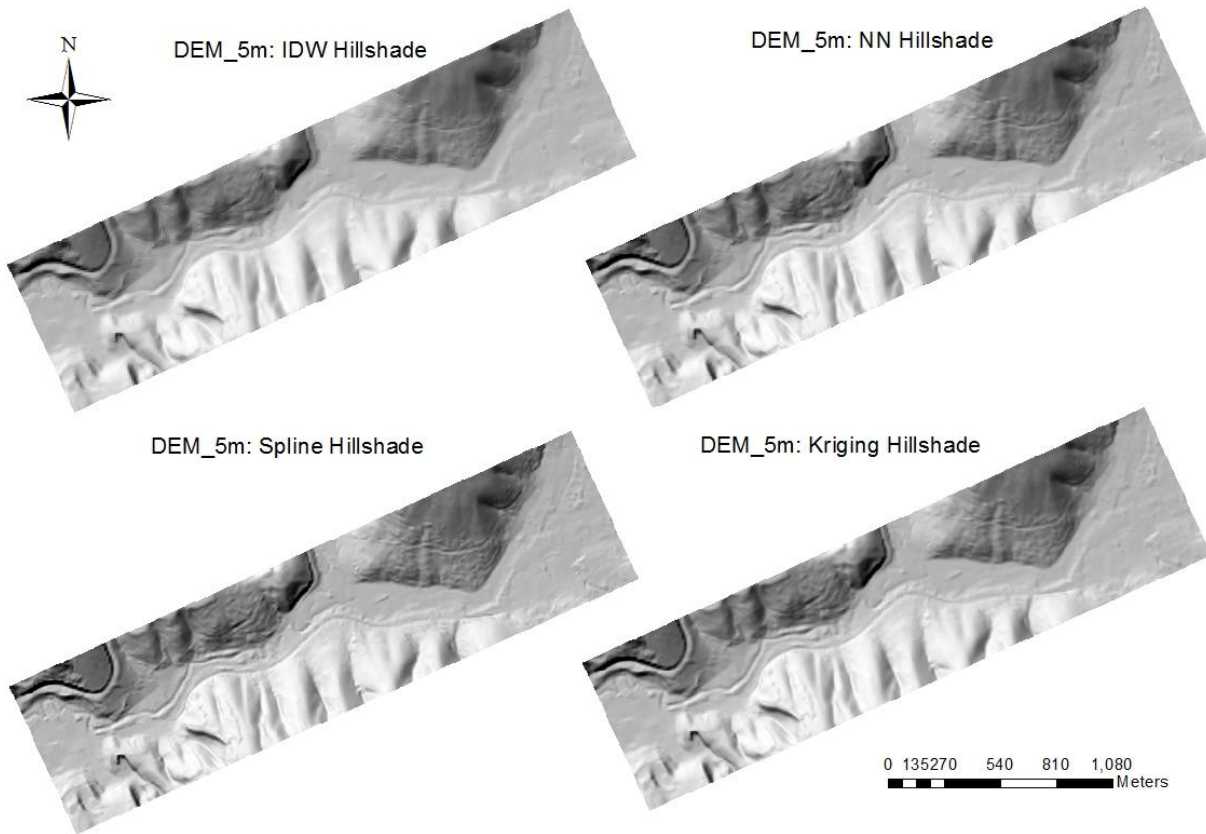
Figure 5.2: Hillshade maps of the different interpolations applied for the 5m grid DEM.

Spatial differencing of the interpolated elevation surfaces conducted in ILWIS Figure 5.3 (shown below) indicates a similar phenomenon whereby the difference in elevation of the three raster layers as compared to the IDW layer was found to be in sub-meter range for most of the study domain, the floodplain exhibiting the smaller differences. Moreover, such minor elevation difference among the interpolated surfaces was also indicated by statistical comparison with control points at random points spread majorly in the floodplain. 108 GPS points were used for the purpose and the summary is given in the Table 5.1 below. The close figures of the four interpolation techniques in the mean error, STD and RMSE suggest a similar performance; marginally IDW performs better. (NB: The generally high value of the elevation difference between the interpolated surfaces and the control points was a result of the reduced accuracy of the handheld GPS on some measurements, refer section 5.2.1).

Table 5.1: Statistical comparison of the different interpolations applied

DEM Resolution	Min Error	Max Error	Mean Error	STD	RMSE
IDW	-53.2	47.9	-2.67	-3.98	14.89
NN	-53.4	47.7	-2.77	-4.09	14.94
SPLINE	-53.7	47.5	-2.84	-4.18	14.98
KRIGING	-53.4	47.6	-2.80	-4.13	14.95
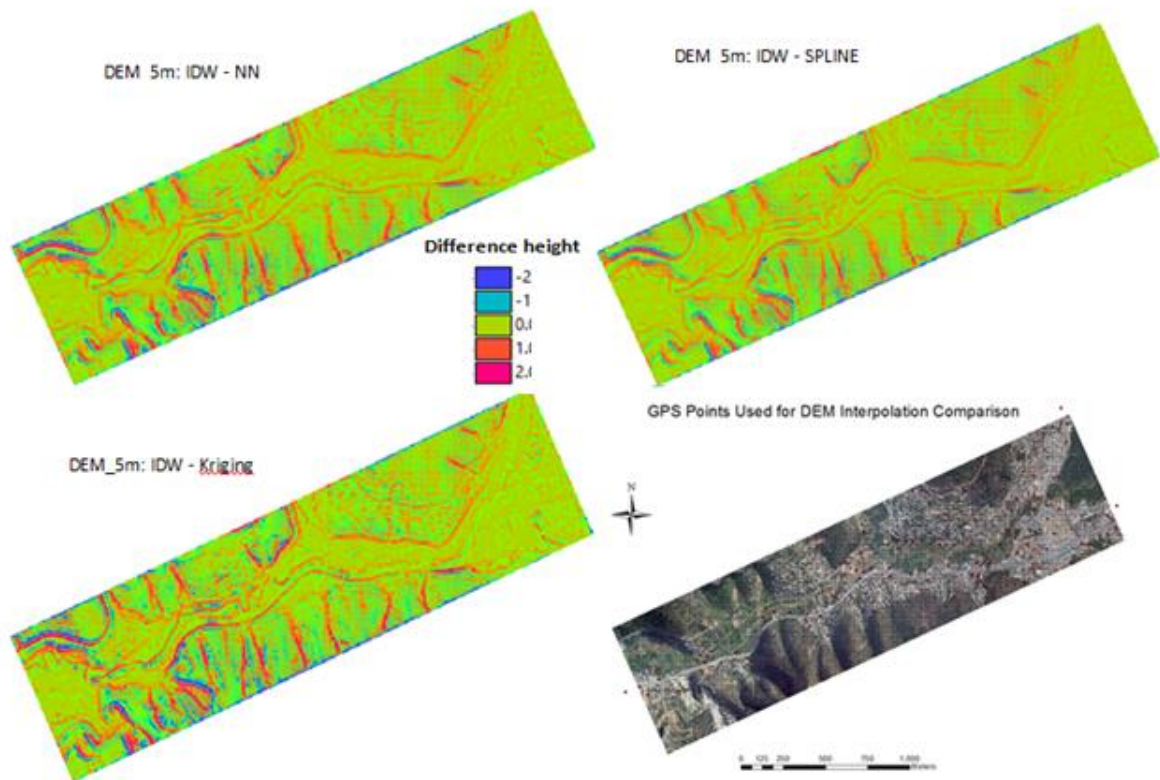
Figure 5.3: ILWIS Difference maps of the interpolated DEM and GPS points used for statistical comparison of the different interpolations applied.

From the above analysis, it was evident that no significant difference was observed among the different interpolation techniques applied in the study domain in terms of representing the topography especially in the relatively flat floodplain. Hence, as the 10m × 10m elevation grid, the road and river (culvert included) elevation points collected were sufficient to capture the surface variation of the study domain topography for the targeted flood simulation, the IDW technique with power of two was selected and interpolation was done at 5m, 10m, 15m and 20m resolutions for the road surface points, river bottom points and the 10m × 10m elevation grid which was used to obtain the base terrain elevation (DEM) of the study domain. The effect on the interpolation results from the use of power other than two requires further investigation.

5.1.3. Terrain Representation

Extraction operations on the resulting interpolated raster elevation values of roads and rivers resulted in interrupted and unconnected cells on all the different resolutions, except that of the 5m, which might affect the (continuous) flow of water later in the model domain. This was caused when the digitized road and/or river polygon misses the cell centre of the overlapping raster pixel, the effect being pronounced at larger cell sizes (> 10m). Moreover, overlay operations of the different elevation layers were not successful due to the limited functionality of ArcGIS in raster processing. Alternatively, all the raster layers were exported from ArcGIS as 'TIFF' file to be imported in ILWIS 3.3 Academic version (via GDAL). Unfortunately, ILWIS was also not successful in extracting connected cells for all the resolutions of the road and river layers. Hence, the road and river polygons were converted to lines (Polygon to Line tool of Data Management) and used for the extraction in ArcGIS environment resulting in connected boundary cells which overlap with the line feature (Road Extraction Layer in Figure 5.4). These layers were then exported to ILWIS and merged with new raster layers created to fill-up the missing pixels (Road Fill layer

in Figure 5.4 inside of the river and road boundaries pixels, whenever found left out by the extraction, which were too many for the coarse resolution layers. ILWIS 'Map Calculation' functionality was used to extract the final road and river elevation raster layers from the interpolated surface of the different resolutions.
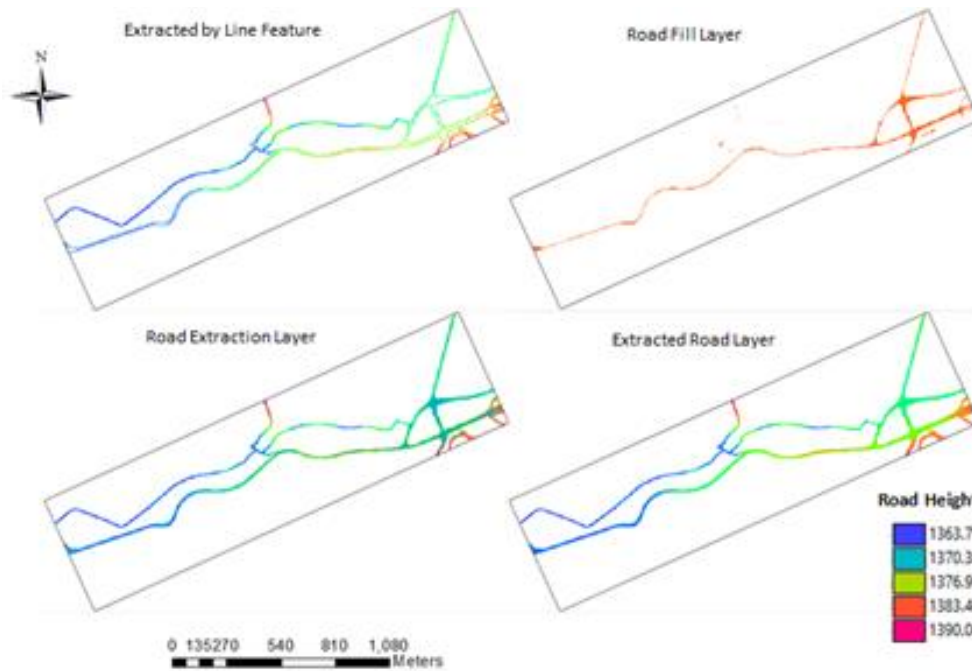
Figure 5.4: A sample 5m resolution road layer extraction procedure.

The road and river layers produced from the above operation, however, had some artefacts on the 10m, 15m and 20m resolutions resulting from connection of adjacent cells at parallel roads and meandering sections of the river. It was important to remove such connections as they do not exist in reality but also if not corrected they will overwrite other topographic surface definitions such as buildings located between the two parallel roads to the right of the Nyabugogo taxi park and create additional connections on the river incurring unwanted consequences on the flood simulation. As it is shown in the Figure 5.5 below, the 10m river layer for instance, an artificial island of one pixel was created as a result of the wrongly connected adjacent cells above this pixel. Hence, all such artefacts were carefully corrected by manually removing as small number of pixels as possible in order to reduce intervention on the dataset. Moreover, wherever ambiguous the removed pixels were the ones having less area overlapping with the river polygon and selection was made to maintain the natural meander of the river as much as possible. The summary of the removed pixels is given in the Table 5.2 below:

Table 5.2: Removed artefacts (pixels) from final road and river raster layers.

Elevation Layer	5m	10m	15m	20m
Road	-	-	2 pixels	4 pixels
River	-	3 pixels	3 pixels	4 pixels
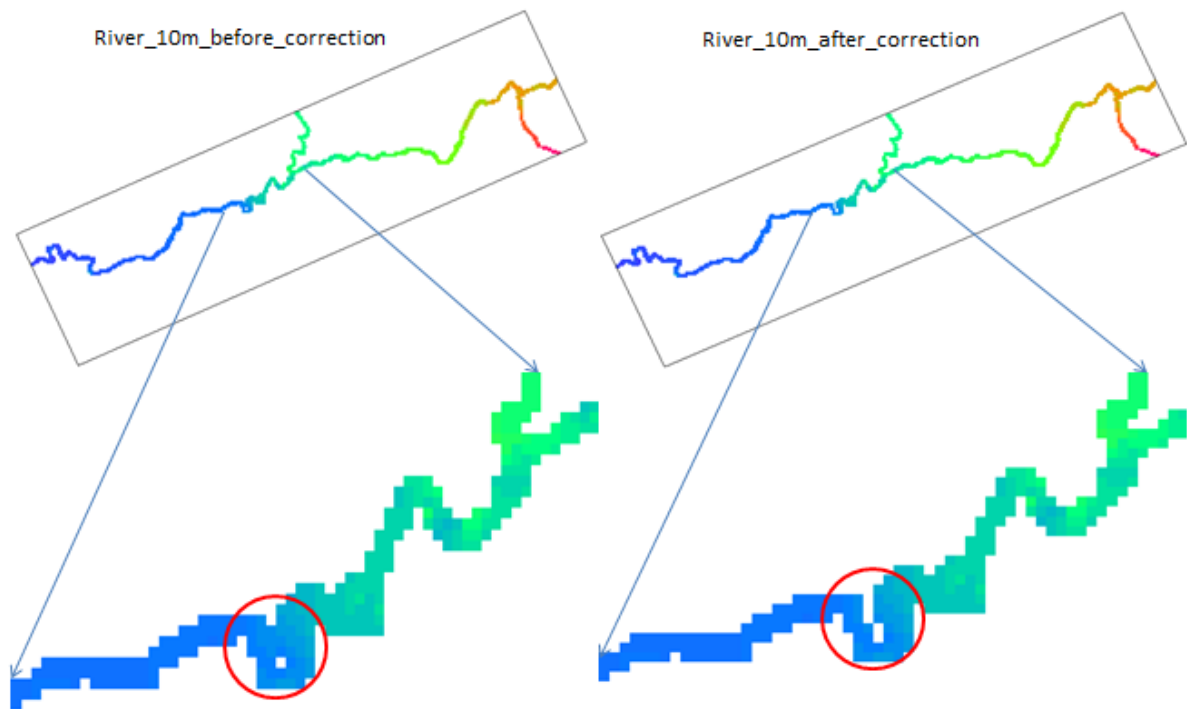
Figure 5.5: A sample 10m resolution river layer before and after manual removal of artefacts.

The building height raster layer of each resolution was generated upon the rasterization of an *attribute map* of the building height shapefile in ILWIS. Once all the input elevation raster layers were prepared for each resolution, the construction of the DTM for flood inundation simulation was possible. However, precaution was taken to avoid overwriting of elevation values at overlapping pixels of the road, river and building layers. This phenomenon was common in the large cell sizes, indicative of inadequacies of such resolutions in representing the natural topography and the associated terrain features possibly having significant consequences for the model flood propagation. As the building height layer only contains height of buildings measured above the terrain surface it was added first on to the bare surface elevation (DEM) thereby raising the elevation values of those pixels containing a building height value while the elevation of all the other cells remains intact. All the major and small roads of the study domain were situated at relatively higher elevations while the Nyabugogo River discharges the upstream flow following the steepest descent along the lowest depressions of the topography. Hence the road layer was then used to replace the elevation values of only the overlapping pixels from the resulting elevation raster layer of the above operation. Subsequently, a similar replacement of elevation values of the pixels from the river layer resulted in the generation of the final detailed DTM for all the 5m, 10m, 15m and 20m resolutions Figure 5.6 below shows a colour shaded relief of the DTM at 20m and 5m resolutions.
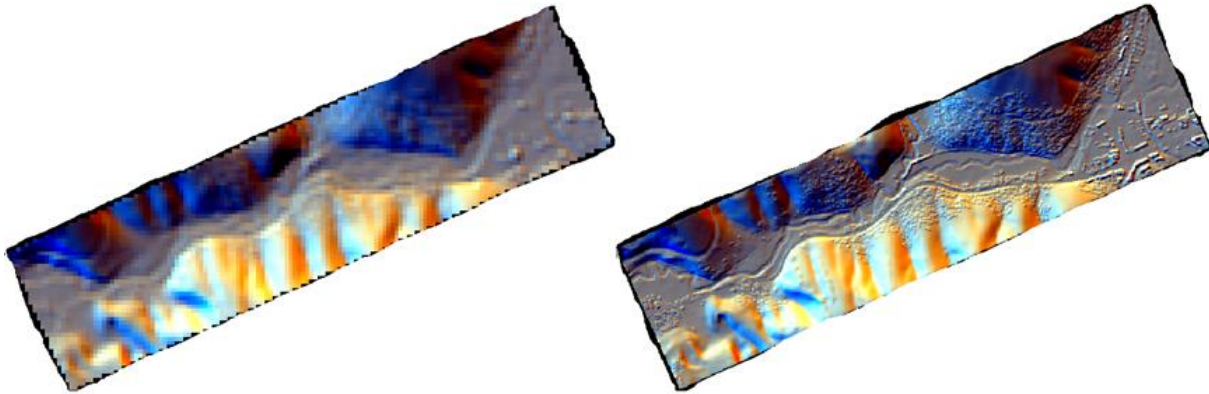
Figure 5.6: Colour-shade of final DTM for 20m (right) and 5m (lest) resolutions

The overall procedure of DTM construction is summarized in the flowchart given in Figure 5.7 below.
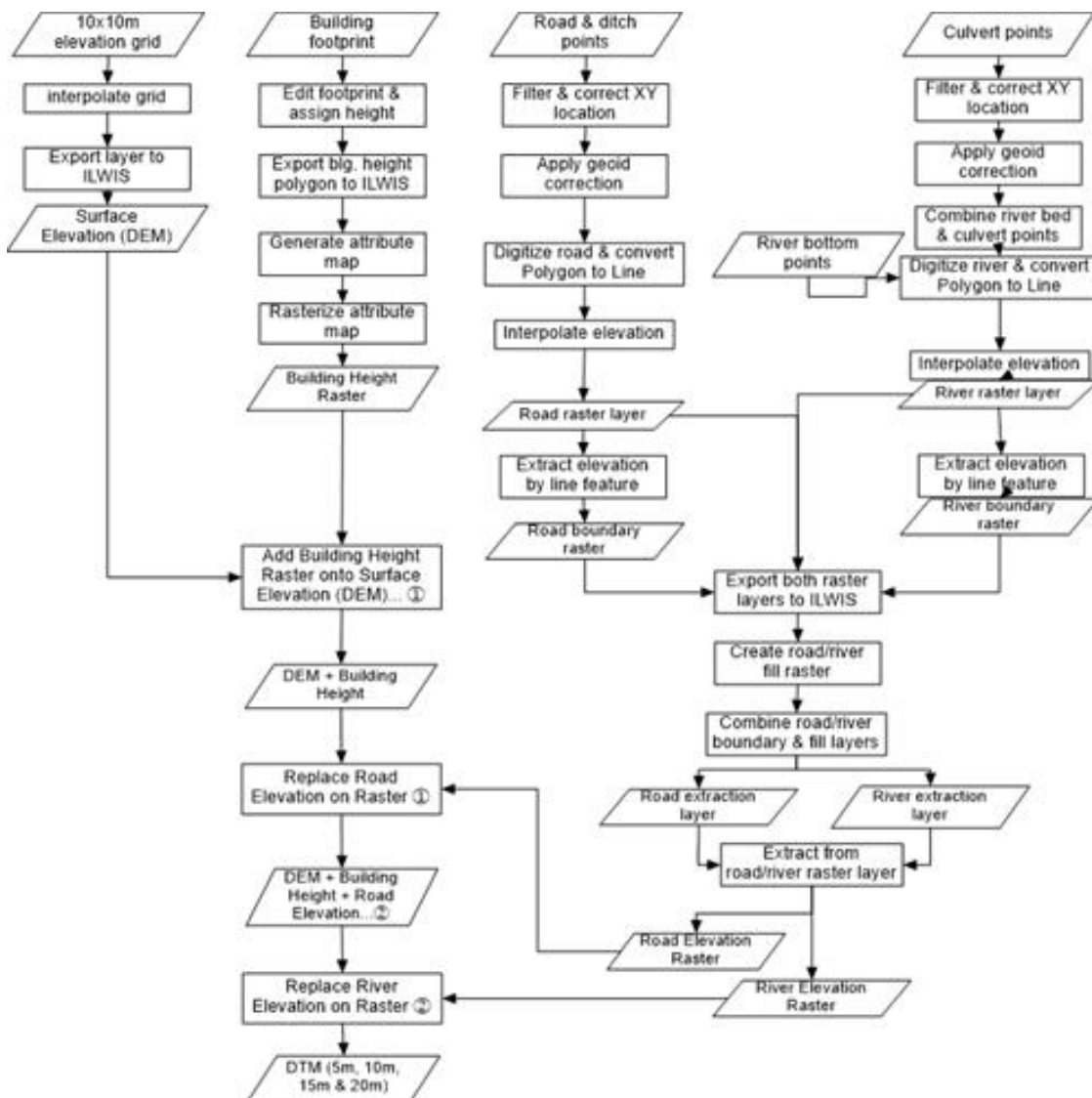
Figure 5.7: Flowchart of DTM generation for all the four resolutions.

5.2.   DEM Accuracy Assessment

5.2.1.   Reference Elevation

The ground control points collected from the field by using a handheld Garmin 52S GPS displayed a significant error as compared to the reference elevation grid as shown in Table 5.1. As it is displayed in the histogram below in Figure 5.8 only 14 measurements and 27 measurements out of the total 108 GCPs were in the range of a ±1m and ±2m error, respectively and even some 21% of the measurements have more than ±10m error. This significant vertical difference is attributed to the air pressure variation with the time of the day but also between the days the measurements were taken.
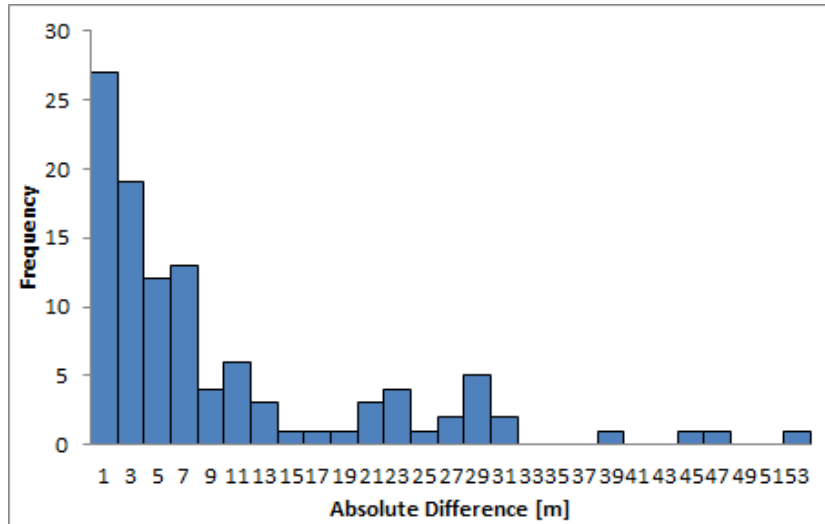
Figure 5.8: Histogram elevation error of the GCPs collected by a handled Garmin 52S GPS

September is the start of the second rainy season in Rwanda hence clouds and small showers were apparent that also amounted to the detriment of the GPS signal. Investigation of the collected GPS readings revealed no systematic or consistent error, hence correction was not viable. Moreover, such vertical error could not be tolerated for the purpose of flood modelling hence, instead, 200 point elevations of the 10m × 10m elevation grid shown in Figure 5.9-(left) were used as a reference for accuracy assessment of the different DEMs. These reference point elevations are spread over the entire study domain to capture all the significant topographic features.
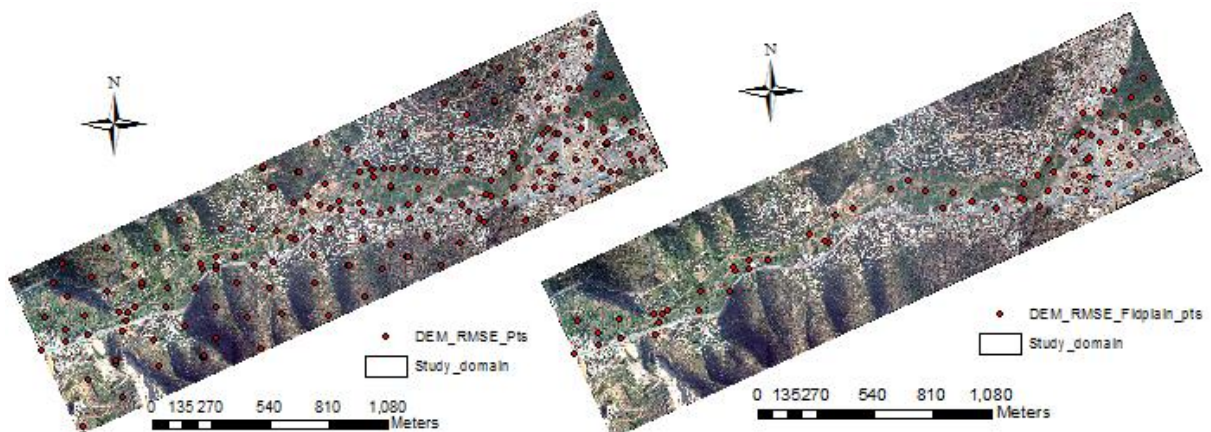
Figure 5.9: Reference point elevations used for DEM comparison.

5.2.2. Effect of Resolution

Topographic representation and hence representation of the physical processes of the real world are highly dependent on the selected grid resolution. Small grid sizes enable accurate representation of complex urban topography whereas large grid sizes lose important system details as a result of the averaging employed. Hence, it is important to investigate the effect of resolution on topographic representation. The interpolated elevation surface of the 10m × 10m elevation grid was analysed for four DEM resolutions: 5m, 10m, 15m and 20m by different techniques. A visual comparison of the 20m and 5m DEM resolutions is given in Figure 5.10 below. It can be clearly observed that the 20m resolution smoths the elevation difference to the extent that it failes to represent the contrast between the hill ridges and valleys. The 5m resolution on the other hand clearly depicts this contrast and it also gives some detail in the relatively flat floodplain (see the river bottom depressions and the hillside roads indicated by an arrow).
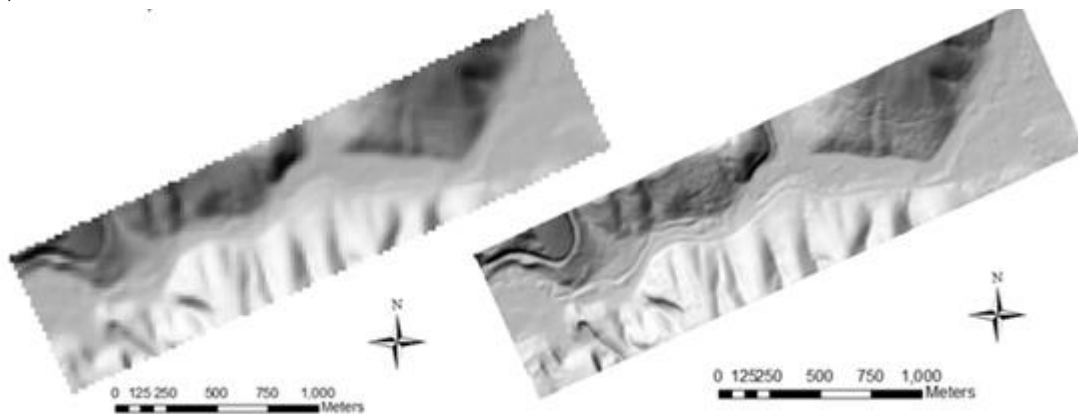
Figure 5.10: Hillshade maps of 20m (left) and 5m (right) DEM resolutions.

A statistical comparison of the different DEM resolutions was conducted using the reference point elevations given in Figure 5.9-(left). An increasing trend of both minimum and maximum error is observed with the increase of the grid size from 5m to 20m. This trend does not hold for the mean error as the positive and the negative error cancel out each other. However, the deterioration of topographic representation from high to low DEM resolution is clearly displayed in the large increase of the RMSE values which is caused by the averaging of increased pixel area. Table 5.3 gives the summary of the comparison.

Table 5.3: Statistical comparison of the different DEM resolutions.

DEM Resolution	Min Error	Max Error	Mean Error	STD	RMSE
5M	-1.5	1.6	-0.03	0.03	0.51
10M	-2.5	2.5	-0.02	0.05	0.71
15M	-5.6	6.1	-0.06	0.09	1.64
20M	-6.7	9.8	0.27	0.14	2.17

Moreover, a difference mapping technique was applied to quantify the elevation difference introduced as a result of the grid size increase. The larger grid sizes were resampled to 5m and deduction of the original 5m DEM was made. Figure 5.11 shows the result of the differencing for the resampled 20m and 10m

respectively. A vertical error of up to ±8m resulted in the 10m case whereas this error is doubled for the 20m case. A systematic error of large magnitudes is observed on the hills in both cases as rapid changes of elevation occur on the sides of the hills which are not captured by the large grid sizes. However, sub-meter error is observed on the floodplain as the relatively flat topography of the floodplain is not largely affected by the averaging.
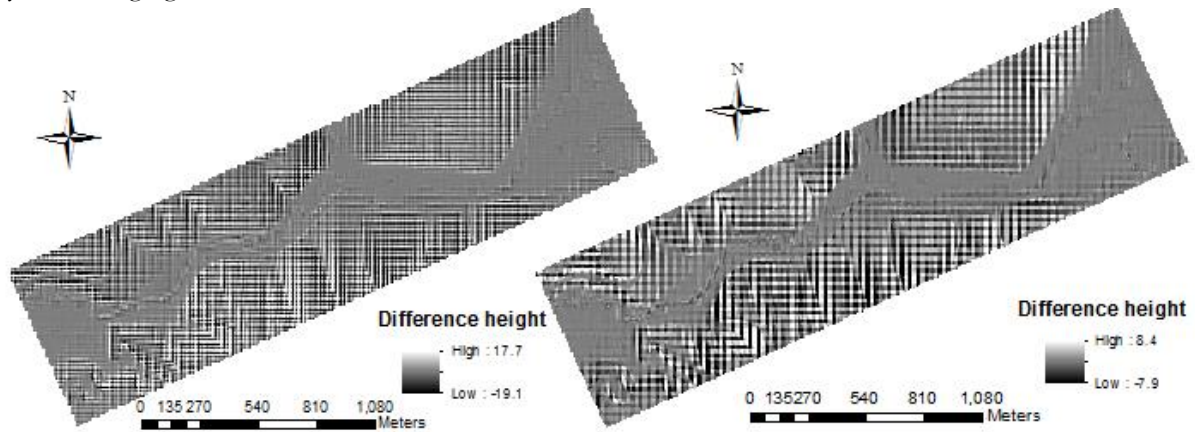
Figure 5.11: Difference map of resampled 20m (left) and 10m (right) to 5m.

The Nyabugogo floodplain is confined by the steep hills on both sides that have a large slope as shown in red in the slope map below. The 20m resolution slope map shown in Figure 5.12-(left) below introduces artificial slope on the hillsides due to the averaging of the large pixel area thereby smoothing the actual slope. As it is also shown in Table 5.4 the maximum and mean slope hence reduces with the increase in grid size. The drop in the standard deviation with grid size also indicates limitation of the larger grid sizes in representing topographic slope variation. The analysis of topographic slope representation is even critically important in large scale flood modelling studies and rainfall induced inundation of complex urban environment located on steep topography.
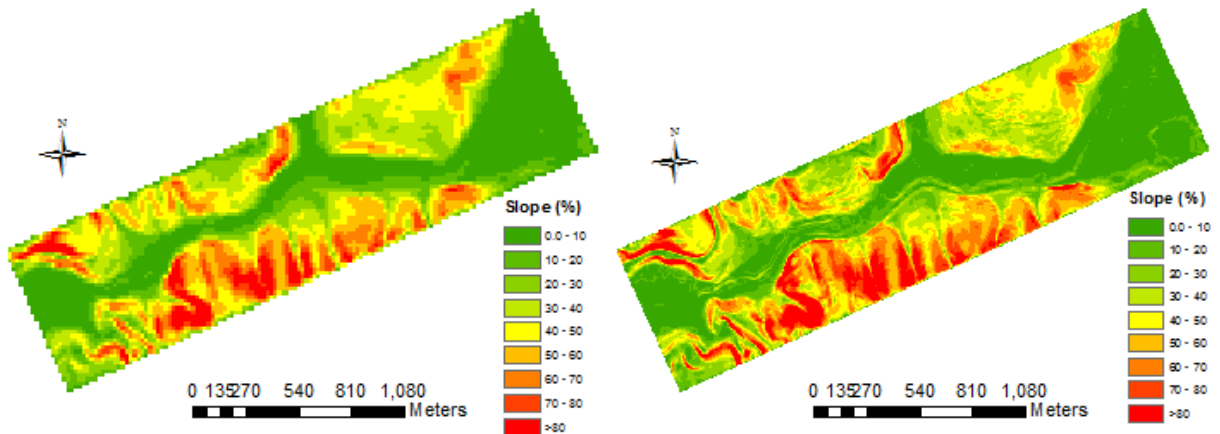
Figure 5.12: Slope map of 20m (left) and 5m (right) DEM.

Table 5.4: Statistics of slope maps of different resolutions.

DEM_Type	Min	Max	Mean	STD	River bed slope (%)
DEM (5m)	0.013	211.16	33.87	27.12	0.17
DEM (10m)	0.016	161.67	33.32	26.28	0.18
DEM (15m)	0.054	137.71	32.65	25.37	0.19
DEM (20m)	0.020	123.63	31.84	24.34	0.19

The overall river bed slope however is not significantly affected by the change in resolution due to the fact that it lies on the relatively flat floodplain where the overall slope in the nearly 3880m long river channel is less than 0.25%. A similar result is reported by Manyifika (2015).

The effect of resolution is even pronounced when it comes to the representation of specific terrain features apart from the general topography. A section of the river and road layers used to construct the DTM are shown below for the Nyabugogo central taxi area. In contrary to the reality, it can be seen on Figure 5.13-(left) that the 20m resolution introduces additional area (see also Table 5.5) to the river and road sections which will affect the propagation velocity of the flood simulation. The 5m resolution correctly represents the dimensions of the river and road features as shown in Figure 5.13-(right). Moreover, in the 20m resolution some pixels of the river and road layers overlap other close features such as buildings. This causes unwanted uncertainty in the flood simulation where the function of the buildings in altering propagation might not be correctly represented.
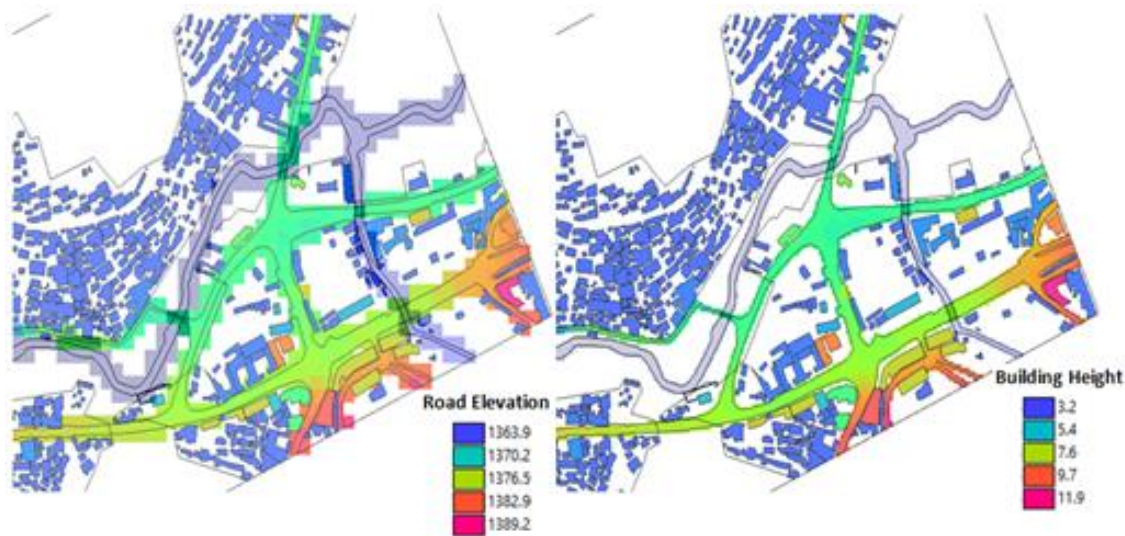
Figure 5.13: Road and River representation at 20m (left) and 5m (right) resolutions.

Table 5.5: Area of road in the different DEM resolutions.

DEM Type	# of Pixels	Area (m²)	%Increase of Area w.r.t. DEM (5m)
DEM (5m)	6215	155375	-
DEM (10m)	2072	207200	33.35479
DEM (15m)	1140	256500	65.08447
DEM (20m)	761	304460	95.95173

A similar effect is observed in representing buildings in the different DTM resolutions. Real world buildings are irregularly shaped and are not aligned in parallel to the raster grid system applied in the model. The 5m resolution shown in figure Figure 5.14-(right) below is small enough to construct the shape of the buildings which are mostly larger than 5m in dimension. This fit however deteriorates with the increase in grid size as shown in the 20m resolution (Figure 5.14-left). The rasterization algorithm of the building shapefiles majorly determines the assigning of grids as building pixels. As a result some small and isolated buildings are ignored. Also due to the large pixel size non-building areas are assigned as building pixels thereby introducing unwanted resistance to flood wave propagation.
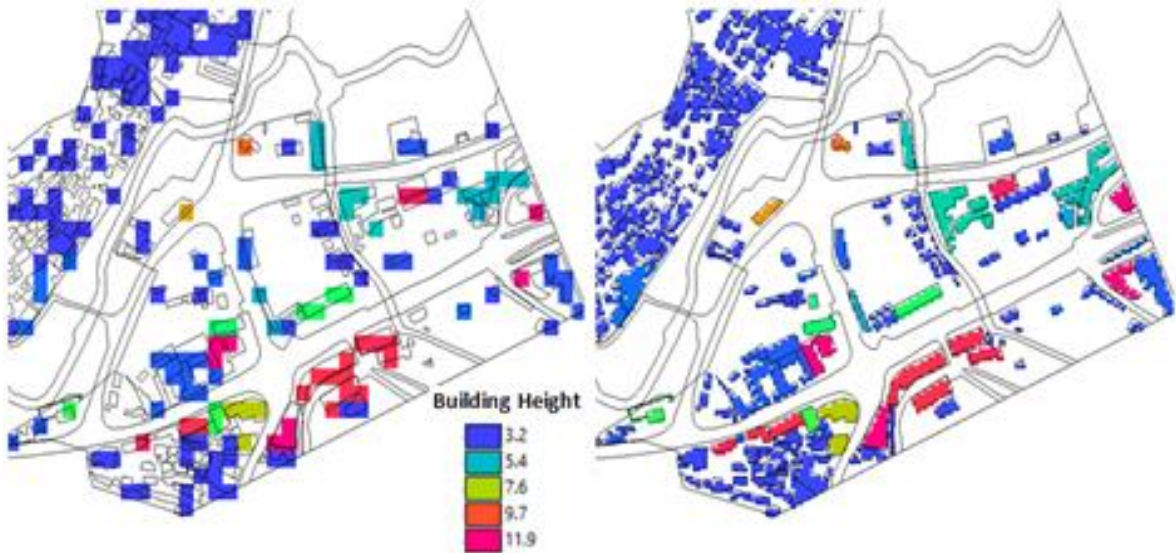
Figure 5.14: Building representation at 20m (left) and 5m (right) resolutions.

The above analysis is evident that finer grid sizes are capable of capturing topographic variations and terrain features that affect flood wave propagation on complex urban environments. Coarse grid resolutions on the other hand miss significant topographic details and create artificial representation of terrain features such as roads and buildings.

5.2.3. Comparison of Satellite Based DEM with Local DEM

Satellite based DEM are alternative sources of topographic information for flood modelling studies. Hereafter the accuracy of the freely available global elevation datasets, namely ASTER (version 2) and SRTM (version 3) are tested. For reasons of simplicity the original 30m resolution was adopted and no cleaning and corrections have been made. These satellite based DEM products are compared to the local DEM at 30m resolution and the point elevation data (given in Figure 5.9-left) were used to assess vertical accuracy. As it can be seen from Figure 3.3 ASTER displays erratic elevation changes while SRTM displays pockets of depressions along the floodplain.

Table 5.6: Statistics of the different type of DEM.

DEM Type	Min	Max	Mean	STD
Local DEM (10m)	1361.3	1591.3	1410.4	47.56
Local DEM (30m)	1361.4	1588.3	1410.3	47.55
ASTER (30m)	1361	1577	1406.95	42.64
SRTM (30m)	1362	1579	1411.38	45.64

From the statistics in Table 5.6, it can observed that both satellite based DEMs underestimate the maximum elevation and also that they fail short of correctly representing elevation variation as indicated by the lower standard deviations as compared to the local DEM. The largest offsets are observed in ASTER while the local DEM at 30m resolution performs better as compared to the 10m resolution. A similar result is obtained by the accuracy assessment as shown in Table 5.7 below. The large minimum error of ASTER suggests that it underestimates elevation mostly associated with the elevated hillsides. Though not as large as ASTER, SRTM also exhibits underestimation of such topography. This

phenomenon has to do with the signal problems of the remote sensing techniques used to acquire elevation. As the local DEM is developed by interpolation of the 10m × 10m elevation grid, it obviously performs better in representing the topography. In general, the RMSE and standard deviation values suggest that SRTM performs better than ASTER. However, it should be noted that these are mean values that represent the overall topography of the study area.

Table 5.7: Accuracy assessment results of the different DEMs for the study domain.

Measure	Local DEM	ASTER	SRTM
Min Error	-10.7	-57.6	-32.6
Max Error	10.6	29.9	31.9
Mean Error	0.02	-2.19	0.93
STD	0.17	0.95	0.78
RMSE	2.69	13.93	10.77

It is known that both satellite based DEM products suffer on steep topography, hence a separate accuracy analysis was done by using 69 point elevations spread only in the floodplain (see Figure 5.9-right). From Table 5.8, it can now clearly be seen that the (extreme) underestimation of ASTER is removed and the same is true for SRTM. Overestimation of the SRTM DEM here is higher as compared to both ASTER and the local DEM which impacted the overall accuracy index, RMSE. The fact that ASTER has the largest standard deviation while maintaining a relatively lower mean error and RMSE values comes from the erratic nature of the elevation surface representation

Table 5.8: Accuracy assessment results of the different DEMs for the floodplain only.

Measure	Local DEM	ASTER	SRTM
Min Error	-6.1	-12.5	-6.8
Max Error	5.1	16.2	20.8
Mean Error	0.14	1.27	1.68
STD	0.06	0.35	0.33
RMSE	0.72	2.98	3.07

To visualize the spatial distribution of the errors of the satellite based DEMs, a difference mapping was done against the local DEM as shown in Figure 5.15 below. A relatively lower error is observed by ASTER in the flat commercial area around the Nyabugogo taxi park as compared to the errors of SRTM DEM. This could also be attributed to the fact that the concentrated buildings affect the SRTM signal. Similar incident can be observed around the Nyabugogo central bus station. Moreover, at the valleys of the hillsides SRTM recorded higher errors as indicated by the cyan color. A general overestimation of the SRTM DEM as compared to the ASTER DEM is evident as shown on the lower left figure which is pronounced on elevated surfaces, the hills.
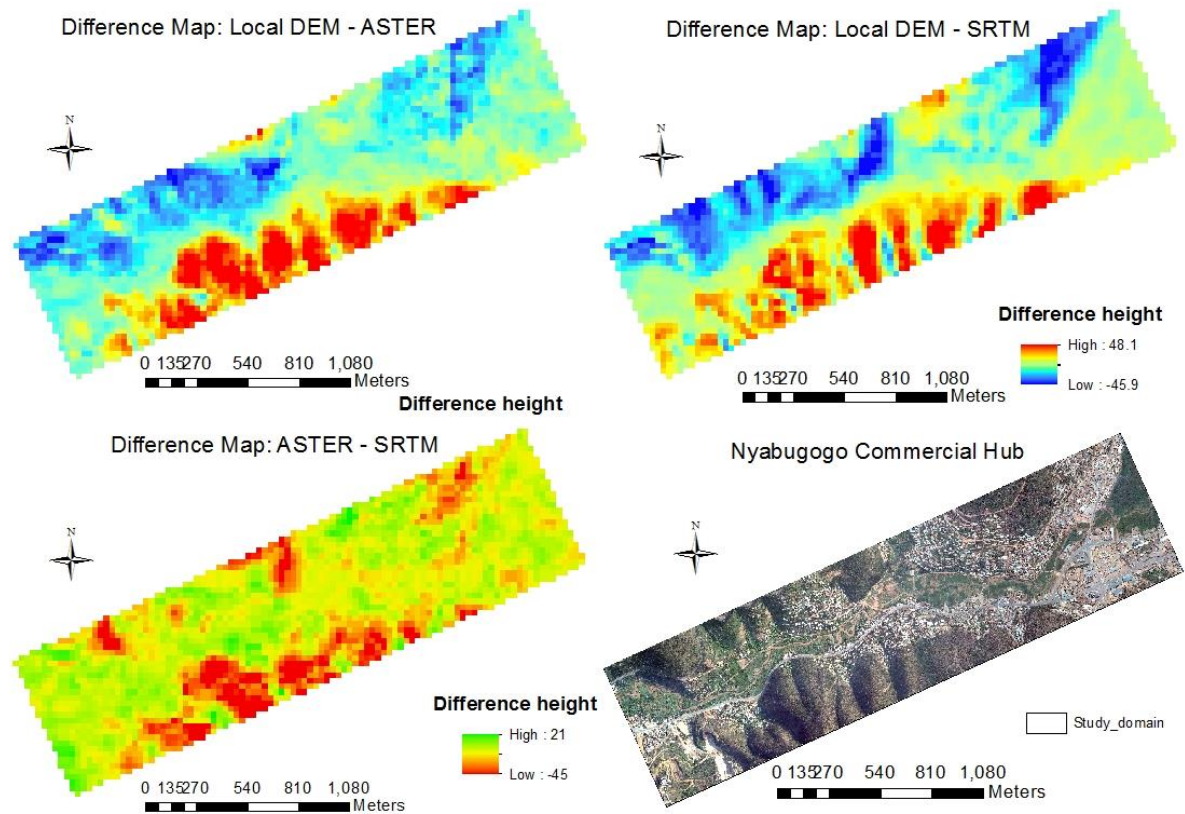
Figure 5.15: Difference Map of the different DEM at 30m resolution

The slope map shown below in Figure 5.16 goes in line to the above discussion where ASTER displays the lowest slope as compared to both SRTM and local DEM. This is prevalent on the hillsides where ASTER has the most underestimation. Moreover, the erratic surface of the ASTER floodplain has also appeared in the slope map. Generally the local DEM displays the largest slope as it better captures the topographic variation of the study area. The comparison of the river bed slope was however not possible as the analysis is merely based on the original DEM and that no corrections and hydrologic processing have been made.
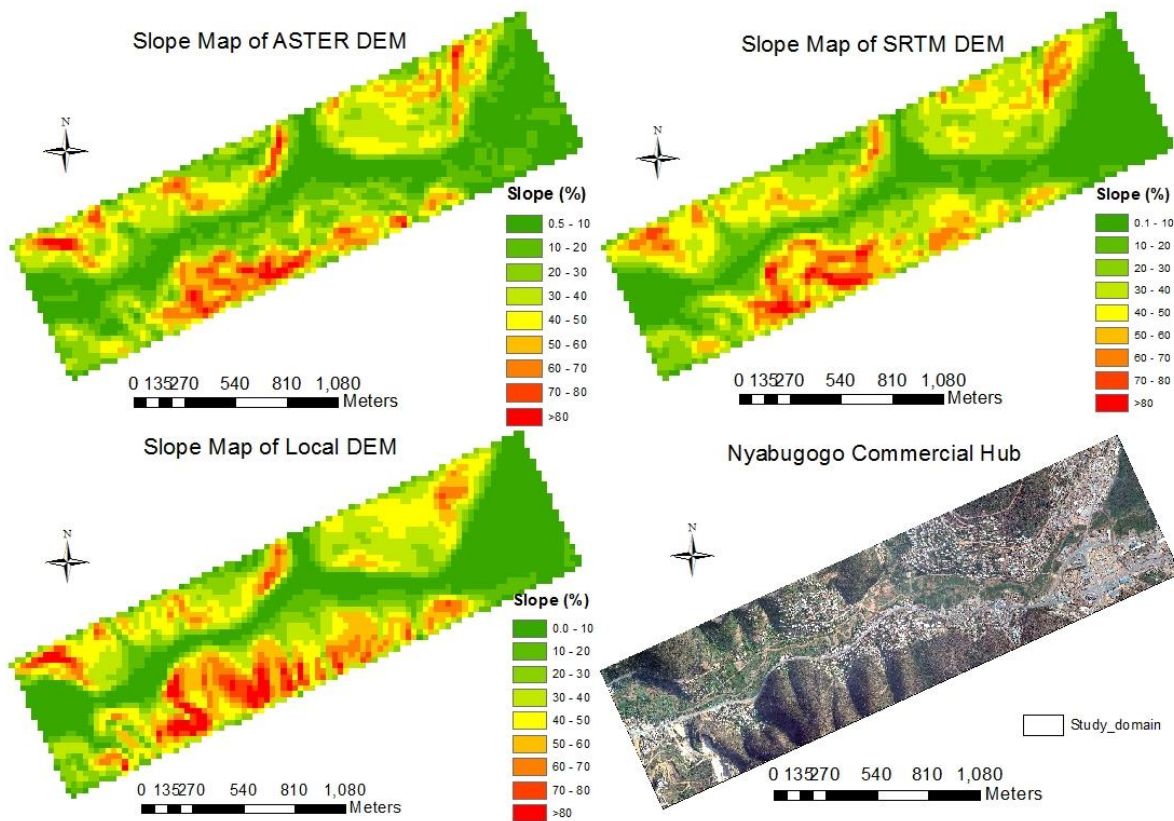
Figure 5.16: Slope map of the different DEM at 30m resolution.

The other topographic index which governs the flood wave propagation is the slope aspect. There are eight possible directions of the aspect, these are the four major directions and intermediate faces between them. Flood wave follows the steepest descent along the forward direction of the aspect. Hence, misrepresentation of the actual aspect of the topography will have a direct consequence on the resulting inundation. A general summary of the aspect in the study domain is given in annex 2 as histograms. An attempt was made to observe the aspect difference of the satellite based DEM in reference to the local DEM. This resulted in a 51.83% and 52.25% similarity of ASTER and SRTM DEM, respectively, within a ±1 aspect direction difference. A ±1 aspect direction difference is assumed acceptable as there are only four possible directions of flow in the 2D flood domain (north, east, south and west) which will force the flow of a ±1 aspect direction to one of these major four directions. A detailed assessment of the aspect in the floodplain however might reveal interesting distinctions between these satellite DEMs in defining the direction of flood wave propagation.

Finally, a sink map of both satellite DEMs was made after a fill sink operation. As it can be seen in Figure 5.17 below the major fill operation was made along the longitudinal river profile. The sink depth is more or less similar in both DEMs. However, in the ASTER DEM a small spread of sink is observed on the flat floodplain near the Nyabugogo central taxi area. This accounts for the erratic ASTER elevation surface and relative underestimation. Both DEMs also indicated a significant depression at two locations along the river indicated by circles in the figure. From the above analysis it can be concluded that SRTM has a slightly better performance when the whole study area was considered whereas ASTER has a slight accuracy in representing the relatively flat floodplain of the study area. Similar result is also reported by

Mukherjee et al. (2012) For optimum representation nevertheless appropriate correction and hydrologic processing of these satellite based DEMs is required.

Figure 5.17: Sink map of satellite based DEM at 30m resolution.

5.3.   Flood Modelling

Once the DEM and DTM of the Nyabugogo commercial hub were prepared, they were imported to SOBEK 1D2D as ArcInfo ASCII files. Apart from the topographic information, the flood model requires o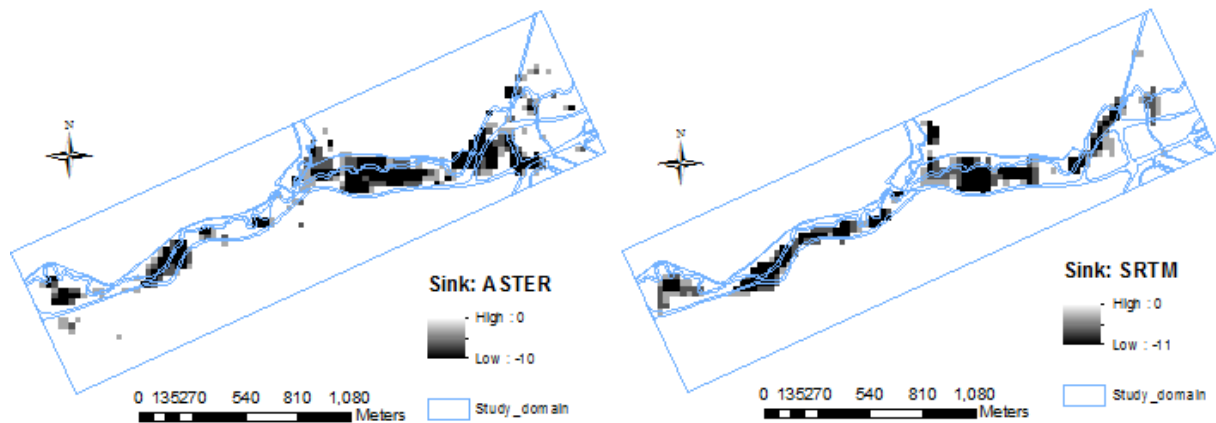ther inputs including forcing terms to be used as boundary conditions, channel cross sections and roughness data. The upstream boundary condition was defined in the form of integrated system response hydrograph of the upstream catchment as given in Figure 3.4. A specified (variable) head boundary (Dirichlet condition) was used to define the hydrologic state at the downstream boundary condition so as to ensure a gravitational free flow. The river bottom profile and cross sections collected by Manyifika (2015) were used to represent the 1D river network. A surface roughness map for three different building representations was also prepared (see Figure 4.6) and imported as ArcInfo ASCII file.

5.3.1.   1D2D Model Setup and Simulation

Global model definitions were assigned at the Settings wizard of the SOBEK model interface (see Figure 4.5). A 24 hour model simulation period and a 30 minute simulation time step were used to simulate the inundation resulting from the peak rainfall which fell between the 4th and 5th of March, 2012. The modelling process started by setting up the 1D river system by a network of reaches and nodes connected to the 1D US and DS boundary nodes of Nyabugogo river. The other two boundary conditions, namely Mpazi drainage and Yanze watershed were then connected to the Nyabugogo river network by means of linkage nodes. Linkage nodes were selected to maintain the interpolation of profile of the Nyabugogo River at the confluence points. Flow calculation points were carefully assigned at every vertex of the river network and between vertexes at distance so as to keep an even distribution for better model performance. The distance between neighbouring calculation points should not be too large so that the physical process can be properly represented and accuracy is not compromised. Such distance should neither be too small in order to maintain numerical stability and reduce simulation time (Delft/Hydraulics, 2014). An average link distance of 30m was maintained between the calculation points in the model.

The 1D network profile was defined by 50 trapezoidal cross-sections which constitute the river bottom and surface (bank) elevations, and dimensions of the trapezoid as shown in Figure 4.5. These cross sections are spread throughout the 1D river network enabling a proper representation of the river system (see Figure 4.4). Moreover, two bridge and two culvert structures were defined on the major Nyabugogo

River and the Mpazi drainage channel respectively. A fixed Manning's coefficient was adopted to represent bottom friction. The profile definition of these cross sections was transformed to the full river network by linear interpolations at the calculation points and linkage nodes. The complete 1D river network was then linked to the 2D grid by means of connection nodes at the boundary of the model domain and calculation points along the 1D river network. The 1D2D linkage mechanism is explained in section 4.3.3. A spatial surface roughness value was also assigned to the 2D grid.

The first simulation was tested at 20m resolution which took about 3 hours and 48 minutes. A 20m local DEM was used as 2D grid to represent the study area topography. Figure 5.18 below shows the result of the maximum flood depth recorded throughout the total simulation time step. Large flood depth and extent can be seen close to the downstream boundary. Moreover, strange flood depth values are recorded at the location pointed by the arrow. A side view functionality of the SOBEK NETTER interface was used to investigate the nature of this problem as shown in Figure 5.19. It is now clearly seen that the unrealistic heap on the river bottom profile caused the large depth of inundation as the river flow will accumulate behind the heap until it eventually starts to overtop. Furthermore, the highly undulating river bottom profile throughout the 1D network calls for appropriate correction so as to maintain a realistic gentle slope. Several causes such as instrument error could have caused this phenomenon.
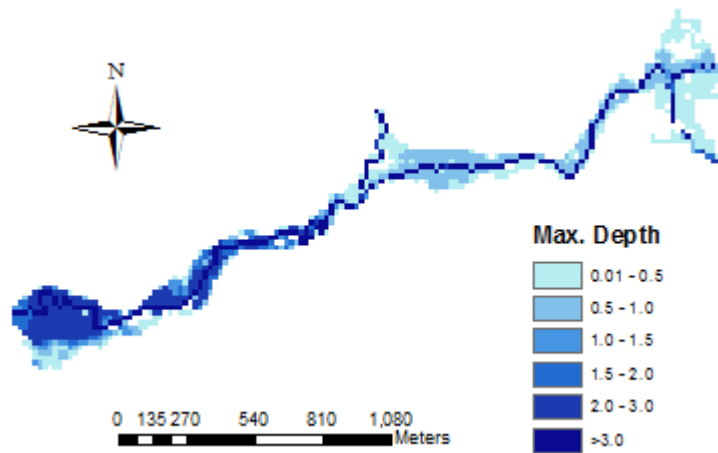

Figure 5.18: Maxim flood depth map at 20m DEM resolution.
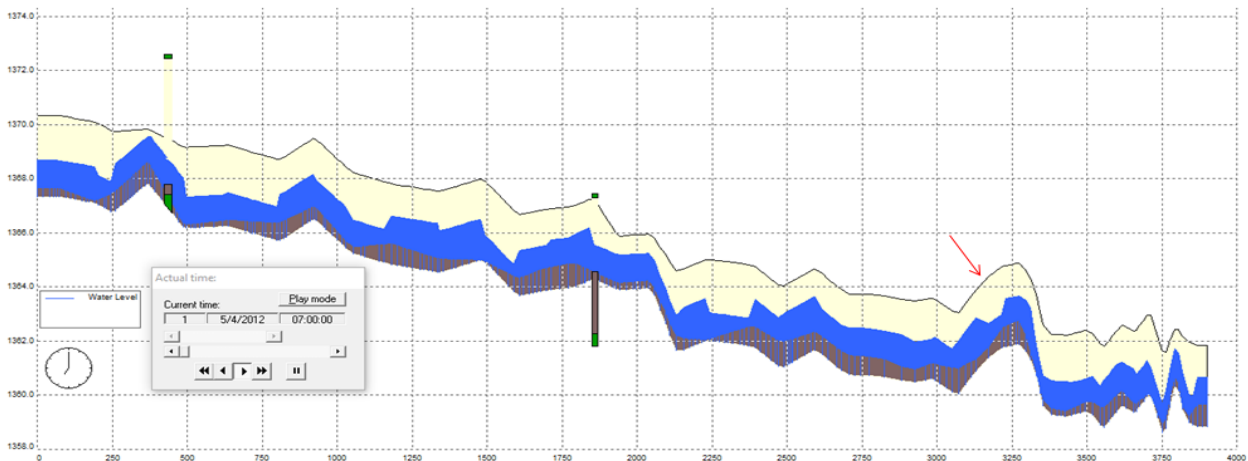
Figure 5.19: Side view of the longitudinal profile of the model at 20m resolution.

From the field visit it was noted that Nyabugogo is a typical sedimented river channel and hence a manual correction of the river bed slope was applied to reduce the heap heights and raise depression/pits and the result is presented in Figure 5.20 below. In SOBEK inundation of a 2D grid is triggered by the overflow of the 1D river channel network, therefore accurate representation of the river bottom profile is of high significance for accurate flood modelling.
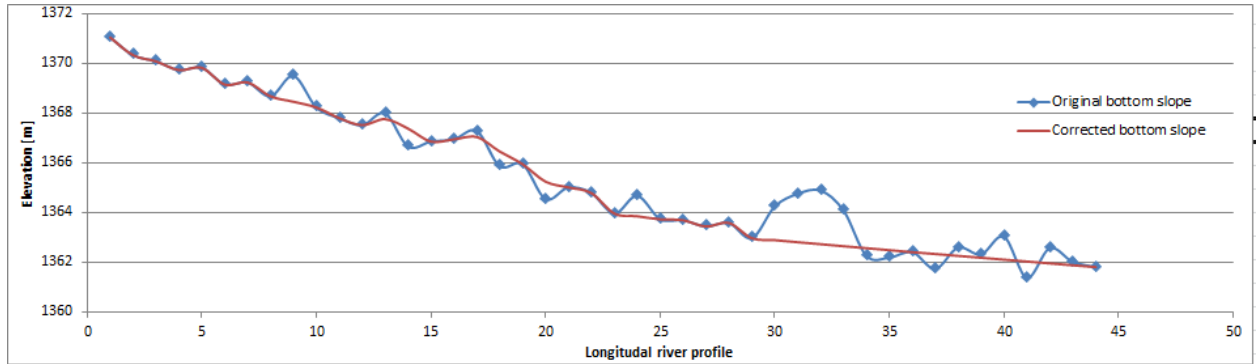
Figure 5.20: Manual river bottom profile correction.

The average depth of Nyabugogo River is 3m. The fact that the river stays wet and discharges a large flow throughout the total simulation period is depicted by the deep blue colour of the maximum depth map on Figure 5.18. At the downstream boundary the model discharges the inflow only at the 2D/1D boundary node according to the specified variable head boundary. As the model domain is diagonally shaped it was not possible to introduce a 2D line boundary node which could drain the stored water as overland flow. Several tests were then made to drain the large column of water that was stored as a result. A large cross section was first introduced close to the downstream boundary. The dimensions of the preceding cross section were increased by three folds for the new cross section spanning about 40m maximum flow width. However no significant change was observed on flood depth and extent. This revealed that the problem was caused by the specified head boundary condition expressed only as the level of water in the channel which was less than four meters. In this case the model encounters an extreme (in the order of thousands) hydraulic gradient at the model boundary. Since this is not an acceptable condition, the model automatically assigns the elevation head of the neighbouring calculation point to the boundary node. To avoid this situation a free flow condition was set by lowering the (fixed) stage of the downstream boundary node from the neighbouring cell inside the model. This resulted in the removal of the large column of water that was stored inside the model as shown in Figure 5.21. As a result a drastic drop in the simulation time step occurred; it only took few minutes.
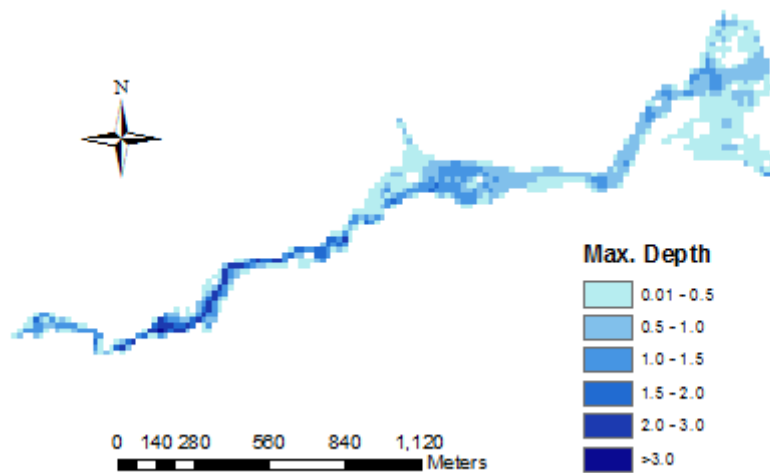
Figure 5.21: Maxim flood depth map after river bottom and DS boundary condition correction at 20m DEM resolution.

Now that the model is adjusted for irregularities of the river bottom profile and the DS boundary condition, a steady state simulation was run to test the robustness of the model. The simulation was made both at low and high flows of the three US boundary conditions (3.8 and 25.5 m³/sec respectively for Nyabugogo US). Generally river flow follows natural topography and same behaviour is displayed in the steady state simulation of the model. As it is evident in Figure 5.22 below, the adjustments made enabled the model to properly simulate both the low and high flow conditions. The high flow steady state simulation is in fact a good indication of the model's capacity to withstand different forcing conditions. In both low and high flow conditions, a column of water accumulates behind the two bridge structures. This is also what happens in reality when a flow of water encounters a structure along its course. A vertical friction also develops at such instances and it will slowly drain. On relatively steep sections of the river profile however the depth of flow drops as a result of the increased velocity that quickly drains the flow; that satisfies the principle of conservation of mass.
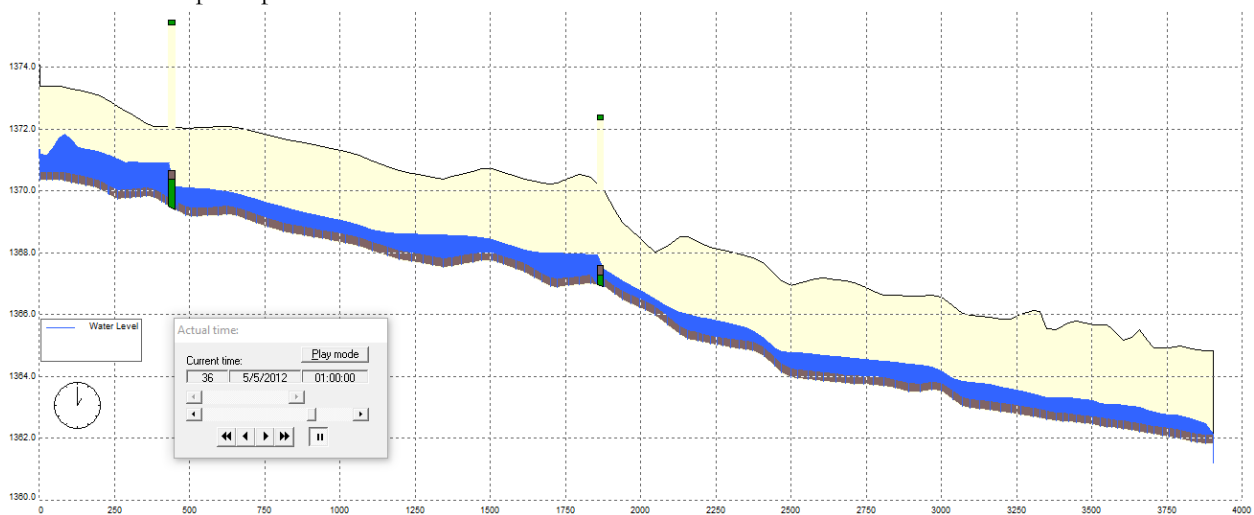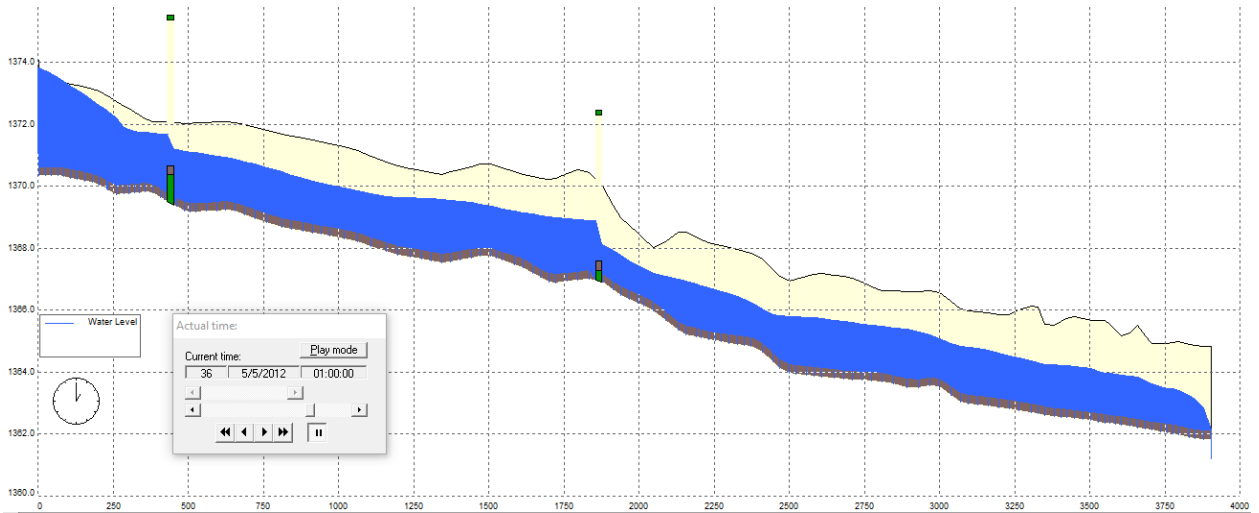
Figure 5.22: Side view of 1D steady state low flow (top) and high flow (bottom) simulations.

To evaluate whether the model handles a proper drying of wet 2D grids, another simulation was performed with an extended hydrograph for additional 24 hours. Two cases were tested; one is when the base flow was extended and the other is when the system receives no water. The hydrographs of the two cases are shown Figure 5.23 below:
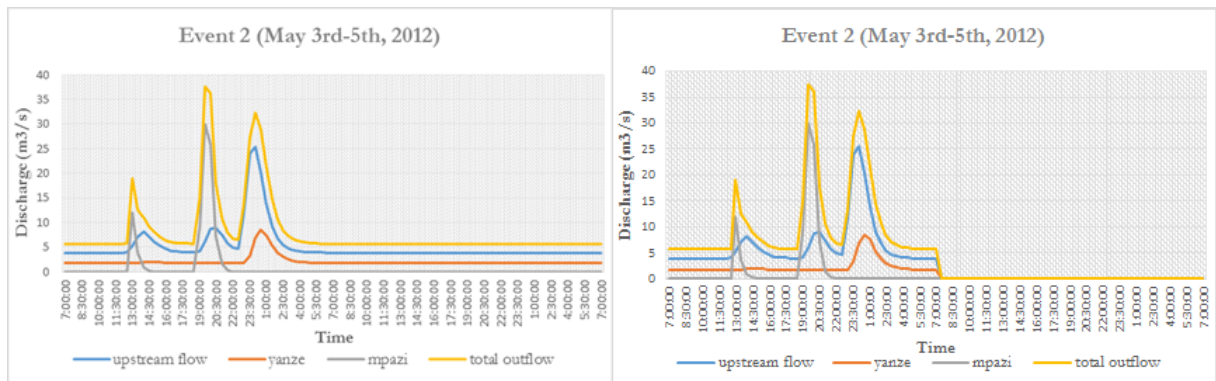
Figure 5.23: Extended upstream flow hydrograph with base flow (left) and no flow (right).

Wet 2D grid cells, which are isolated or distant from the 1D channel network remained wet in both cases as the model simulates drying or wetting patterns only by means of hydraulic gradient whereas in the real world many more processes take place such as infiltration and evaporation. In the case of the extended base flow simulation, the channel continually drains the base flow and as a result some 2D grid cells located close to the 1D channel still remain inundated from the previous overflow. When the flow is dried after the first 24 hours of the simulation wet 2D grid cells surrounding the 1D network start to empty to the channel, as indicated in the Figure 5.24 below.
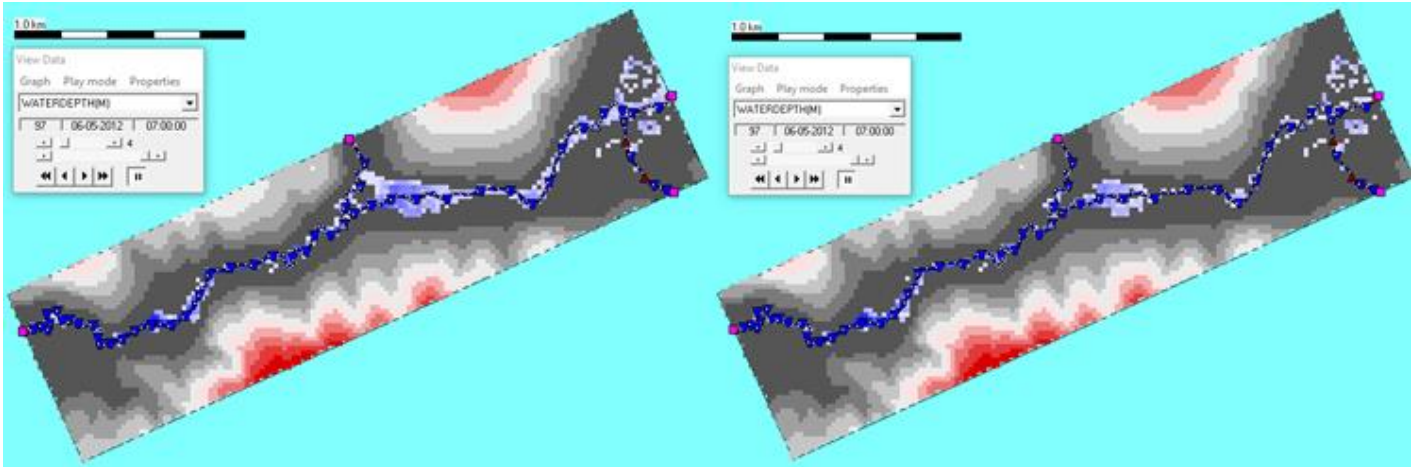
Figure 5.24: SOBEK NETTER interface of drying 2D grids: base flow (left) and no flow (right).

Model Calibration

Observed state variables are critically important to calibrate models. In flood modelling, measurements of flood characteristics such as flood depth and extent can be used for calibration purposes. Calibration was carried out by optimizing surface roughness, expressed here as Manning's coefficient values to match simulated flood characteristics with observed measurements (see Table 5.9). In this study, however, no measurement was available on the inundation that resulted due to the peak rainfall under analysis. Manyifika (2015) has collected few flood depth observations by interviewing local people and observing flood marks (see Figure 3.6). These observations were merely used to obtain an overall insight of the recurring urban flood in Nyabugogo commercial hub.

Table 5.9: Surface roughness values for model calibration.

Land Cover	Surface Roughness: Manning's n [s/m^{-3}]			
	Trial1	Trial2	Trial3	Trial4
Green area	0.04	0.038	0.042	0.05
Residential	0.035	0.033	0.037	0.045
Commercial	0.032	0.03	0.034	0.042
Building	1	1	1	1
River	0.03	0.028	0.032	0.04
Road	0.025	0.023	0.027	0.035

Four trials were made in an attempt to match the observed flood marks and simulated flood depth values. Calibrating the model with in the ranges of scientifically recommended Manning's coefficient values was not achieved as it can be seen from Figure 5.25. Hence the calibration process was ignored pertaining to the fact that the observed flood marks do not have any relation with the even under investigation.
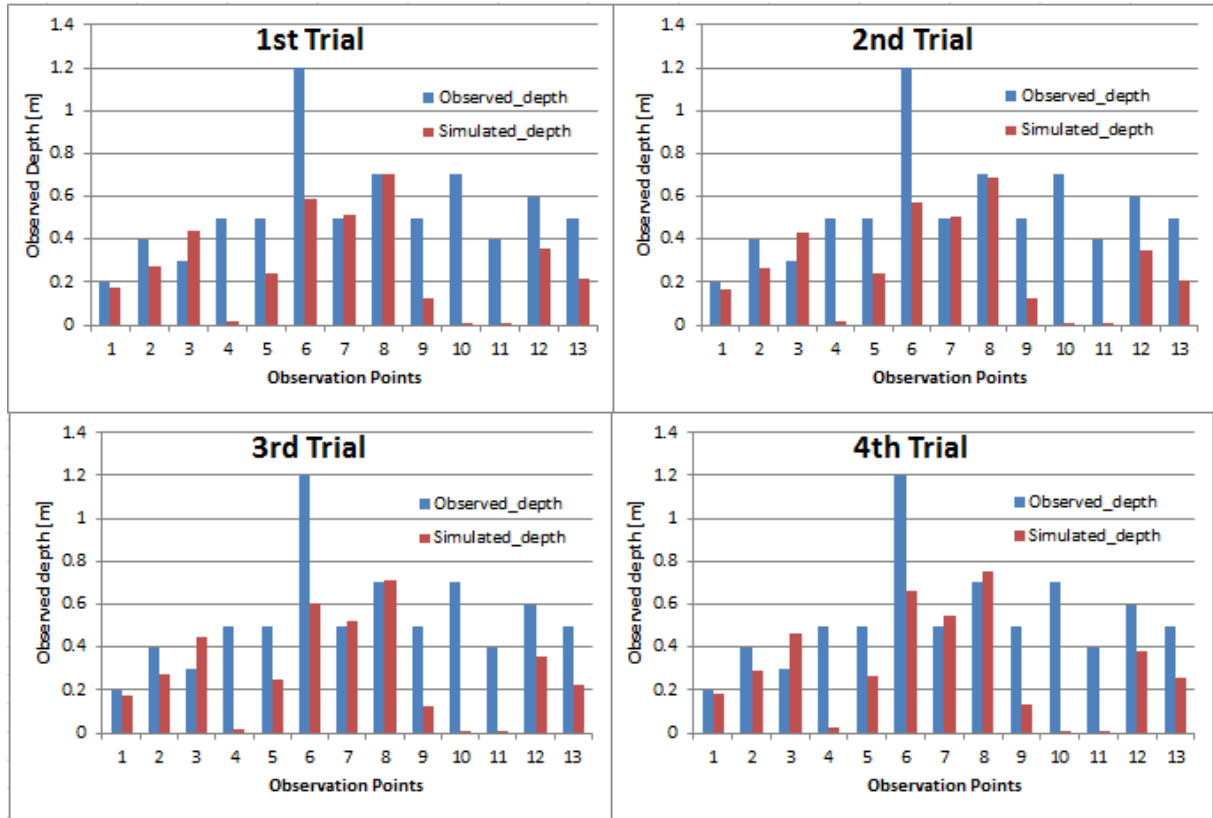
Figure 5.25: Calibration trials with Manning's surface roughness coefficient.

5.3.2. Effect of Spatial Resolution

Proper representation of the different terrain features of complex urban topography is fundamental for accurate urban flood modelling. The spatial resolutions of DEMs define the 2D grids of flood models. Fine DEM resolution facilitates the accurate representation of topography and real world physical processes but it comes with high computational cost. Coarse resolution, on the other hand, significantly optimizes computational cost at the expense of losing important topographic details as averaging is done over relatively large area. Hydraulic gradient which defines the flood propagation is largely governed by the elevation head in overland flow of 2D grid. Four major DEM resolutions have been used in this study (5m, 10m, 15m and 20m) to represent topography of the study domain. The effect of resolution hence was once again assessed by comparing flood simulation results such as flood depth, flood extent, flood velocity.
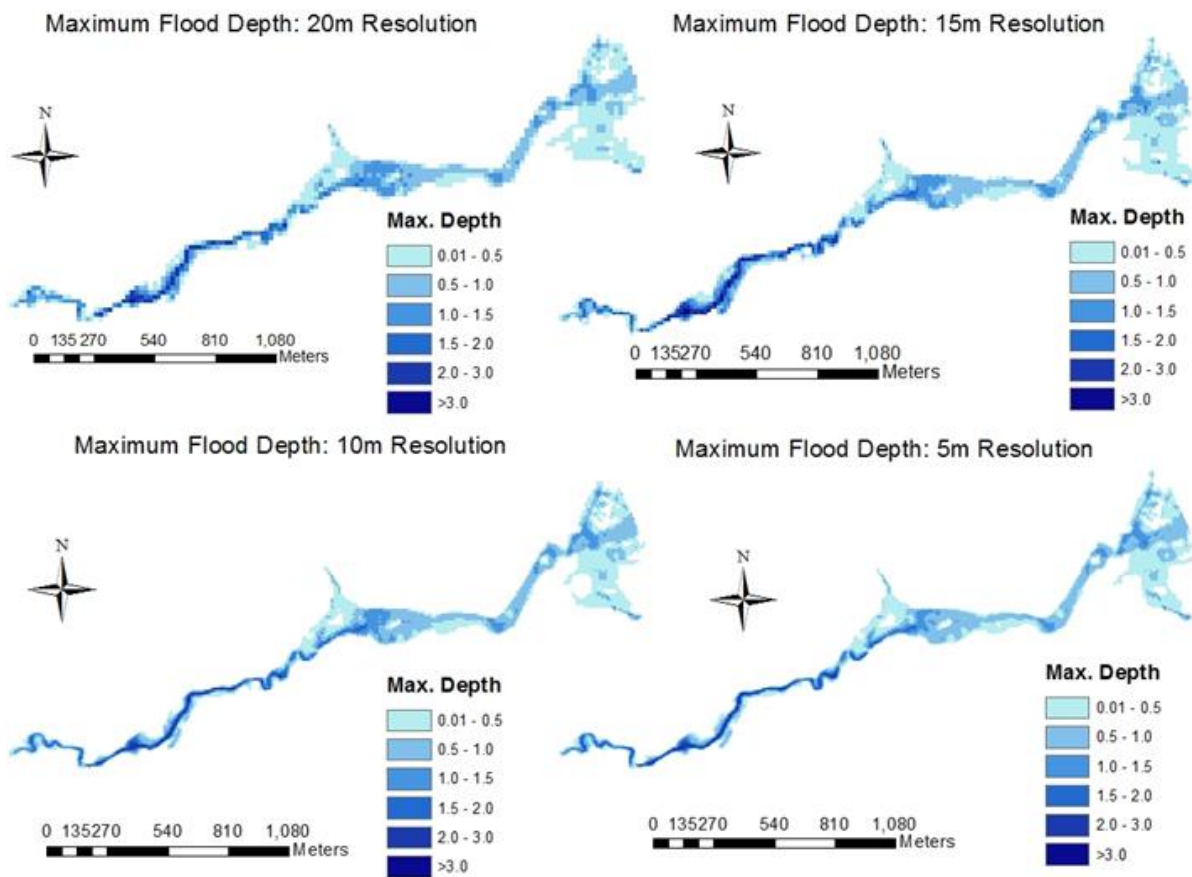
Figure 5.26: Maximum flood depth map of 20m, 15m, 10m and 5m resolutions.

SOBEK stores the simulated flood characteristics of every simulation time step. Figure 5.26 shows the maximum flood depth recorded in any time step and is indicative of the flood extent and column of water to be stored in each 2D grid cell. The maximum flood depth displays a general decline with the decrease in grid size. This can be observed by the decay of the blue tone on the inundated pixels. All the four resolutions managed to represent inundations of local depressions such as upstream of the Yanze river confluence, but with varying depth of inundation. A significant decrease of inundated area is observed on the 10 and 5m resolutions. In the large grid size of 15 and 20m resolutions, once overtopping occurs, the entire grid area will be wet. This increases the inundation extent, which is significantly higher than the smaller resolutions where overland flow might not occur to neighbouring grid depending on the hydraulic gradient. Moreover, the averaging at large scale of course resolutions ignores small scale dynamics of overland flow influencing the flood wave propagation.

Similar upstream and downstream boundary conditions were specified for all the resolutions. The strange behaviour of large flood depth in large grid size contradicts the principle of mass conservation where the stored amount of water in the model domain is the difference between the amount supplied and discharged. Table 5.10 table enlists the maximum flood depth statistics of nine different resolutions which is summarized in Figure 5.27. It can be observed that the rate of increase in flood depth and inundation area increases with resolution.

Table 5.10: Maximum flood depth statistics of different resolutions.

DEM Resolution	Maximum Flood Depth [m]				Area [m²]
	Min	Max	Mean	STD	
5m	0.012	3.15	0.68	0.53	301700
7.5m	0.012	2.97	0.66	0.50	302175
10m	0.012	3.03	0.69	0.54	306600
12.5m	0.013	3.25	0.69	0.53	310313
15m	0.014	3.47	0.76	0.63	324675
17.5m	0.011	2.89	0.67	0.53	329525
20m	0.012	3.05	0.70	0.55	330400
25m	0.016	3.99	0.79	0.70	338750
30m	0.016	4.03	0.91	0.77	385200
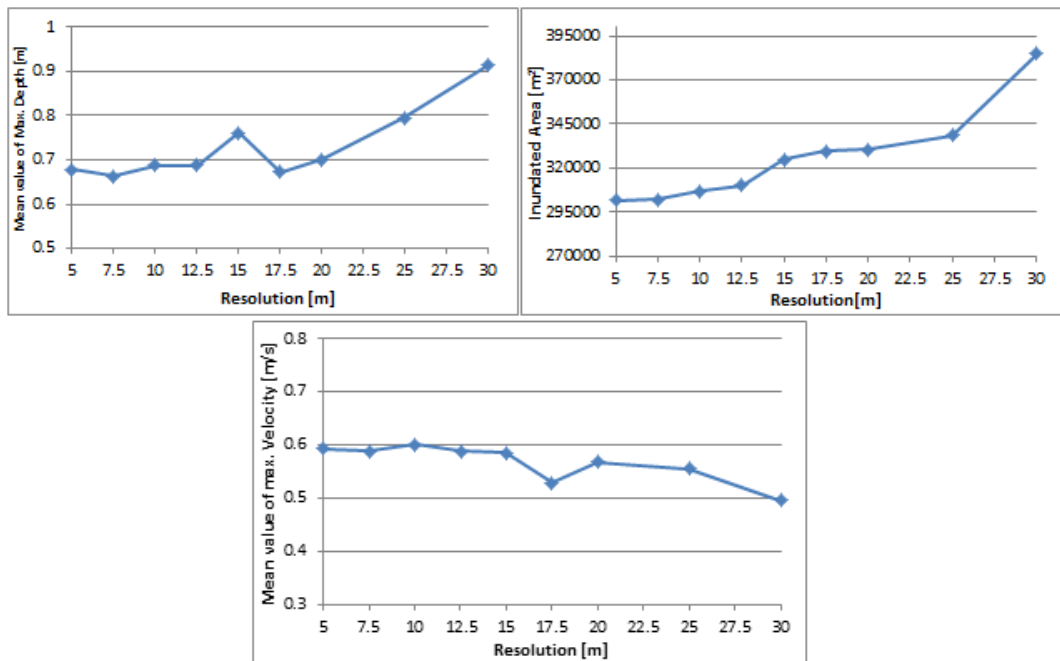
Figure 5.27: Mean of Maximum depth (left), maximum velocity (bottom) and inundation area (right) of the different DEM resolutions.

The effect of averaging is also observed in the maximum flood wave velocity given in Figure 5.28. The smoothing effect introduced as a result of averaging over large area lead to the decrease of flood wave propagation in course resolutions (see also Figure 5.27-bottom). The maximum velocity is majorly governed by river bottom profile and topography of the 2D grid. The largest velocity is recorded on the Mpazi drainage channel and at the DS boundary. This is because of the relatively steep slope of the Mpazi channel and the introduced hydraulic gradient (free flow condition) at the DS boundary. Moreover, at locations of large inundation relatively smaller velocities are observed as lateral flows of inundation are expectedly lower than longitudinal flow velocity.
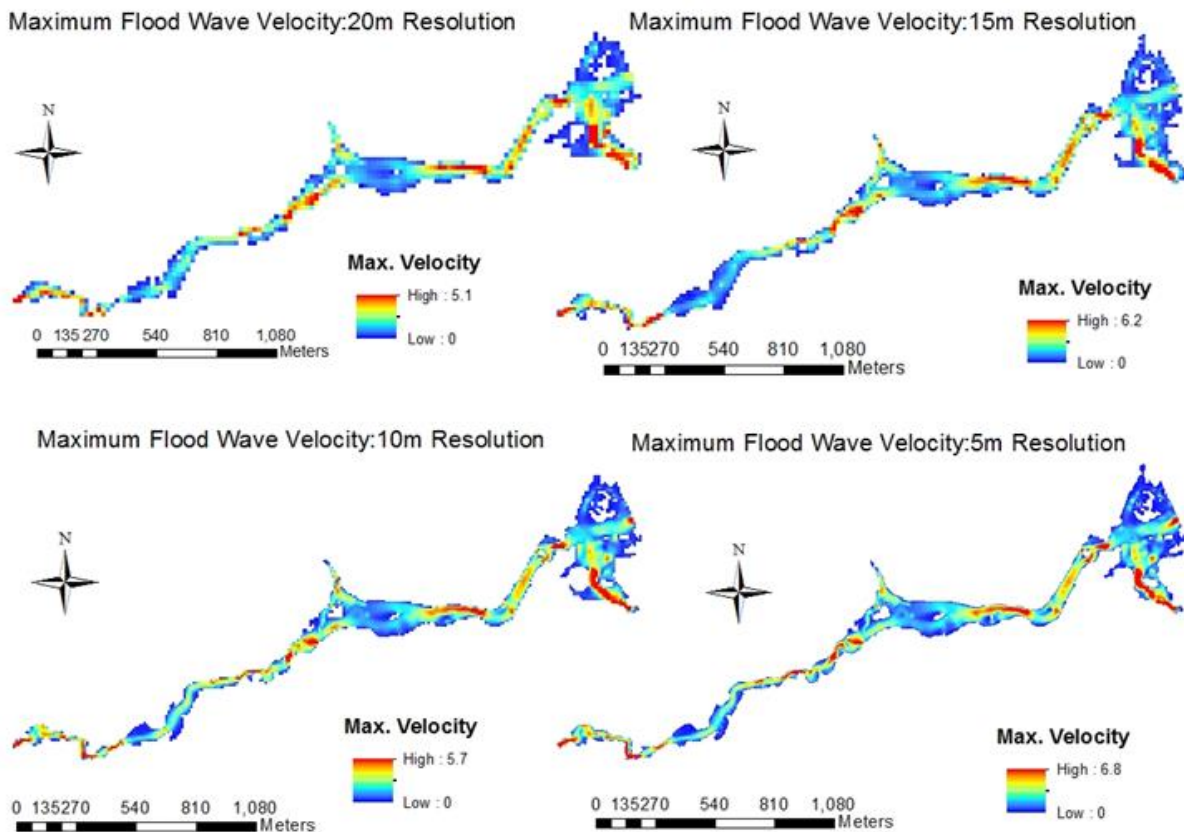
Figure 5.28: Maximum flood wave velocity map of 20m, 15m, 10m and 5m resolutions.

5.3.3. Effect of Road Representation

Roads function as conventional flow paths during the overtopping of river banks. To quantify the effect of roads on flood wave propagation, an additional 1D channel network was setup and linked to the existing river network. The link between the two channel networks and the interlocking road networks was made by the use of connection nodes. Unlike the river channel, the 1D road network profile is undulating following the topography of the study area. Moreover, part of the road was aligned to the foot of the hills resulting in an increased undulation. Hence to achieve a connectivity of the number of road-river and road-road crossings, profile interpolation of all the connecting networks was necessary. This was achieved by connection nodes. The use of connection nodes at road-river intersections was safe due to the fact that flow is merely governed by hydraulic gradient. This means that the downward flow of the river channel continues safely as the road profile was significantly elevated compared to the river bottom profile.

To examine the function of the 1D road network, the 1D river channel network was excluded and an artificial steady flow of 2m³/sec was introduced as the US boundary condition at the three uppermost road boundary nodes. As it is shown in Figure 5.29 below, the flow quickly turns to overland flow near the US road boundary nodes as a result of the road profile definition which generally was aligned to the surface topography. Once the overland flow occurred, it followed the steepest descent along the river channel all the way up to the DS boundary. The large column of water that accumulated at the DS boundary was for the reason that there was no 1D2D connection node at the DS boundary of the river channel to discharge the flow out of the model domain.
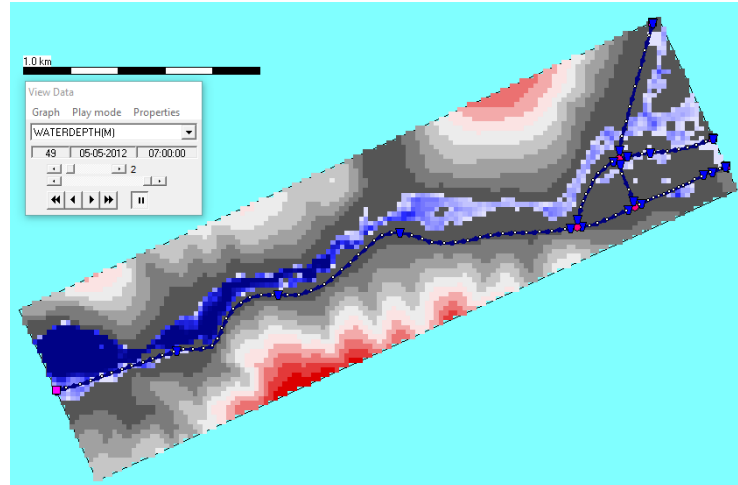
Figure 5.29: Snapshot of 1D road network test simulation.

After this initial test, the 1D road network was then coupled with the 1D river channel network and the actual boundary conditions of the river network were adopted. Since the connection nodes themselves function as calculation points, overtopping of the river channel at these nodes was conveyed along the 1D road network. This phenomenon was observed during the peak flows of the Mpazi drainage and Nyabugogo River. In such incidences, a significant volume of water was transported by the road network thereby affecting the flood wave propagation. Figure 5.30 below shows the SOBEK NETTER interface snapshot where the sections of the road that were activated as a result of the overtopping at the two road-river connection nodes (the activated road links are coloured blue). The peak flow from Mpazi drainage was found to be the largest contributor to the flow over the road network. This happens at the connection node located on the second culvert of the Mpazi drainage channel where the outlet of the culvert is blocked by accumulated sediment forcing the gushing flow to spread along the road network.

Figure 5.30: Snapshot of a zoomed-in road section during a combined 1D road and 1D river simulation.

The 1D2D model simulation of such road schematization resulted in the reduction of flood extent by slightly more than 1% and 0.7% for the 20m and 5m DEM resolutions respectively. No substantial change was observed on the flood depth. The introduction of the 1D road network significantly influenced the 2D lateral flood propagation around the central bus station in the 20m resolution. The effect of the road network on the flood extent was largely confined to the Nyabugogo central bus station area where a network of road-river intersection exists. Moreover, the relatively flat topography of this area facilitates the

transport of water over the road network. This effect does not propagate towards the downstream of the model domain as the road follows the foot of the hill which is mostly distant from the river course and also at higher elevation. Figure 5.31 shows the effect of 1D road network schematization around the Nyabugogo central bus station.
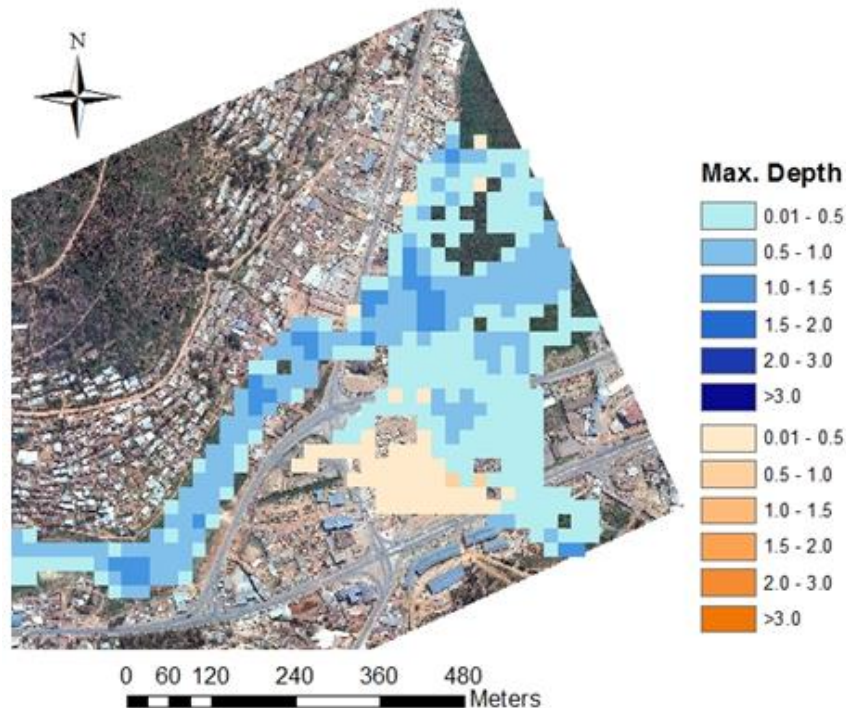
Figure 5.31: Section maximum depth map (in blue) with 1D road network schematization, overlaid on the maximum flood depth map of a normal DEM (in orange).

The effect of road in regulating urban flood wave propagation was further investigated by using the DTM of the study domain. As it is discussed in section 5.1.3 the DTM was prepared by raising the elevation of terrain features such as roads and building over the surface elevation defined by the DEM. To examine the effect of roads in particular, the building elevation was excluded from the DTM. Reasonably accurate road network representation was achieved by the 5m resolution and hence it was used to analyse the 1D2D model simulation results. As it is shown in the figure below a significant change was observed on the maximum depth map. The flood extent increased by almost 21% and the increase was mainly located around the central bus station area where the effect of the road network was more prevalent. The overall mean of the maximum flood depth increased by almost 50%. The elevated road surface clearly has blocked the lateral spread of flow overtopping the river banks thereby creating additional wet zones in the marshy riverine area with increased inundation depth as well. The maximum velocity hotspots were mostly intact except for the locations where large inundation depth was recorded (see Figure 5.32). The chart given on Figure 5.33 summarizes the effect of road under the different representations applied. Representation of road as a 1D channel network did not result in a significant change on flood depth and velocity. However, when the road elevation was added to the DEM, the flood depth increased by as large as 52% and hence a significant reduction in the flood wave velocity was also observed. Therefore, it is evident that an accurate representation of the road network in the DTM is critically important for 1D2D hydrodynamic urban flood simulation studies.
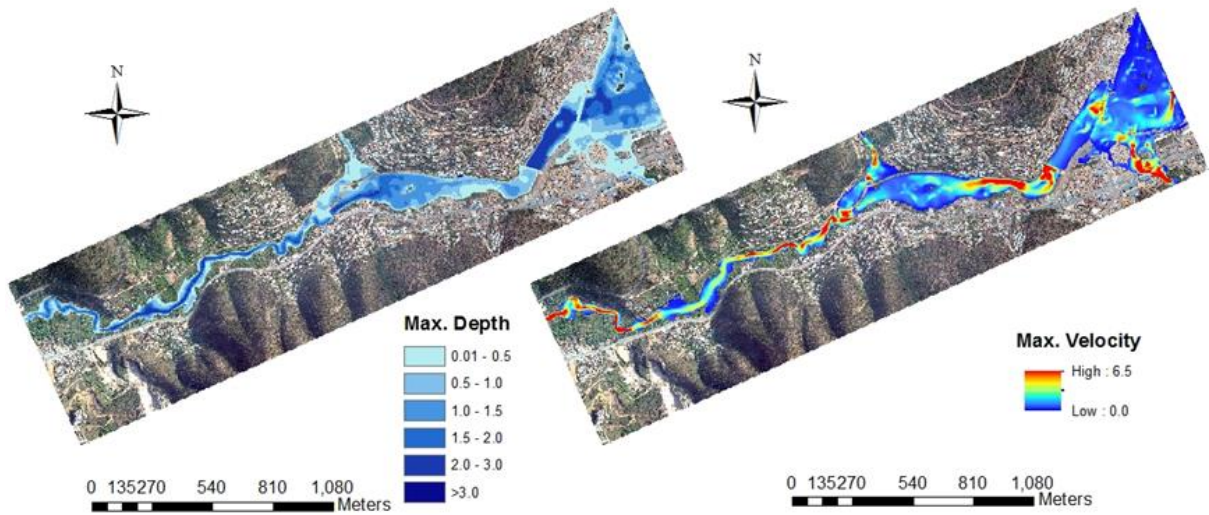
Figure 5.32: Maximum depth (left) and maximum velocity (right) maps when road is elevated over the DEM surface.
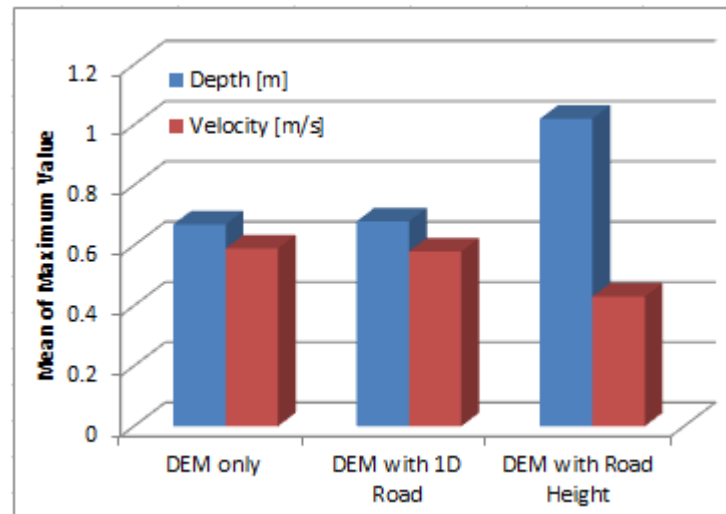
Figure 5.33: Effect of road representation on urban flood characteristics.

5.3.4. Effect of Building Representation

To properly understand flood wave propagation in urban topography appropriate representation of buildings and other surface structures is critical. Buildings alter the dynamics of flood wave propagation by resisting, storing and conveying overland flow. One technique to address this effect of buildings is to assign high surface roughness values that will retard flow over 2D grid cells that are assigned as building pixels. Three different representations of the surface roughness were tested; solid, partially solid and hollow (see section 4.5). When buildings are represented as solid objects, largest surface roughness value (Manning's coefficient= 1.0) is assigned to represent the resistance to flow. Moreover, the elevation of the building pixels is raised to the height of the building (Haile and Rientjes, 2005) so that the physical representation of the solid object is achieved. Under such conditions the overland flow is blocked and starts to accumulate until it eventually finds its way around the building. While the blocking causes the inundation depth to raise, the change of direction results in a change of the flood wave velocity. Moreover, in complex urban environments where buildings are mostly dense, representation of buildings as solid objects significantly affects the flood extent too. This is caused when the elevated building pixels force the flow to change its direction to extend to neighbouring pixels.

The second representation is to treat buildings as partially solid objects. In this case buildings do not block the flow (as their elevation is not raised), rather they delay the flow by storing it and releasing it later on. To enable this function a moderately high surface roughness value was assigned. This technique has an implication on both flood depth and extent as the flood wave is temporarily kept in the building pixel. When a surface roughness value equivalent to the neighbouring pixel is used on the building pixels, the building is represented as a hollow object. Here no distinction occurs between building and other pixels in terms of storage and conveyance of the flood water and hence no specific effect of the buildings occur on the flood characteristics. Figure 5.34 shows the simulation results of the three building representations at 5m resolution. Maximum depth was observed when buildings were represented as solid objects while the maximum inundation extent and maximum flood wave propagation were observed in the partially-solid representation. A similar result is reported by other studies including Manyifika (2015) and Haile (2005).
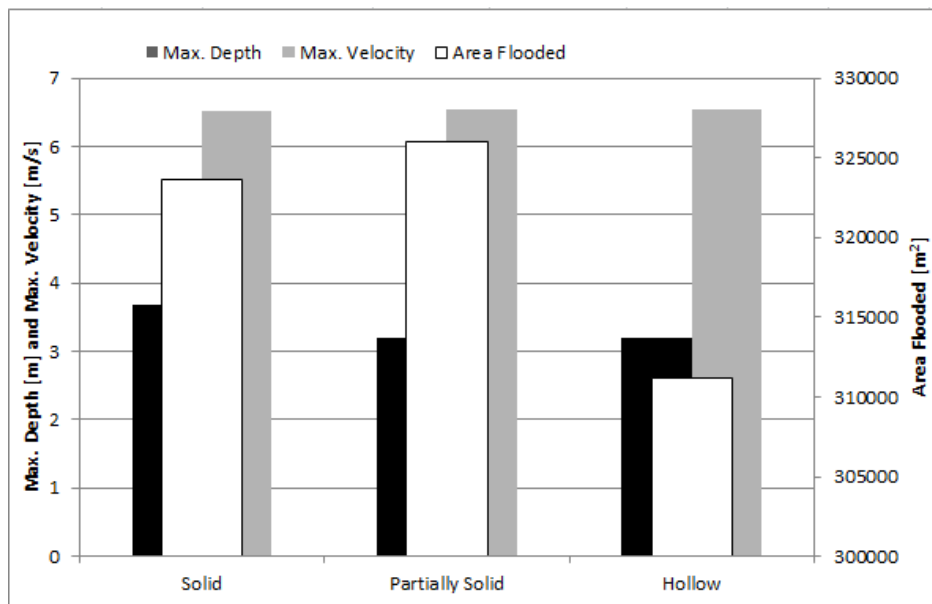
Figure 5.34: Summary of simulation results for the different types of building representation.

Most of the buildings in the Nyabugogo commercial hub (and in particular around the central bus station) were concrete structures as observed during the field work. In reality, a flood wave finds its way in to the building under door/window openings and hence potentially a large volume of water is stored inside buildings. In addition, when the flood wave encounters the wall of a building a vertical friction arises which depends on the type/material of the building wall. To accurately model detailed urban flood propagation by incorporating the flood water-building interaction requires a detailed analysis of roughness coefficients and hence a large sum of data will be needed. In this study however, this aspect was ignored and all buildings were treated as simple solid structures with no vertical friction.

To understand the effect of raising the building pixel elevation to the measured building height a, a simulation was run by using the DEM including the building height. Following the discussion of section 5.2.2., the comparison of flood extent and maximum flood depth was made using the 5m resolution as it properly represents the dimension of most of the buildings in the study area. As shown in Figure 5.35 below, a nearly 3% increase of flood extent occurred when the building elevation was raised which completely inundated the central bus station and even extended further as shown by the red circle. Take note also that the maximum flood depth map on the right (i.e. the DEM without the building height)

inundated pixels representing buildings on the ground, clearly fails short of simulating a realistic flood wave propagation of the urban neighbourhood where buildings themselves are not inundated but rather surrounded by the inundation. The simulation using DEM merged with the building height, however, modelled such condition thereby resulting in a more realistic flood inundation of urban environments (example is indicated by the red arrows on Figure 5.35).
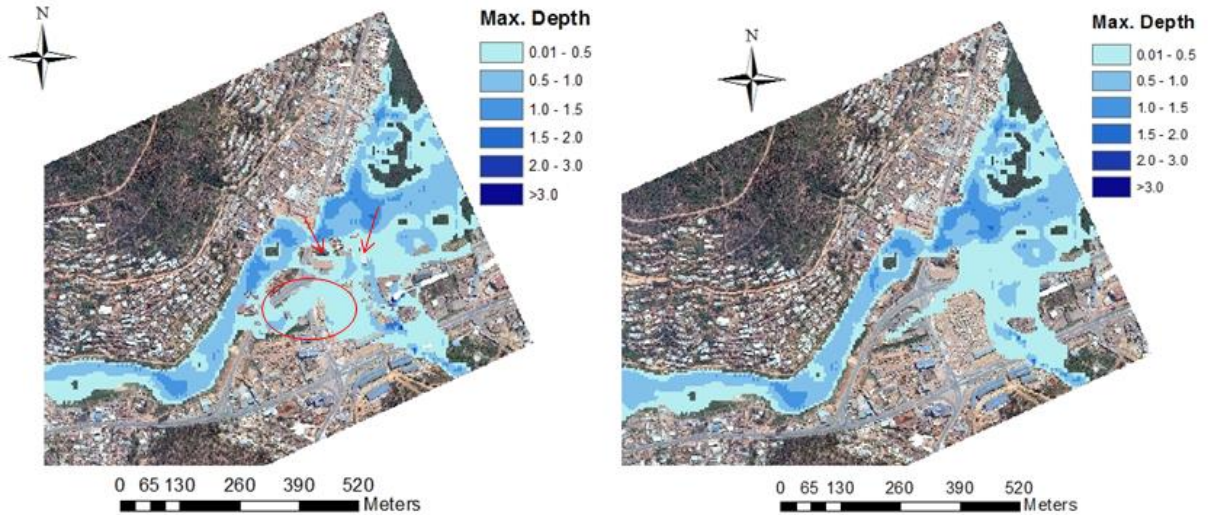
Figure 5.35: Maximum flood map: DEM + building height (left) and DEM only (right) at 5m resolution.

Finally, the combined effect of buildings and roads in defining the flood wave propagation of the Nyabugogo commercial hub was investigated by using the detailed digital terrain model (see section 5.1.3.). The river elevation layer was however decoupled from the DTM for the reason that both the river bottom and river bank elevations were fed into the 1D river channel network as cross section profile definitions. Hence, once an overtopping of the 1D channel network occurs it will wet the pixels representing the river banks, the elevation of which is already accounted for by the base DEM used. Moreover, the 1D road network (represented as 1D channel network) was also removed to allow for the complete effect of raised road elevation of the DTM.
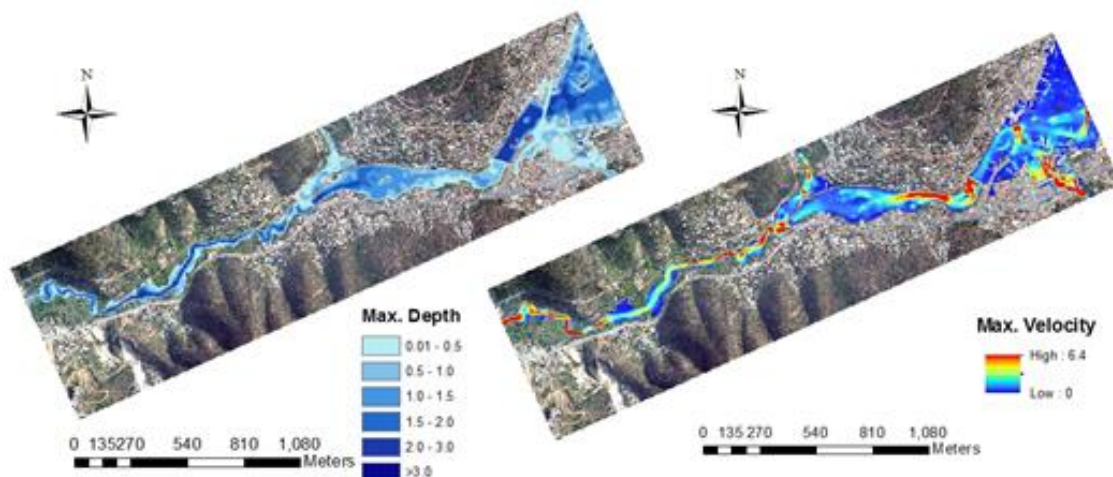
Figure 5.36: Maximum flood depth (left) and maximum flood wave velocity (right) at 5m DTM resolution.

It is clear from Figure 5.36 that the combined effect of buildings and roads in the form of DTM resulted in an increased inundation extent. Compared to the flood characteristics observed when only the DEM was used, at 5m DTM resolution, the flood extent increased by as large as 23% and also the mean of the maximum flood depth increased by 51%. As a result the mean of the maximum velocity also dropped by 25%. The representation of buildings and road as elevated surfaces in a detailed DTM introduces a substantial change to the flood characteristics of complex urban environments. Hence, it can be concluded that the use of a detailed DTM, where components of the urban terrain are accurately represented, is fundamental to reliable modelling of flooding in complex urban environments such as that of the Nyabugogo commercial hub.

5.3.5. Sensitivity Analysis

For the sensitivity analysis only the 20m DEM was used and a fixed surface roughness was assigned. The sensitivity of the flood model for surface roughness was however analysed by (Manyifika, 2015) which revealed that the model is highly sensitive to the channel bottom friction. Sensitivity of the model for DS boundary condition was first analysed. The specified head DS boundary was progressively raised and lowered to see how much the effect will propagate in to the flood model domain.
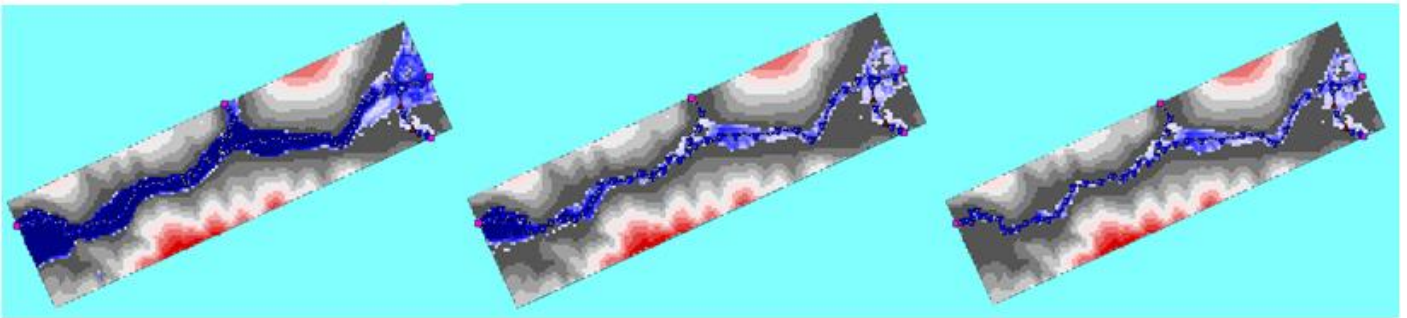
Figure 5.37: DS boundary condition sensitivity, maximum flood depth maps (+10m, +5m and +1m difference with the model domain resp.)

The specified stage was first raised to a difference of 10m from the last model domain elevation. As it is shown in Figure 5.37 above, the large column of water immediately started to flood the model domain. This is the result of the large negative hydraulic gradient that is created between the model domain and the outside boundary node. Then stage was raised to 5m difference which avoided the back flow of water but still created hindrance to the free flow causing inundation around the DS boundary. The inundation at the DS boundary disappeared when the downstream boundary node stage was raised to a difference of only 1m as shown on Figure 5.37-right. The positive hydraulic gradient in the direction of flow enabled a free flow discharge of the river channel.

The effect of DS boundary condition under four specific head definitions is shown in Figure 5.38. The elevation head inside the model domain at the downstream boundary was 1361.83m. For the first two cases (i.e. for 1m above the elevation head inside the model domain and at the same level, respectively), the effect disappeared within a 300m length. However, when a lower DS head is specified no effect propagates back to the model domain as the flow is completely discharged by free flow. Hence, it can be concluded that the effect of DS boundary condition is so minimal that it can be safely ignored. Moreover, in this specific study the major inundation happens close to the upstream boundary condition around the Nyabugogo central bus station. In general, for urban flood modelling it is advisable to select a DS boundary further away from the model domain so as to avoid any DS effect propagation in to the model domain.
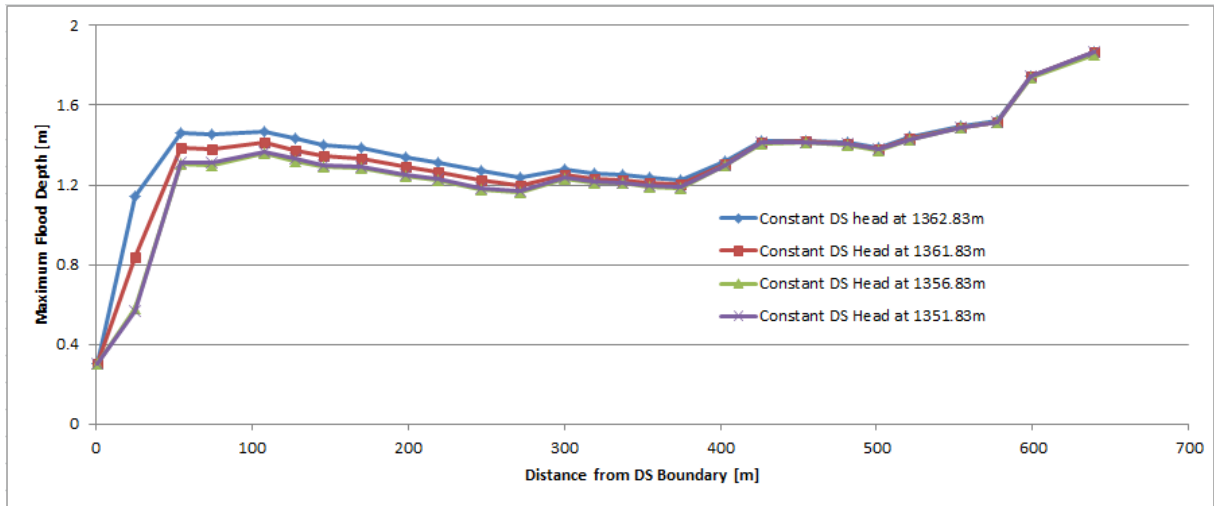
Figure 5.38: Sensitivity to downstream boundary condition.

The model sensitivity for upstream boundary condition was also tested by progressively varying the US boundary discharge hydrograph from 25% to 200%. Expectedly the maximum flood depth increased with the increase in the boundary inflow however the rate was not proportional to the rate of boundary flow increase. In fact a small decline on the rate of maximum depth increase was observed. This is because with the increase in flow, new 2D grids become wet and the inundation might increase rather spatially. The Nyabugogo river channel is already full by the base flow that only 25% of the upstream discharge hydrograph causes a maximum inundation of more than two meters and a similar effect is also observed on the flood extent. The resulting flood characteristics with the change of the upstream boundary inflow is summarised in Table 5.11 below.

Table 5.11: Sensitivity to upstream boundary condition.

US Boundary Flow	Maximum Depth [m]		Maximum Velocity [m/s]		Inundated Area [m²]
	Max	Mean	Max	Mean	
BC=25%	2.3	0.44	2.8	0.29	224400
BC=50%	2.6	0.55	3.3	0.42	268400
BC=75%	2.8	0.63	4.8	0.49	306000
BC=100%	3.1	0.70	5.1	0.55	330400
BC=150%	3.4	0.80	6.0	0.63	370800
BC=200%	3.6	0.89	5.5	0.67	403200

5.3.6. ASTER and SRTM for 1D2D Modelling

The unprocessed 30m resolution DEM of ASTER and SRTM was finally used to represent topography in the 1D2D hydrodynamic flood modelling. Figure 5.39 below shows the maximum flood depth map. It can be clearly observed that both ASTER and SRTM DEMs did not produce the expected flood simulation results. The inundations are concentrated on specific locations and the flood extent also did not show a systematic propagation with respect to the river. Flood extent reduced by 23% and 29% when the ASTER and SRTM DEMs were used as compared to the local DEM at 30m resolution. Most of the inundated area coincided with the observed sink (see Figure 5.17) in both satellite based DEMs. Moreover SRTM also failed to capture the major inundation area just above the confluence of Nyabugogo and

Yanze River. From these observations, it can be concluded that for this specific study area the use of ASTER and SRTM DEM in a 1D2D hydrodynamic model without applying appropriate corrections will give erroneous flood characteristics. Moreover the course 30m resolution of these satellite based elevation products clearly missed important topographic details making it more difficult for the application of detailed urban flood modelling. As the base elevation these unprocessed satellite based DEMs define was flawed, it was not possible to incorporate and test the effect of road and building elevations on a 1D2D hydrodynamic flood model simulation. Studies such as Jarihani et al., (2015) have shown that upon the appropriate corrections both products could give an acceptable flood inundation characteristics, especially for large scale applications. It is hence recommended to apply corrections such as vegetation smoothing and hydro-processing before use is made in hydrodynamic modelling.
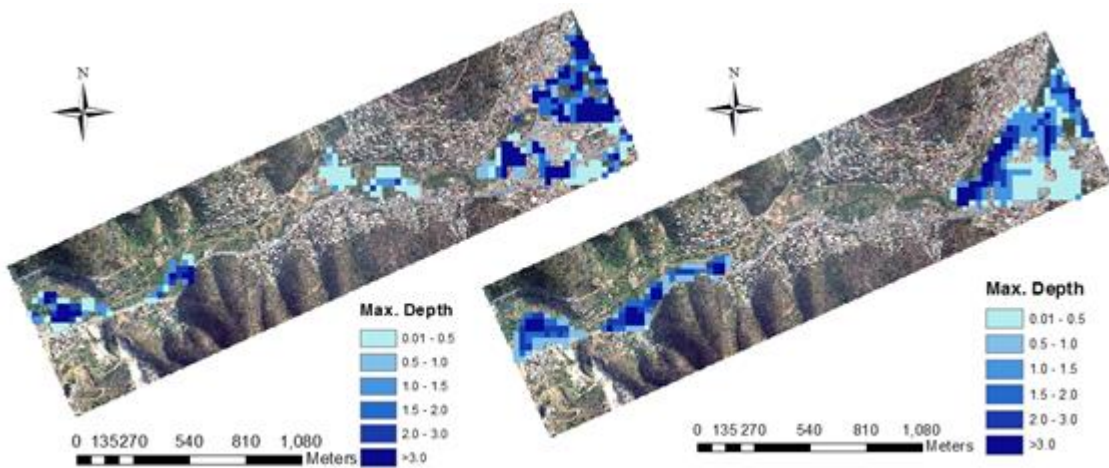

Figure 5.39: Maximum flood depth map of ASTER (left) and SRTM (right) at 30m resolution.

6.   CONCLUSION AND RECOMMENDATIONS

6.1.   Conclusion

Understanding the behaviour of urban flood wave propagation requires determining the role of urban terrain features in regulating the overland flow. In complex urban environments, buildings and roads in particular govern the flood characteristics. Hence, accurate representation of these terrain features largely determines the accuracy of food model simulation results. Recent advancements in remote sensing technology resulted in techniques that enable the replication of urban terrain with high resolution remote sensing imagery. LiDAR data is a typical example of this. However, such datasets are not always available and involve huge cost that most local authorities do not afford. Hence, alternative techniques should be developed to supplement the topographic data requirement of flood simulation models.

In this study, a locally available 10m × 10m elevation grid was used to define a base elevation DEM. Road profile and building height were obtained from field measurements and merged with the DEM to generate a detailed digital terrain model of the Nyabugogo commercial hub, Kigali, Rwanda. Unprocessed and freely available satellite based DEM, namely ASTER and SRTM were also examined as surrogate topographic data. These elevation dataset were used to provide topographic representation for the 1D2D flood model simulation by SOBEK software.

As mentioned above, accurate representation of topography is fundamental for accurate flood model simulation. Hence, emphasis was given for the construction of a detailed urban terrain model. Generating the profile of road network was a challenging task in this regard as most of the roads in the study area were not in alignment with the raster grid adopted by the flood model. Establishing appropriate connectivity, hence, was of high significance to conceptualize the function of roads in transporting the overland flow of water. Similarly, the representation of the different shape and alignment of buildings, which are represented as pixels raised to their approximate height as measured in the field, was also challenging.

Four model resolutions were adopted in this study; 5m, 10m, 15m and 20m. The finer resolutions were able to produce sufficient representations whereas significant inaccuracies were observed with the increase in grid size (especially 15m and 20m). When merging the different elevation layers to setup the DTM, a significant overlaps of the terrain features was observed in the 20m resolution, for instance. Such artefacts limit the optimum representation of the complex urban environment, thereby affecting the flood wave propagation in the model simulations.

In this study, comparison of ASTER and SRTM DEM was made with reference point elevations and against the local DEM. The freely available global elevation datasets of ASTER and SRTM are alternative sources of topographic information which are critically important when other sources of elevation data are not available. The accuracy assessment of these elevation datasets in representing the Nyabugogo commercial hub revealed several artefacts, similar to the findings of other studies. A significant difference in the slope and aspect of these DEMs as compared to the local DEM was a major concern as it governs the overland flow after overtopping the river banks. Though it was not addressed in this study, appropriate corrections of these satellite based products is necessary for use in urban flood modelling studies.

The causes for the unrealistic inundation of the downstream and other locations along the course of Nyabugogo River were investigated and mitigations were introduced in terms of adjusting the downstream boundary stage and river bottom undulation corrections. These changes removed excessive inundations that were the mere consequences of the model inputs and setups applied. The river bottom profile was manually corrected by applying linear interpolation on the measured elevations of the cross sections. However, for optimal simulation results, care should be taken to accurately represent river bottom profile.

The reliability of the 1D2D hydrodynamic flood model was tested by simulating steady state low and high flow conditions. The model's sensitivity to upstream and downstream boundary conditions was also investigated. It was found that the downstream boundary effect did not propagate to the model domain. However, in conditions where this is not the case SOBEK 1D2D allows to extend the 1D channel network further downstream of the model domain so that the effect of such downstream boundary condition could be safely excluded.

The major limitation of the study was the unavailability of observed flood data to calibrate and validate the model. The available flood depth data were very few and had no relation to the peak rainfall event analysed. Surface roughness values of literature were used to define the Manning's coefficient. To evaluate the effect of buildings, a distributed roughness coefficient (for six land cover classes) was used for conditions of solid, partially solid and hollow building representations. In agreement to previous findings, maximum flood depth and extent were observed when buildings were represented as solid and partially solid, respectively.

To examine the effect of the road network in transporting overland flow, a 1D channel approach was tested to represent the road network. Depending on the hydraulic gradient flood water started to travel along the road network once it overtopped the river channel at the point of road-river confluence. This is the phenomenon that actually happens in reality. Moreover, the use of the detailed DTM in the 1D2D flood model resulted in an increased flood depth and extent. This increase was observed mostly around the central bus station area where a network of roads and dense buildings were present. Pixels representing buildings were not flooded and hence the overland flow extended towards neighbouring pixels around buildings. The flood wave propagation velocity on the other hand decreased as it was encountered by buildings.

Overall, a reasonable representation of the complex urban environment of Nyabugogo commercial hub was achieved through the development of a detailed DTM. The use of this DTM in a 1D2D hydrodynamic flood modelling resulted in a significant change of the flood characteristics as compared to the results simulated by using only the base DEM. A satellite derived forcing data (CMORPH 8km × 30min) prepared by Manyifika (2015) was adopted in this study as the upstream boundary condition. A detailed topographic representation of the study area was developed and a reliable 1D2D hydrodynamic model was setup, hence this study can be used for further flood modelling analysis using high resolution forcing data for optimum simulation results.

6.2. Recommendations

- The development of a detailed digital terrain model from field measurement is a laborious task and prone to manual error. Moreover, feasibility of measuring small scale topographic details is also limited, for example, measuring road side curbs. High resolution remote sensing technologies

such as LiDAR and IfSAR overcome this difficulty and provide accurate representation of complex urban topography. It is hence recommended to use such topographic dataset for high resolution hydrodynamic flood modelling.

- In modelling urban flood inundation, buildings block the flood wave propagation and subsequently the flood depth increases thereby a vertical friction is created between the column of water and the building wall. Different types of buildings exert different friction. Hence to accurately model the effect of buildings on flood characteristics, it is advisable to assign appropriate building specific vertical friction values.

- Appropriate correction including vegetation smoothing, hydrological processing should be applied before using satellite based topographic data such as ASTER and SRTM DEM for urban flood modelling,

LIST OF REFERENCES

Aktaruzzaman, M., & Schmitt, T. G. (2009). *Detailed digital surface model generation and automatic object detection to facilitate modelling of urban flooding. ISPRS Workshop.* Hannover. Retrieved from http://www.siwawi.arubi.uni-kl.de/index2_2011.php?link=aktaruzzaman&lang=en

Bates, P. D., & De Roo, A. P. J. (2000). A simple raster based model for flood inundation simulation. *Journal of Hydrology*, *236*(1-2), 54–77.

Baugh, C. a., Bates, P. D., Schumann, G., & Trigg, M. a. (2013). SRTM vegetation removal and hydrodynamic modeling accuracy. *Water Resources Research*, *49*(9), 5276–5289. http://doi.org/10.1002/wrcr.20412

Bizimana, J. P., & Schilling, M. A. (2010). Geo-Information Technology for Infrastructural Flood Risk Analysis in Unplanned Settlements: A Case Study of Informal Settlement Flood Risk in the Nyabugogo Flood Plain, Kigali City, Rwanda. In P. S. Showalter & Y. Lu (Eds.), *Geospatial Techniques in Urban Hazard and Disaster Analysis* (Vol. 2, pp. 51–69). Dordrecht: Springer. http://doi.org/10.1007/978-90-481-2238-7

Bladé, E., Gómez-Valentín, M., Dolz, J., Aragón-Hernández, J. L., Corestein, G., & Sánchez-Juny, M. (2012). Integration of 1D and 2D finite volume schemes for computations of water flow in natural channels. *Advances in Water Resources*, *42*, 17–29. http://doi.org/10.1016/j.advwatres.2012.03.021

Bourgine, B., & Baghdadi, N. (2005). Assessment of C-band SRTM DEM in a dense equatorial forest zone. *Comptes Rendus Geoscience*, *337*(14), 1225–1234. http://doi.org/10.1016/j.crte.2005.06.006

Chen, A. S., Evans, B., Djordjević, S., & Savić, D. a. (2012). A coarse-grid approach to representing building blockage effects in 2D urban flood modelling. *Journal of Hydrology*, *426-427*, 1–16. http://doi.org/10.1016/j.jhydrol.2012.01.007

Chen, J., Hill, A. A., & Urbano, L. D. (2009). A GIS-based model for urban flood inundation. *Journal of Hydrology*, *373*(1-2), 184–192. http://doi.org/10.1016/j.jhydrol.2009.04.021

Colosimo, G., Crespi, M., De Vendictis, L., & Jacobsen, K. (2009). Accuracy evaluation of SRTM and ASTER DSMs. In *29th EARSeL Symposium* (p. 9). Chania, Greece.

Costabile, P., Macchione, F., Natale, L., & Petaccia, G. (2015). Flood mapping using LIDAR DEM. Limitations of the 1-D modeling highlighted by the 2-D approach. *Natural Hazards*, *77*(1), 181–204. http://doi.org/10.1007/s11069-015-1606-0

Delft/Hydraulics. (2014). *SOBEK 2.12: User's Manual.* The Netherlands.

Di Baldassarre, G. (2012). *Floods in a Changing Climate : Inundation Modelling.* Cambridge: Cambridge University Press.

Downing, T., Watkiss, P., & Dyszynski, J. (2009). *Economics of Climate Change in Rwanda.* Stockholm, Sweden: Stockholm Environment Institute.

Dutta, D., Herath, S., & Musiake, K. (2003). A mathematical model for flood loss estimation. *Journal of Hydrology*, *277*(1-2), 24–49. http://doi.org/10.1016/S0022-1694(03)00084-2

Frey, H., & Paul, F. (2011). On the suitability of the SRTM DEM and ASTER GDEM for the compilation of: Topographic parameters in glacier inventories. *International Journal of Applied Earth Observation and Geoinformation*, *18*(1), 480–490. http://doi.org/10.1016/j.jag.2011.09.020

Gilles, D. W. (2010). *Application of numerical models for improvement of flood preparedness.* MSc Thesis, University of Iowa. Retrieved from http://ir.uiowa.edu/cgi/viewcontent.cgi?article=1858&context=etd

Grohmann, C. H. (2015). Effects of spatial resolution on slope and aspect derivation for regional-scale analysis. *Computers & Geosciences*, *77*, 111–117. http://doi.org/10.1016/j.cageo.2015.02.003

Guo, Q., Li, W., Yu, H., & Alvarez, O. (2010). Effects of topographic variability and Lidar sampling density on several DEM interpolation methods. *Photogrammetric Engineering & Remote Sensing*, *76*(6), 701–712.

Haile, A. T. (2005). *Integrating Hydrodynamic Models and High Resolution DEM (LIDAR) for Flood Modelling.* MSc Thesis, University of Twente Faculty of Geo-Information and Earth Observation (ITC). Retrieved from http://www.itc.nl/library/papers_2005/msc/wrem/haile.pdf

Haile, A. T., & Rientjes, T. H. M. (2005). *Effects of LiDAR DEM resolution in flood modelling: A model sensitivity study for the city of Tegucia-galpa, Honduras. Proceedings of ISPRS Workshop Laser Scanning 2005.* Enschede. Retrieved from http://www.isprs.org/proceedings/XXXVI/3-W19/

Hénonin, J., Russo, B., Mark, O., & Gourbesville, P. (2013). Real-time urban flood forecasting and modelling – a state of the art. *Journal of Hydroinformatics*, *15*(3), 717. http://doi.org/10.2166/hydro.2013.132

Hénonin, J., Russo, B., Roqueta, D. S., Sanchez-, R., Donna, N., Domingo, S., ... Mark, O. (2010). Urban flood real-time forecasting and modelling : a state-of-the-art review. In *MIKE by DHI Conference* (pp. 6–8). Copenhagen.

Horritt, M. S., & Bates, P. D. (2001). Effects of spatial resolution on a raster based model of food flow. *Journal of Hydrology*, *253*, 239–249. http://doi.org/10.1016/S0022-1694(01)00490-5

Horritt, M. S., & Bates, P. D. (2002). Evaluation of 1D and 2D numerical models for predicting river flood inundation. *Journal of Hydrology*, *268*(1-4), 87–99. http://doi.org/10.1016/S0022-1694(02)00121-X

Horritt, M. S., Di Baldassarre, G., Bates, P. D., & Brath, A. (2007). Comparing the performance of a 2-D finite element and a 2-D finite volume model of floodplain inundation using airborne SAR imagery. *Hydrological Processes*, *21*(20), 2745–2759. http://doi.org/10.1002/hyp.6486

Hunter, N. M., Bates, P. D., Horritt, M. S., & Wilson, M. D. (2007). Simple spatially-distributed models for predicting flood inundation: A review. *Geomorphology*, *90*(3-4), 208–225. http://doi.org/10.1016/j.geomorph.2006.10.021

Jarihani, A. a., Callow, J. N., McVicar, T. R., Van Niel, T. G., & Larsen, J. R. (2015). Satellite-derived Digital Elevation Model (DEM) selection, preparation and correction for hydrodynamic modelling in large, low-gradient and data-sparse catchments. *Journal of Hydrology*, *524*, 489–506. http://doi.org/10.1016/j.jhydrol.2015.02.049

Koriche, S. A. (2012). *Remote Sensing Based Hydrological Modelling for Flood Early Warning in the Upper and Middle Awash River Basin*. MSc Thesis, University of Twente Faculty of Geo-Information and Earth Observation (ITC). Retrieved from http://www.itc.nl/library/papers_2012/msc/wrem/koriche.pdf

Mani, P., Chatterjee, C., & Kumar, R. (2013). Flood hazard assessment with multiparameter approach derived from coupled 1D and 2D hydrodynamic flow model. *Natural Hazards*, *70*(2), 1553–1574. http://doi.org/10.1007/s11069-013-0891-8

Manyifika, M. (2015). *Diagnostic assessment on urban floods using satellite data and hydrologic models in Kigali, Rwanda*. MSc Thesis-University of Twente: Faculty of Geo-Information Science and Earth Observation (ITC). Retrieved from http://www.itc.nl/library/papers_2015/msc/wrem/manyifika.pdf

Mason, D. C., Giustarini, L., Garcia-Pintado, J., & Cloke, H. L. (2014). Detection of flooded urban areas in high resolution Synthetic Aperture Radar images using double scattering. *International Journal of Applied Earth Observation and Geoinformation*, *28*, 150–159. http://doi.org/10.1016/j.jag.2013.12.002

Md Ali, A., Solomatine, D. P., & Di Baldassarre, G. (2015). Assessing the impact of different sources of topographic data on 1-D hydraulic modelling of floods. *Hydrology and Earth System Sciences*, *19*(1), 631–643. http://doi.org/10.5194/hess-19-631-2015

Meesuk, V., Vojinovic, Z., Mynett, A. E., & Abdullah, A. F. (2014). Urban flood modelling combining top-view LiDAR data with ground-view SfM observations. *Advances in Water Resources*, *75*, 105–117. http://doi.org/10.1016/j.advwatres.2014.11.008

Mukherjee, S., Joshi, P. K., Mukherjee, S., Ghosh, A., Garg, R. D., & Mukhopadhyay, A. (2012). Evaluation of vertical accuracy of open source Digital Elevation Model (DEM). *International Journal of Applied Earth Observation and Geoinformation*, *21*(1), 205–217. http://doi.org/10.1016/j.jag.2012.09.004

Patro, S., Chatterjee, C., Singh, R., & Raghuwanshi, N. S. (2009). Advanced Bash-Scripting Guide An in-depth exploration of the art of shell scripting Table of Contents. *Okt 2005 Abrufbar Uber Httpwww Tldp orgLDPabsabsguide Pdf Zugriff 1112 2005*, *2274*(November 2008), 2267–2274. http://doi.org/10.1002/hyp

Rahman, A. (2006). *Digital surface model (DSM) construction and flood hazard simulation for Development Plans in Naga City, Philippines*. MSc Thesis-University of Twente: Faculty of Geo-Information Science and Earth Observation (ITC). Retrieved from http://www.itc.nl/library/papers_2006/msc/ereg/rahman.pdf

REMA. (2013). *Rwanda State of Environment and Outlook Report*. Kigali, Rwanda: Rwanda Environment Management Authority.

Research and Public Awareness Unit/MIDIMAR. (2012). *Identification of Disaster Higher Risk Zones on Floods and Landslides in Rwanda*. Kigali, Rwanda: Ministry of Disaster Management And Refugee Affairs.

Rientjes, T. (2014). Modelling in Hydrology (Lecture Notes), (Water REsources and Environmental Management. ITC/University of Twente).

Schubert, J. E., & Sanders, B. F. (2012). Building treatments for urban flood inundation models and implications for predictive skill and modeling efficiency. *Advances in Water Resources*, *41*, 49–64. http://doi.org/10.1016/j.advwatres.2012.02.012

SWEDESURVEY. (2010). *Project Rwanda National Land Use and Development Master Plan. Report for Production of ortho photo in Rwanda.*

Syme, W. J. (2008). Flooding in Urban Areas-2D Modelling Approaches for Buildings and Fences. In *9th National Conference on Hydraulics in Water Engineering* (pp. 23–26). Darwin, Australia.

Tarekegn, T. H., Haile, A. T., Rientjes, T., Reggiani, P., & Alkema, D. (2010). Assessment of an ASTER-generated DEM for 2D hydrodynamic flood modeling. *International Journal of Applied Earth Observation and Geoinformation*, *12*(6), 457–465. http://doi.org/10.1016/j.jag.2010.05.007

Tennakoon, K. B. M. (2004). *Parametrization of 2D Hydrodynamic Models and Flood Hazard Mapping for Naga City, Philippines.* Retrieved from http://www.itc.nl/library/papers_2004/msc/upla/tennakoon.pDF

Thomas, J., Joseph, S., Thrivikramji, K. P., & Arunkumar, K. S. (2014). Sensitivity of digital elevation models: The scenario from two tropical mountain river basins of the Western Ghats, India. *Geoscience Frontiers*, *5*(6), 893–909. http://doi.org/10.1016/j.gsf.2013.12.008

Tighe, M., & Chamberlain, D. (2009). Accuracy Comparison of the SRTM, ASTER, NED, NEXTMAP® USA Digital Terrain Model over Several USA Study Sites. In *ASPRS/MAPPS 2009 Fall Conference*. San Antonio, Texas. Retrieved from http://info.asprs.org/publications/proceedings/sanantonio09/Tighe_2.pdf

Tsinda, A., & Gakuba, A. (2010). Sustainable Hazards Mitigation in Kigali City (Rwanda). In *46th ISOCARP Congress* (pp. 1–11).

van de Sande, B., Lansen, J., & Hoyng, C. (2012). Sensitivity of Coastal Flood Risk Assessments to Digital Elevation Models. *Water*, *4*(3), 568–579. http://doi.org/10.3390/w4030568

Vaze, J., Teng, J., & Spencer, G. (2010). Impact of DEM accuracy and resolution on topographic indices. *Environmental Modelling and Software*, *25*(10), 1086–1098. http://doi.org/10.1016/j.envsoft.2010.03.014

Wang, C., Wan, T. R., & Palmer, I. J. (2010). Urban flood risk analysis for determining optimal flood protection levels based on digital terrain model and flood spreading model. *The Visual Computer*, *26*(11), 1369–1381. http://doi.org/10.1007/s00371-009-0414-5

WMO. (2013). The Global Climate 2001–2010: A Decade of Climate Extremes Summary Report, (1119), 20. http://doi.org/WMO-No. 1119 THE - ISBN: 978-92-631-1119-7

Yu, D., & Coulthard, T. J. (2015). Evaluating the importance of catchment hydrological parameters for urban surface water flood modelling using a simple hydro-inundation model. *Journal of Hydrology*, *524*, 385–400. http://doi.org/10.1016/j.jhydrol.2015.02.040

ANNEXES

Annex 1: Upstream discharge hydrograph.

Date[dd/mm/yyyy]	Time[hh:mm:ss]	Discharge[m3/s]		
		Nyabugogo	Mpazi	Yanze
4/5/2012	7:00:00	3.8	0	1.7
4/5/2012	7:30:00	3.8	0	1.7
4/5/2012	8:00:00	3.8	0	1.7
4/5/2012	8:30:00	3.8	0	1.7
4/5/2012	9:00:00	3.8	0	1.7
4/5/2012	9:30:00	3.8	0	1.7
4/5/2012	10:00:00	3.8	0	1.7
4/5/2012	10:30:00	3.8	0	1.7
4/5/2012	11:00:00	3.8	0	1.7
4/5/2012	11:30:00	3.8	0	1.7
4/5/2012	12:00:00	3.8	0	1.7
4/5/2012	12:30:00	4	0	1.7
4/5/2012	13:00:00	5.2	12	1.8
4/5/2012	13:30:00	7	3.7	1.8
4/5/2012	14:00:00	8.2	0.8	1.9
4/5/2012	14:30:00	7	0.2	1.9
4/5/2012	15:00:00	6	0	1.9
4/5/2012	15:30:00	5.2	0	1.9
4/5/2012	16:00:00	4.6	0	1.8
4/5/2012	16:30:00	4.2	0	1.8
4/5/2012	17:00:00	4.1	0	1.8
4/5/2012	17:30:00	4	0	1.8
4/5/2012	18:00:00	3.9	0	1.8
4/5/2012	18:30:00	3.9	0	1.7
4/5/2012	19:00:00	4.2	8.9	1.7
4/5/2012	19:30:00	6.1	29.8	1.7
4/5/2012	20:00:00	8.7	25.8	1.8
4/5/2012	20:30:00	8.9	7.1	1.8
4/5/2012	21:00:00	7.4	1.5	1.8
4/5/2012	21:30:00	5.8	0.3	1.8
4/5/2012	22:00:00	4.9	0	1.8
4/5/2012	22:30:00	4.7	0	1.8
4/5/2012	23:00:00	11.6	0	1.8
4/5/2012	23:30:00	24	0	3.3
5/5/2012	0:00:00	25.4	0	6.8
5/5/2012	0:30:00	20.3	0	8.5
5/5/2012	1:00:00	13.9	0	7.5
5/5/2012	1:30:00	9.1	0	5.3
5/5/2012	2:00:00	6.7	0	3.8
5/5/2012	2:30:00	5.5	0	3
5/5/2012	3:00:00	4.7	0	2.5
5/5/2012	3:30:00	4.4	0	2.2
5/5/2012	4:00:00	4.1	0	2
5/5/2012	4:30:00	4	0	1.9
5/5/2012	5:00:00	3.9	0	1.8
5/5/2012	5:30:00	3.9	0	1.8
5/5/2012	6:00:00	3.9	0	1.8
5/5/2012	6:30:00	3.8	0	1.8
5/5/2012	7:00:00	3.8	0	1.7

Annex 2: Aspect histograms of the different DEMs.

Aspect histogram of local DEM

Aspect histogram of ASTER DEM

Aspect histogram of SRTM DEM